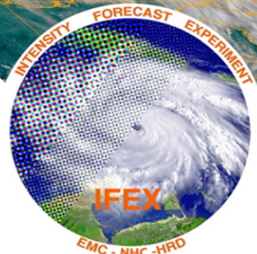
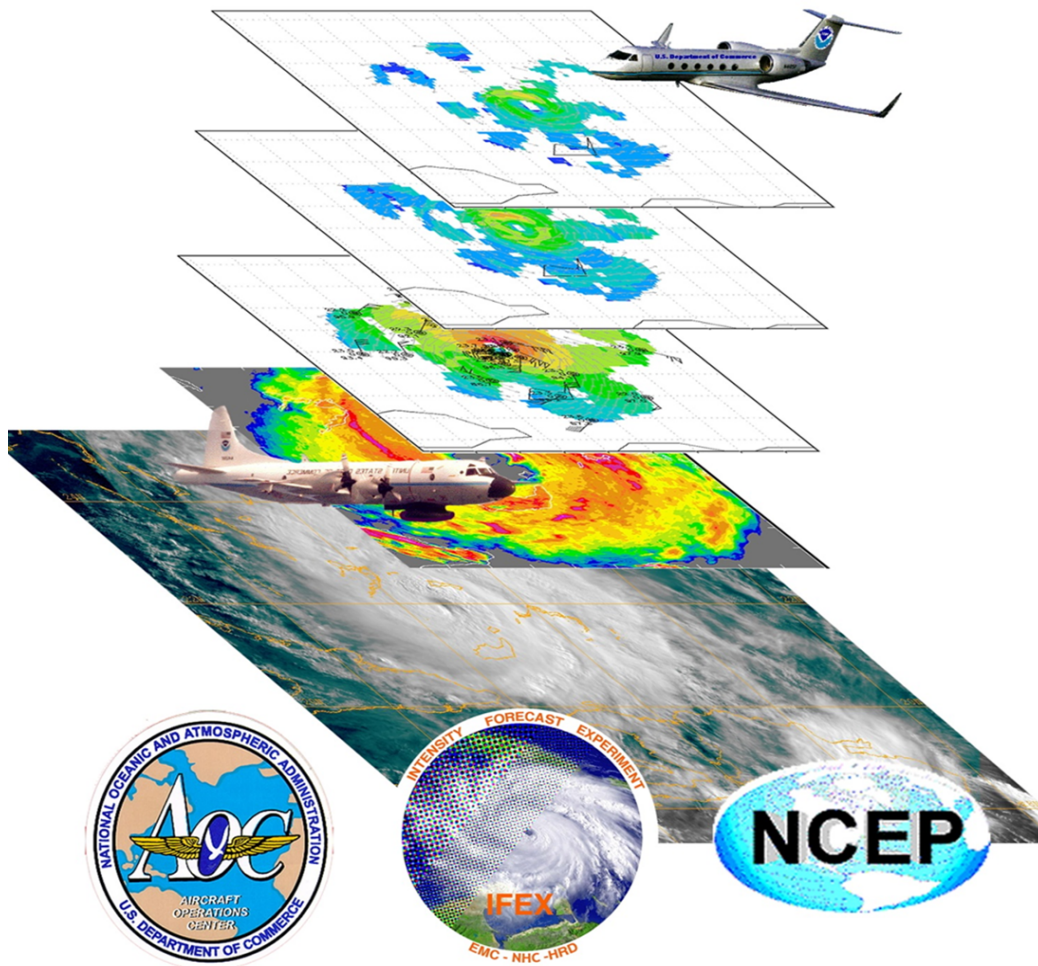


# 2018 Hurricane Field Program



**2018 HURRICANE FIELD PROGRAM PLAN  
INTENSITY FORECAST EXPERIMENT**

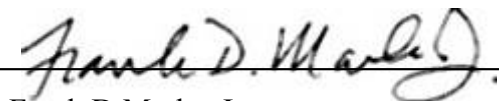
National Oceanographic and Atmospheric Administration (NOAA)  
Atlantic Oceanographic and Meteorological Laboratory (AOML)  
Hurricane Research Division (HRD)  
4301 Rickenbacker Causeway  
Miami, FL 33149

**KEY PERSONNEL DEFINED:**

HRD DIRECTOR	<b>Frank Marks</b>
HRD DEPUTY DIRECTOR	<b>Shirley Murillo</b>
FIELD PROGRAM DIRECTOR	<b>Jonathan Zawislak</b>
FIELD PROGRAM DEPUTY DIRECTOR	<b>Robert Rogers</b>
HRD ADMINISTRATIVE	<b>Jennifer Calderon</b>
AOC DESIGNEE	<b>Jim McFadden</b>
DDAL REPRESENTATIVES	<b>Jonathan Zawislak, Heather Holbach</b>

**PREPARED BY:**

NOAA/AOML/HRD and U.MIAMI/RSMAS/CIMAS: **Jonathan Zawislak, Sim Aberson, Ghassan Alaka, Lisa Bucci, Hui Christophersen, Joe Cione, Peter Dodge, Jason Dunion, John Gamache, Heather Holbach (NGI/FSU), John Kaplan, Paul Leighton, Paul Reasor, Robert Rogers, Kelly Ryan, Kathryn Sellwood, Jason Sippel, Jun Zhang**  
NOAA PARTNERS: **Eric Blake (NWS/NHC), Michael Brennan (NWS/NHC), Paul Chang (NOAA/NESDIS), George Halliwell (NOAA/AOML/PhOD), Zorana Jelenak (NOAA/NESDIS), Chris Landsea (NWS/NHC), Rick Lumpkin (NOAA/AOML/PhOD)**  
IFEX Collaborators:  
**Trey Alvey (U. Utah), Mark Boothe (NPS), Mark Bourassa (FSU), Alan Brammer (SUNY Albany), Tim Dunkerton (NWRA), Michael Montgomery (NPS), Benjamin Jaimes (U. Miami/RSMAS), Blake Rutherford (NWRA), Elizabeth Sanabia (USNA), Nick Shay (U. Miami/RSMAS), Chris Thorncroft (SUNY Albany), Ryan Torn (SUNY Albany), Josh Wadler (U. Miami/RSMAS)**



---

Frank D Marks, Jr  
Director, Hurricane Research Division

Date

TABLE OF CONTENTS

---

<b>INTRODUCTION</b> .....	1
1. Description of Intensity Forecasting Experiment (IFEX) .....	1
2. Experiments Overview .....	2
3. HFP Plan Organization .....	4
<b>OPERATIONS</b> .....	5
1. Available Aircraft and Deployment Locations .....	5
2. Field Program Duration .....	5
3. Research Mission Operations .....	5
4. Field Operations .....	5
4.1 <i>Scientific Leadership Responsibilities</i> .....	5
4.2 <i>Principal Duties of HRD Scientific Personnel</i> .....	6
4.3 <i>Communication of HFP Activities</i> .....	6
5. Operational Constraints .....	6
<b>DATA MANAGEMENT</b> .....	7
1. Data Management and Availability .....	7
2. Basin-scale HWRP Real-time Products .....	7
3. HRD Data Products List .....	8
<b>INSTRUMENT DESCRIPTIONS</b> .....	9
1. Flight-level Measurements .....	9
2. Tail Doppler Radar (TDR) .....	9
3. Lower Fuselage (LF) Radar .....	9
4. Stepped-Frequency Microwave Radiometer (SFMR) .....	9
5. GPS Dropwindsonde and Ocean Profilers .....	10
6. Cloud Microphysics .....	10
7. Doppler Wind LIDAR (DWL) .....	11
7.1 <i>Technical Details</i> .....	11
7.2 <i>Pattern/Module Requirements</i> .....	11
7.3 <i>Analysis Strategy</i> .....	12
8. Compact rotational Raman LIDAR (CRL) .....	12
8.1 <i>Technical Details</i> .....	12
8.2 <i>Motivation</i> .....	14
8.3 <i>Synergies with other P-3 Measurements</i> .....	14
8.4 <i>Pattern/Module Requirements</i> .....	14
8.5 <i>Analysis Strategy</i> .....	15
8.6 <i>References</i> .....	16
9. Imaging Wind and Rain Airborne Profile (IWRAP) .....	17
10. Wide Swath Radar Altimeter (WSRA) .....	17
11. Coyote UAS .....	17
<b>TAIL DOPPLER RADAR (TDR) EXPERIMENT: Science Description</b> .....	19
<b>SFMR EXPERIMENT: Science Description</b> .....	23
Science Objective #1: SFMR High Incidence Angle Measurements (HiSFMR).....	23
Science Objective #2: G-IV SFMR Validation .....	27

## TABLE OF CONTENTS

---

<b>GENESIS STAGE EXPERIMENT: Science Description</b> .....	31
Science Objective #1: Precipitation Mode (PMODE) .....	31
Science Objective #2: Pouch .....	35
Science Objective #3: Favorable Air Mass (FAM) .....	39
<b>EARLY STAGE EXPERIMENT: Science Description</b> .....	44
Science Objective #1: Analysis of Intensity Change Processes Experiment (AIPEX) .....	44
Science Objective #2: Convective Burst Structure and Evolution Module (CBM) .....	53
Science Objective #3: Arc Cloud Module .....	61
<b>MATURE STAGE EXPERIMENT: Science Description</b> .....	64
Science Objective #1: Internal Processes .....	64
TC DIURNAL CYCLE .....	64
GRAVITY WAVE .....	68
SECONDARY EYEWALL FORMATION (SEF) .....	70
EYE-EYEWALL MIXING .....	74
Science Objective #2: Environment Interaction .....	76
TC IN SHEAR .....	76
ARC CLOUD .....	79
Science Objective #3: New Observing Systems (NOS) .....	82
COYOTE .....	82
NESDIS OCEAN WINDS .....	83
<b>END STAGE EXPERIMENT: Science Description</b> .....	87
Science Objective #1: Landfall .....	87
Science Objective #2: Weakening / Extratropical Transition (ET) .....	91
<b>SYNOPTIC FLOW EXPERIMENT: Science Description</b> .....	93
<b>OCEAN SURVEY EXPERIMENT: Science Description</b> .....	95
<b>APPENDIX A: Standard Patterns and Expendable Locations</b> .....	112
<b>APPENDIX B: Decision and Notification Process</b> .....	117
<b>APPENDIX C: Principal Duties of HRD Scientific Personnel</b> .....	122
1. Safety .....	122
2. Conditions of Flight .....	122
3. General Information for All Scientific Mission Participants .....	123
4. HRD SCIENCE CREW Responsibilities .....	123
<b>APPENDIX D: Operational Maps</b> .....	126
<b>APPENDIX E: Aircraft Instrumentation List</b> .....	127
<b>APPENDIX F: DOD/NWS RAWIN/RAOB and NWS Coastal Land-Based Radar</b> <b>Locations</b> .....	129
<b>APPENDIX G Systems of Measure and Unit Conversion Factors</b> .....	131
<b>APPENDIX H: List of Acronyms</b> .....	132

## INTRODUCTION

---

### 1. Description of Intensity Forecasting Experiment (IFEX)

One of the key aspects of NOAA's Mission is, "To understand and predict changes in the climate, weather, oceans, and coasts..." with a long-term goal of achieving a, "Weather-ready Nation," in which society is able to prepare for and respond to weather-related events. This objective specifies the need to improve the understanding and prediction of tropical cyclones (TCs). The NOAA/National Weather Service/National Hurricane Center (NHC) is responsible for forecasting TCs in the Atlantic and East Pacific basins, while NOAA/National Centers for Environmental Prediction (NCEP)/Environmental Modeling Center (EMC) provides numerical weather prediction (NWP) forecast guidance for the forecasters. Together they have made great strides in improving forecasts of TC track. With support from the research community, forecast errors of TC track have decreased by about 50% over the past 30 years. However, there has been much less improvement in forecasts of TC intensity, structure, and rainfall. This lack of improvement is largely the result of deficiencies in routinely collecting inner-core data and assimilating it into the modeling system, limitations in the numerical models themselves, and gaps in understanding of the physics of TCs and their interaction with the environment. Accurate forecasts will rely heavily on the use of improved numerical modeling systems, which in turn will rely on accurate observational datasets for assimilation and validation.

The operational Hurricane Weather Research and Forecasting (HWRF) model uses an assortment of physical parameterizations intended to represent subgrid-scale processes important in TC evolution. Such a modeling system holds the potential of improving understanding and forecasting of TC track, intensity, structure, and rainfall. In order to realize such improvements, however, new data assimilation techniques must be developed and refined, physical parameterizations must be improved and adapted for TC environments, and the models must be reliably evaluated against detailed observations from a variety of TCs and their surrounding environments.

To conduct the research necessary to address the issues raised above, since 2005 NOAA has been conducting an experiment designed to improve operational forecasts of TC intensity, called the Intensity Forecasting EXperiment (IFEX; Rogers et al., BAMS, 2006, 2013). The IFEX goals, developed through a partnership involving the NOAA/Atlantic Oceanographic and Meteorological Laboratory (AOML)'s Hurricane Research Division (HRD), NHC, and EMC, are to improve operational forecasts of TC intensity, structure, and rainfall by providing data to improve the operational numerical modeling system (i.e., HWRF) and by improving understanding of the relevant physical processes. These goals will be accomplished by satisfying a set of requirements and recommendations guiding the collection of the data:

## INTRODUCTION

---

- GOAL 1: Collect observations that span the TC life cycle in a variety of environments for model initialization and evaluation
- GOAL 2: Develop and refine measurement technologies that provide improved real-time monitoring of TC intensity, structure, and environment
- GOAL 3: Improve understanding of the physical processes important in intensity change for a TC at all stages of its life cycle

A unique, and critical, aspect of IFEX is the focus on providing measurements of TCs at all stages of their life cycle. While the focus of hurricane research flights during the past 30 years has been predominantly on mature storms, leading to a dataset biased toward these types of systems, IFEX now also places a focus on the genesis and early stages of storms. This emphasis will not only provide critical observations during a period in the storm life cycle when there is perhaps the greatest uncertainty in the track and intensity forecasts, but also fills an observing gap during the early stages of a storm's development where case and composite studies have lacked.

### 2. Experiments Overview

This season, HFP-IFEX includes experiments for each stage of the TC life cycle: “Genesis”, “Early”, “Mature”, and “End” of life cycle.

The “*Genesis Stage Experiment*” consists of objectives that require observations during the pre-Tropical Depression (TD), or “Invest” (designated by NHC) period of a developing (or non-developing) storm. Each of three objectives focus on progressively larger-scale aspects of a disturbance: one that evaluates the co-evolution of precipitation (such as convective bursts), and the response of the developing vortex at multiple levels to that precipitation, another that seeks to investigate the kinematic and thermodynamic characteristics of the “pouch” as it evolves towards a “self-sustaining entity” (i.e., a TC), and a third aimed at describing the evolving favorability of the large-scale environment surrounding a developing (or non-developing) disturbance.

The “*Early Stage Experiment*” will consist of objectives that require observations in TCs at TD, Tropical Storm (TS), or Category 1 hurricane intensity. The first objective is to identify processes responsible for the intensification (or non-intensification) during these early stages, including those that experience (rapid) intensification in moderately sheared environments. This objective emphasizes sampling in a shear-relative framework, particularly in the upshear quadrants where changes in the precipitation distribution is intimately linked to future intensity change. The second objective investigates the structure and impact of convective bursts cycling around the TC center on intensity change, while a third objective requires measurements across arc cloud boundaries emanating away from the TC center. These measurements will increase our understanding on the formation and evolution of arc clouds and their impacts on TC structure and intensity in the short-term.

## INTRODUCTION

---

The “*Mature Stage Experiment*” will consist of objectives that require observations in stronger hurricanes (Category 2 intensity or greater). Science objectives during this stage are separated into those that will evaluate internal processes to the TC and those that will investigate the interaction of a TC with its environment. Observations are sought on a number of important internal processes that could result in structural and intensity changes in a TC; these include the diurnal cycle, gravity wave activity, secondary eyewall formation and eyewall replacement cycles, and the mixing that occurs between the eye and eyewall. The objective on environmental interaction encompasses sampling storms experiencing an evolving environmental vertical wind shear profile, and the influence of arc clouds as they emanate from away from the center into the surrounding environment. The third objective is consistent with IFEX GOAL #2 and is to evaluate the use of new observing systems to sample the hurricane structure, including the boundary layer (using the unmanned aerial system, Coyote) and its environment (e.g., the air-sea interface).

The “*End Stage Experiment*” consists of objectives that require observations during the weakening or extratropical transition period of storm, and/or during landfall. As with other stages, these experiments focus on the structural changes that occur in a TC. The landfall objective additionally focuses on the validation of surface wind speed estimates and forecasts, as well as rainbands and their potential to generate severe weather.

Other experiments included in the HFP Plan (HFPP) are the following:

- “*Ocean Survey*”: Ocean observations obtained from sonobouys (e.g., AXBTs, AXCTDs, and AXCPs) will be used to better understand a TC’s interaction with the underlying ocean (such as enthalpy flux), and obtained at enough resolution to rigorously test coupled TC models.
- “*Synoptic Flow*”: This experiment will investigate new strategies for optimizing the use of aircraft observations to improve forecasts of TC track, intensity, and structure. It suggests targeting regions in and around the TC with aircraft where ensemble prediction systems suggest the most sensitivity of TC-related forecast metrics (position, intensity, and track).
- “*Tail Doppler Radar*”: The primary goal of this experiment is to gather wind measurements that will provide three-dimensional wind analyses of the TC that can also be used to create a more accurate initialization for HWRF.
- “*SFMR Experiment*”: The goals of this experiment are to improve surface wind speed algorithms when the instrument is looking at off-nadir (high,  $> \pm 5^\circ$ ) incidence angles, and to validate SFMR measurements from the G-IV by coordinating sampling with the P-3.

## INTRODUCTION

---

### 3. HFP Plan Organization

The HFP-IFEX missions presented in this document are separated into individual science experiments. Each experiment outlines Science Objectives that map onto to one or more IFEX GOAL listed in subsection (1). Science Objectives are described for each experiment in their, “Science Description” documents. The “Science Description” includes the motivation and background on the science behind each objective, relevant hypotheses, a description of the aircraft “Patterns” and “Modules” that will be flown for that objective, and the analysis strategy once data is collected. Accompanying each experiment are also, “Pattern and Module Descriptions,” which provide a summary of details regarding the mission execution (timing, patterns, expendables, etc.). These provide the information needed for the PIs, [FIELD PROGRAM DIRECTOR], and aircraft crew to plan and execute a mission associated with an experiment.

Multiple “Patterns” and “Modules” are possible for each Science Objective in an experiment. Each “Pattern” and “Module” is numbered sequentially within an individual Science Objective, and labeled with a shorthand descriptor; for example, a pattern in the “Environment Interaction” objective of the “*Mature Stage Experiment*” is named, “**P-3 Pattern #1: Environment Interaction (TC in Shear)**”. A second qualifier may be provided; in the previous example, “TC in Shear.”

In most cases (unless otherwise noted), “Patterns” will be identified as one of the “standard” patterns, illustrated in APPENDIX A (e.g., Lawnmower, Square-spiral, Figure-4, Rotated Figure-4, Butterfly). Many of the “Patterns” outlined in the experiments are “standard” patterns that are subsequently modified to meet the sampling needs of the objective.

Within each experiment, reference is made to either “Patterns” or “Modules.” “Patterns” refers to missions that require an entire dedicated mission (i.e., generally greater than 3 h of flight time). “Modules” refer to break-away (e.g., from the “standard” patterns described APPENDIX A), shorter flight segments that generally require less than 3 h or less of flight time for completion.

#### *References*

Rogers, R., and co-authors, 2006: The Intensity Forecast Experiment: A NOAA multiyear field program for improving tropical cyclone intensity forecasts. *Bull. Amer. Meteor. Soc.*, **87**, 1523–1537.

Rogers, R., and co-authors, 2013: NOAA’s Hurricane Intensity Forecasting Experiment: A Progress Report. *Bull. Amer. Meteor. Soc.*, **94**, 859–882.



## OPERATIONS

---

### 1. Available Aircraft and Deployment Locations

Starting on 23 June, the NOAA WP-3D (P-3) (N42RF) aircraft will be available with two flight crews available for back-to-back missions, while the Gulfstream IV-SP (G-IV) (N49RF) aircraft will be available 01 June with two flight crews available for back-to-back missions. Operations for all aircraft will primarily base out of the NOAA/OMAO/Aircraft Operations Center (AOC) in Lakeland, FL with deployments to U.S. coastal locations in the western Gulf of Mexico for suitable Gulf storms, as well as other locations along the U.S. East Coast, St. Croix, and Barbados. Occasionally, post-mission recovery may be accomplished elsewhere. APPENDIX D shows deployment locations and operating range rings (for 2 h on-station time) for both the P-3 (Fig. D-1) and the G-IV (Fig. D-2).

### 2. Field Program Duration

The HFP-IFEX will be conducted from approximately 01 July through 31 October 2018.

### 3. Research Mission Operations

The decision and notification process for research-tasked missions is shown, in flow chart form, in APPENDIX B (Figs. B-1, B-2, and B-3). The decision and notification process for HRD participation in EMC-tasked operational missions will follow a similar flow chart. The names of those who receive primary notification at each decision or notification point are shown in Figs. B-1, B-2, and B-3.

Research operations must consider that the aircraft are required to be placed in the National Hurricane Operations Plan of the Day (POD) 24 h before a mission. If operational requirements are accepted, the research aircraft must follow the operational constraints described in Section 7.

The NOAA P-3 aircraft, equipped as shown in APPENDIX E (Table E-1), will be available for research missions on a non-interference basis with tasked operational missions from 23 June to 31 October 2018. Also, the G-IV aircraft, equipped as show in APPENDIX E (Table E-2) should be available, on a non-interference basis, with tasked operational missions from 01 June to 31 October 2018.

### 4. Field Operations

#### *4.1 Scientific Leadership Responsibilities*

The implementation of the Hurricane Field Program Plan (HFPP) is the responsibility of [FIELD PROGRAM DIRECTOR], who in turn reports directly to [HRD DIRECTOR] and [HRD DEPUTY DIRECTOR]. In the event of deployment, [FIELD PROGRAM DIRECTOR] may assign a ground team manager (e.g., [FIELD PROGRAM DEPUTY DIRECTOR]) to assume overall responsibility for essential ground support logistics, site communications, and site personnel who are not actively engaged in flight. Designated Principal Investigators (PIs) are responsible to [FIELD PROGRAM DIRECTOR], and/or [FIELD PROGRAM DEPUTY

## OPERATIONS

---

DIRECTOR], for the preparation and execution of experiments and their accompanying flight patterns and modules. While in flight, LEAD PROJECT SCIENTISTS are in charge of the scientific aspects of the mission and ensure science goals of the mission are met. They communicate with the AOC flight crew (specifically, the Flight Director) regarding execution of the mission and the planned flight patterns/modules, and address and report issues regarding instrument status to the flight crew and [FIELD PROGRAM DIRECTOR]. The HRD SCIENCE CREW ensures all appropriate mission reports are completed and data downloaded off the aircraft.

### *4.2 Principal Duties of HRD Scientific Personnel*

APPENDIX C describes the possible HRD SCIENCE CREW needed to conduct the experiments and their roles. Actual named assignments are adjusted on a case-by-case basis. Operations will include completion of detailed records by each member of the HRD SCIENCE CREW while on the aircraft.

### *4.3 Communication of HFP Activities*

All HFP activities are communicated to the public via the HRD web blog or social media. In addition, more detailed information on activities will be communicated internally to HRD. When field activities are occurring, an HRD conference call at 1300 UTC with IFEX participants and collaborators is possible, followed by an internal email. The internal email will include up-to-date information on the HRD SCIENCE CREW, hotel, storm and mission status, and schedules. The blog is our main forum where we will provide field operation status, including deployment information of aircraft and personnel for operations outside Miami.

NHC will serve as the communications center for information and will provide interface between AOC, NHC, and CARCAH (Chief, Aerial Reconnaissance Coordinator, All Hurricanes). HRD SCIENCE CREW who have completed a flight will provide information to the [FIELD PROGRAM DIRECTOR], as required.

## **5. Operational Constraints**

NOAA aircraft are routinely tasked by NHC and/or EMC through CARCAH to perform operational missions — these always take precedence over research missions. Research objectives can frequently be met, however, through piggybacking these operational missions. Occasionally, HRD may request, through NHC and CARCAH, slight modifications to the flight plan on operational missions. These requests must not deter from the basic requirements of the operational flight as determined by NHC and coordinated through CARCAH.

Hurricane research missions are routinely coordinated with hurricane reconnaissance operations. As each research mission is entered into the planned operation, a block of time is reserved for that mission and operational reconnaissance requirements are assigned. A mission, once assigned, *must be flown in the time period allotted and the tasked operational fixes met*. Flight departure times are critical. Information on delays to, or cancellations of, research flights must be relayed to CARCAH.

DATA MANAGEMENT

---

**1. Data Management and Availability**

Data management and dissemination will be according to the HRD data policy that can be viewed at [http://www.aoml.noaa.gov/hrd/data\\_sub/](http://www.aoml.noaa.gov/hrd/data_sub/)

Data Management Plans have been produced for nearly all observational and model products made available by NOAA/AOML/HRD (Table DM-1) and are available on request with the HRD [DDAL (Data Display, Archival, and Legacy Working Group) REPRESENTATIVES].

A brief description of the primary data types and contact information made available via HRD are listed in Table DM-1.

Raw data are typically available immediately after a flight, subject to technical and quality assurance limitations. Some P-3 and G-IV raw data can be accessed through NOAA/OMAO/AOC after the mission at <https://seb.noaa.gov/pub/>. Processed data or other data that has undergone further quality control or analyses by HRD scientists are normally available to the Principal and Co-investigators within a period of several months after the end of the HFP.

All requests for NOAA data gathered during the HFP should be forwarded by email to the associated contact person in the HRD data products list (Table DM-1) or via email to [HRD DIRECTOR] or the [DDAL REPRESENTATIVES].

**2. Basin-scale HWRF Real-time Products**

The real-time Basin-scale HWRF is run by the Modeling Team at NOAA/AOML/HRD and can be accessed at the following webpage: [storm.aoml.noaa.gov](http://storm.aoml.noaa.gov)

**2018 NOAA/AOML/HRD Hurricane Field Program - IFEX**

**DATA MANAGEMENT**

**3. HRD Data Products List**

*Table DM-1. List of products and analyses made available by HRD in support of the HFP and the contacts*

<b>INSTRUMENTS</b>	<i>Investigators</i>
Tail Doppler radar (TDR)	John Gamache ( <a href="mailto:john.gamache@noaa.gov">john.gamache@noaa.gov</a> ) Paul Reasor ( <a href="mailto:paul.reasor@noaa.gov">paul.reasor@noaa.gov</a> )
Lower Fuselage (LF) radar	John Gamache ( <a href="mailto:john.gamache@noaa.gov">john.gamache@noaa.gov</a> ) Paul Reasor ( <a href="mailto:paul.reasor@noaa.gov">paul.reasor@noaa.gov</a> )
Stepped Frequency Microwave Radiometer (SFMR)	Heather Holbach ( <a href="mailto:heather.holbach@noaa.gov">heather.holbach@noaa.gov</a> )
Doppler Wind LIDAR (DWL)	Lisa Bucci ( <a href="mailto:lisa.bucci@noaa.gov">lisa.bucci@noaa.gov</a> )
Cloud Physics Probes	Robert Black ( <a href="mailto:Robert.a.black@noaa.gov">Robert.a.black@noaa.gov</a> )
Compact Rotational Raman LIDAR	Jun Zhang ( <a href="mailto:jun.zhang@noaa.gov">jun.zhang@noaa.gov</a> )
<b>PLATFORMS</b>	<i>Investigators</i>
P-3 and G-IV Flight-level	Neal Dorst ( <a href="mailto:neal.m.dorst@noaa.gov">neal.m.dorst@noaa.gov</a> )
Dropsonde	Kathryn Sellwood ( <a href="mailto:Kathryn.sellwood@noaa.gov">Kathryn.sellwood@noaa.gov</a> )
Coyote	Joe Cione ( <a href="mailto:joe.cione@noaa.gov">joe.cione@noaa.gov</a> ) Kelly Ryan ( <a href="mailto:Kelly.ryan@noaa.gov">Kelly.ryan@noaa.gov</a> )
Airborne eXpendable BathyThermograph (AXBT)	Nick Shay ( <a href="mailto:nshay@miami.edu">nshay@miami.edu</a> ) Jun Zhang ( <a href="mailto:jun.zhang@noaa.gov">jun.zhang@noaa.gov</a> )
<b>OBSERVATIONAL PRODUCTS</b>	<i>Investigators</i>
HEDAS Pre-processing	Altug Aksoy ( <a href="mailto:altug.aksoy@noaa.gov">altug.aksoy@noaa.gov</a> )
Center Fixes / Tracks (2-min)	Neal Dorst ( <a href="mailto:neal.m.dorst@noaa.gov">neal.m.dorst@noaa.gov</a> )
<b>INFORMATIONAL</b>	<i>Investigators</i>
Flight Logs (e.g., LPS, Radar, Dropsonde, Boundary Layer, DWL)	Neal Dorst ( <a href="mailto:neal.m.dorst@noaa.gov">neal.m.dorst@noaa.gov</a> )
<b>MODEL PRODUCTS</b>	<i>Investigators</i>
Basin-scale HWRF	Ghassan Alaka ( <a href="mailto:ghassan.alaka@noaa.gov">ghassan.alaka@noaa.gov</a> )
HWRF Hurricane Ensemble Data Assimilation Scheme (HEDAS)	Sim Aberson ( <a href="mailto:sim.aberson@noaa.gov">sim.aberson@noaa.gov</a> ) Altug Aksoy ( <a href="mailto:altug.aksoy@noaa.gov">altug.aksoy@noaa.gov</a> )

## INSTRUMENT DESCRIPTIONS

---

The following are descriptions of instruments being flown on the P-3 and the G-IV aircraft during the season.

### 1. Flight-level Measurements [P-3 and G-IV]

Data from flight-level measurements are provided at 40 Hz (FAST) and 1 Hz and include: positional information, true air and ground speed, radar and pressure altitude, static and dynamic air pressure, air temperature, dew point temperature, d-value, horizontal and vertical wind, water vapor mixing ratio, and extrapolated surface pressure.

### 2. Tail Doppler Radar (TDR) [P-3 and G-IV]

The P-3 tail Doppler radar (TDR) systems have two solid-state transceivers that simultaneously transmit through the fore and aft antennas. The antennas are canted approximately 20 degrees fore or aft of the plane normal to the fuselage of the aircraft. The exact functioning of the TDR for the hurricane season is still being developed. It is expected the single pulse repetition frequency will be about 3000/sec, and a long compressed pulse will be used to produce sensitivity on the order of -10 dBZ at 10 km. A short pulse will be added to provide data in the first 3 km from the aircraft. The frequency of the radar is in the X-band, with a wavelength of approximately 3 cm, and the beam width is approximately 2 degrees.

The G-IV tail Doppler radar system has two transceivers that use traveling wave tube amplification. They transmit simultaneously through the fore and aft antennas. The antennas are canted approximate 20 degrees fore or aft of the plane normal to the fuselage of the aircraft. The single pulse repetition frequency will be about 3000/sec and a long compressed pulse provides sensitivity on the order of -10 dBZ at 10 km. There is no short pulse, so there are no data recorded within 3 km range of the radar. The frequency of the radar is in the x-band, with a wavelength of approximately 3 cm. The beam width is approximately 2.7 degree.

### 3. Lower Fuselage (LF) Radar [P-3]

TBD

### 4. Stepped Frequency Microwave Radiometer (SFMR) [P-3 and G-IV]

SFMR is an airborne microwave radiometer that offers retrieved surface wind speed and rain rate by measuring the surface brightness temperature at nadir at six C-band frequencies between 4.6 and 7.2 GHz. The apparent brightness temperature of the ocean surface is sensitive to the sea surface temperature (SST) and surface foam coverage due to wave breaking; as the surface wind speed increases, so does the coverage of sea foam and, subsequently, the brightness temperature (Nordberg et al. 1971; Rosenkranz and Staelin 1972; Klotz and Uhlhorn 2014). Therefore, brightness temperature increases with surface wind speed for a given SST. A retrieval algorithm uses the relationship between the surface emissivity and wind speed (using a geophysical model function, GMF, and inversion algorithm) to retrieve surface wind estimates along the flight track

## INSTRUMENT DESCRIPTIONS

---

(Uhlhorn et al. 2007). Recently, Klotz and Uhlhorn (2014) corrected a deficiency in the SFMR surface wind speed algorithm for an overestimation of wind speed in weak wind and heavy rain conditions by revising the GMF coefficients for both the rain absorption and wind-induced surface emissivity models. The result was a significantly reduced bias at wind speeds less than hurricane force, and more accurate retrieved rain rates.

This season a dedicated SFMR experiment will utilize a second SFMR mounted on the P-3 to collect data at high-incidence roll angles. The operational SFMR will be collecting off-nadir data at horizontal polarization and the second SFMR will collect off-nadir data at vertical polarization, which simulates data that the SFMR would collect when the aircraft pitches. The goal is to develop corrections in the SFMR algorithm to obtain measurements of wind speed when the aircraft pitch and roll angle exceeds  $\pm 5^\circ$ , which are currently not reported. A second objective in the SFMR experiment is to verify measurements from the SFMR on the G-IV against those from the operational SFMR on the P-3.

### *References*

- Klotz, B. W., and E. W. Uhlhorn, 2014: Improved Stepped Frequency Microwave Radiometer Tropical Cyclone Surface Winds in Heavy Precipitation. *J. Atmos. Oceanic Tech.*, **31**, 2392–2408.
- Nordberg, W. J., J. Conway, D. B. Ross, and T. Wilheit, 1971: Measurements of microwave emission from a foam-covered, wind-driven sea. *J. Atmos. Sci.*, **28**, 429–435.
- Rosenkranz, P. W., and D. H. Staelin, 1972: Microwave emissivity of ocean foam and its effect on nadir radiometric measurements. *J. Geophys. Res.*, **77**, 6528–6538.
- Uhlhorn, E. W., P. G. Black, J. L. Franklin, M. Goodberlet, J. Carswell, and A. S. Goldstein, 2007: Hurricane Surface Wind Speed Measurements from an Operational Stepped Frequency Microwave Radiometer, *Mon. Wea. Rev.*, **135**, 3070–3085.

### **5. GPS Dropwindsonde [P-3 and G-IV] and Ocean Profilers [P-3]**

The GPS dropwindsonde (dropsonde) is part of the National Center for Atmospheric Research (NCAR) / Earth Observing Laboratory (EOL) AVAPS (Airborne Vertical Atmospheric Profiling System) Dropsonde system that measures vertical profiles of atmospheric temperature, pressure, humidity, and wind speed as it falls from the aircraft to the surface.

Possible ocean profiling probes (to measure ocean temperature and salinity profiles) that could be used this season include: AXBTs (Airborne Expendable BathyThermograph), AXCPs (Airborne Expendable Current Profilers), and AXCTDs (Airborne Expendable Conductivity, Temperature, and Depth).

### **6. Cloud Microphysics [P-3]**

The P-3 is equipped with cloud microphysics probes that image cloud and precipitation particles and produce particle size distributions. The probes flown include the Droplet Measurement Technologies, Inc. (DMT) ([www.dropletmeasurement.com](http://www.dropletmeasurement.com)) Cloud Combination Probe (CCP) (for aerosol and cloud hydrometeor size distributions from 2 to 50  $\mu\text{m}$ ; 2-D images and

## INSTRUMENT DESCRIPTIONS

---

precipitation size distributions between 25 and 1550  $\mu\text{m}$ , liquid water content from 0.05 to 3  $\text{g m}^{-3}$ ), Precipitation Imaging Probe (PIP) (for hydrometeor sizes between 100  $\mu\text{m}$  and 6.2 mm), and the Cloud and Aerosol Spectrometer (CAS) (for aerosol and cloud hydrometeor size between 0.5 and 50  $\mu\text{m}$ ).

### 7. Doppler Wind LIDAR (DWL) [P-3]

#### 7.1 Technical Details

Due to operational instrument limitations, only limited continuous high-resolution wind observations exist in the TC boundary layer and in regions of low or no precipitation. A coherent-detection Doppler wind profile (P3DWL) system will be installed on the NOAA P-3 for the season and can collect wind profiles through the detection of aerosol scatters motion in areas of optically thin or broken clouds or where aerosols are  $\sim 1$  micron or larger. In addition to potential improvement due to assimilation into numerical weather models, these measurements may shed light on physical processes in data sparse regions such as in the hurricane boundary layer, Saharan Air Layer (SAL), regions in-between rainbands, and in the ambient tropical environment around the TC.

The DWL is capable of performing a variety of scanning patterns, both above and below the aircraft. Depending on the scanning pattern, the vertical resolution of the wind profiles is 25-50 m and the horizontal resolution is 1-2 km. Below the aircraft, the instrument can observe winds at or near the surface ( $\sim 25$  m). When sampling above the aircraft, it can observe as high as  $\sim 14$  km (in the presence of high cirrus). However, in the presence of optically thick convection or within  $\sim 400$  m of the instrument, the DWL is unable to collect measurements.

The DWL was used in the West Pacific field campaign THORPEX in 2008 where data collected in the near-TC environment improved both track and intensity forecasts. DWL has successfully retrieved continuous observations in high-wind regimes where few measurements are typically collected. Measurements obtained in the boundary layer provide a means of evaluating near-surface momentum field where surface energy exchange is an important process for hurricane evolution. The DWL provides observations that allow for axisymmetric wind field coverage due to its complementary relationship to TDR. This distribution of measurements is theorized to improve hurricane prediction by capturing asymmetries in the vortex.

#### 7.2 Pattern/Module Requirements

DWL scanning pattern criteria are as follows:

- Weak or asymmetric TCs: Four scans down 20 with a 5 second nadir followed by one scan up 20 with 5 second vertical. If signal strength in the up scan is very weak, only scan down.
- Boundary layer/SEF measurements: DN 20 mode (12 point stepstare) with 5 second vertical stare between 360 degree scans.
- SAL: Two scans at down 20 with a 5 second nadir followed by one scan up 20 with 5 second vertical. If signal strength in the up scan is very weak, change to 4 scans down, one scan up. If no signal upward, only scan down.

## INSTRUMENT DESCRIPTIONS

*7.3 Analysis Strategy*

An analysis of TC structure will be performed by evaluating boundary layer height, inflow characteristics (layer depth, strength of the peak, angle), and gradient wind in secondary eyewall. An analysis of SAL includes capturing the details of the easterly jet. To evaluate the impact of DWL observations on hurricane forecasts, OSE's will be performed using both line-of-sight and post-processed vector wind data. Observations collected from the DWL in conjunction with other observing platforms will be used to evaluate the model representation of different aspects of a TC, such as the boundary layer, SAL intrusions, and sheared TCs. Multiple modeling frameworks are expected to be used.

**8. Compact rotational Raman LIDAR (CRL) [P-3]***8.1 Technical Details*

The CRL is powered by a Nd:YAG laser with 50 mJ pulse energy running at 30 Hz. The normal ocular hazard distance of CRL is less than 200 m, which allows eye-safe operation during aircraft normal operation away from airport. It uses a compact, lightweight transmitting-receiving system, which can be easily mounted to the P-3 nadir port. As illustrated in Fig. CRL-1, the CRL integrated telescope, laser, and receiving system fits into a box of 13x20x26 inches weighing approximately 100 lbs. The CRL was initially developed to obtain 2-D distributions of water vapor, aerosols, and clouds and was first deployed on the University of Wyoming King Air (UWKA) in 2010 (Liu et al. 2014). The successful demonstration of CRL led the development of MARLi. In early 2015, low-J and high-J pure rotational Raman channels (J is the rotational quantum number) were added to provide temperature measurements (Wu et al. 2016).

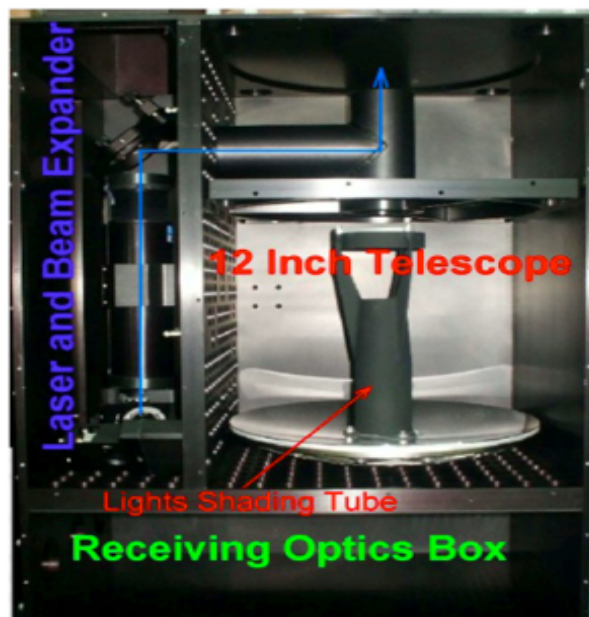


**Figure CRL-1.** Photograph of CRL inner structure. Different parts of lidar system are highlighted.



## INSTRUMENT DESCRIPTIONS

Although the 50-mJ laser limits water vapor measurement to short range under high solar background conditions, the CRL still can provide excellent data for characterizing the spatial variability of aerosol, water vapor, and temperature during night or under normal solar background conditions. The CRL was deployed onboard the UWKA from 1 June to 15 July 2015 over the Great Plains during the recent Multi-Agency PECAN (Plains Elevated Convection At Night) deployment. The CRL operated reliably and collected 120-hrs of excellent data around convective clouds. Fig. CRL-2 shows aerosol, water vapor, and temperature measurements obtained by the CRL on 1 July 2015. The co-varying of aerosol, water vapor, and temperature are clearly illustrated by over 4 hours of measurements around a Mesoscale Convective System (MCS). The first hour of data shows gradual variations of temperature, water vapor, and aerosol when the UWKA flew from the base station to the storm. The UWKA then flew a tight racetrack pattern to approach the storm, resulting in symmetric water vapor mixing ratio (WVMR), aerosol lidar scattering ratio (LSR) patterns. Around the storm, the spatial variations of WVMR and LSR are much sharper. From 0700–0800 UTC, the UWKA flew across the boundary of the cold pools, which had over 3°C temperature drop at the flight level, three times. Resolving such fine-scale 2-D variations of aerosol, water vapor, and temperature is only possible with airborne Raman lidar measurements.

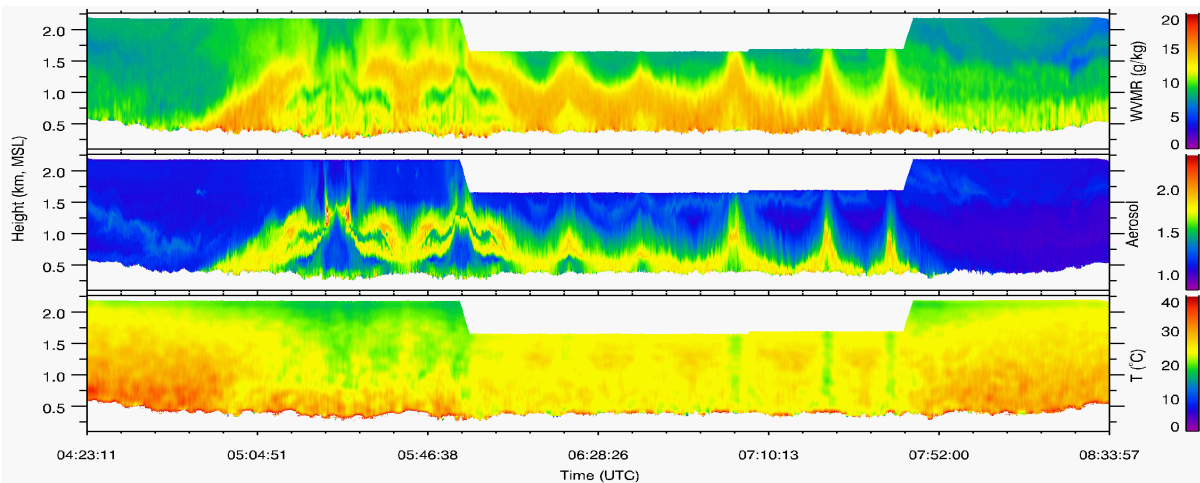


**Figure CRL-2.** CRL measurements of WVMR (top), aerosol LSR (middle), and temperature (bottom) from repeated sampling of the inflow into a MCS on 1 July 2015. The white areas at the lower boundary of the image indicate the surface.

CRL signals are sampled with an A/D card at 250 MHz, which corresponds to a 0.6 m vertical resolution. The temporal/horizontal resolution will be set depending on the application. The data acquisition system is capable of saving individual profiles, which correspond to about 3.6 m horizontal resolution at a typical P-3 cruise speed of 108 m s<sup>-1</sup>. The highest resolution data is important for studying ocean surface wave characteristics, fine-scale sea spray structure, and ABL height variation. Different post-averaging can be done to improve signal-to-noise ratio as necessary for different atmospheric features.

## INSTRUMENT DESCRIPTIONS

---

### *8.2 Motivation*

Despite potential benefits with increasing model horizontal resolution, TC forecast models still face many challenges in intensity prediction (e.g., Bender et al. 2007; Davis et al. 2008; Tallapragada et al. 2014; Zhang et al. 2017). As the horizontal resolution of operational hurricane forecast models approaches 2 km (and eventually reaches 1 km), these models begin to resolve TC inner-core and boundary layer structures. However, TC atmospheric boundary layer (ABL) structures are challenging to observe. Since 1997, Global Positional System (GPS) dropsondes have been the main tool to provide ABL structure (e.g., Franklin et al. 2003). Nonetheless, dropsonde observations are limited by sample size and coarse horizontal resolution, such that previous ABL studies mainly used a composite approach (Barnes 2008; Zhang et al. 2011; 2013). High-resolution temperature and water vapor measurements are only available at the flight level, which is typically above the boundary layer. Although unmanned aircraft based observations will fill some gaps in the near future (Cione et al. 2016), fine-scale two-dimensional (2-D) thermodynamic structures of TC ABL are still lacking.

To transform our capabilities for characterizing the TC ABL thermodynamics, we propose to install the CRL, developed at the University of Wyoming, on a NOAA P-3 aircraft to simultaneously provide fine-scale temperature, water vapor, and aerosol profiles when P-3 is out of clouds. Due to small laser used for CRL, the measurement range may be limited to within 2-km below P-3. Measured ABL structures in TCs will improve our understanding of the physical processes in the TC ABL, which can be used to further upgrade model physics representations. The new observations also can be used to initialize model simulations and to evaluate model simulation results.

The main objectives of the first CRL deployment on the P-3 are:

- 1) Characterize the spatial variability of ABL water vapor, temperature, and aerosol vertical structures;
- 2) Survey environment variability of thermal structure in the lower free troposphere;
- 3) Characterize sea spray and ocean wave structure under different wind regimes.

### *8.3 Synergies with other P-3 Measurements*

Dropsonde, UAS (Coyote) and CRL, together with P-3 in-situ measurements, will provide detailed measurements of the temperature and water vapor structure. Dropsonde measurements provide essential vertical thermodynamic profiles at a coarse horizontal resolution, while P-3 and UAS in-situ measurements provide high horizontally resolved measurements at discrete heights. CRL 2-D cross-sections of water vapor and temperature (as well as UAS in-situ measurements) could fill data gaps between dropsonde observations and in-situ observations. Combined DWL and CRL measurements also offer an opportunity for a more complete analysis of combined wind and thermodynamic measurements for more effective TC ABL characterization.

### *8.4 Pattern/Module Requirements*

To support studies on air-sea interaction and the ABL, P-3 flights within the ABL or near the altitude of the ABL top are required to provide fine-scale ABL temperature, water vapor, and aerosol structures with the CRL. Typically, to sample the full ABL structure the optimal flight

## INSTRUMENT DESCRIPTIONS

---

altitude with the inner core is right below cloud base. Such flight pattern will allow us to resolve cold pool, roll structure, ABL top mixing, sea spray and near-surface water vapor and temperature structure. Together with flight-level wind and thermodynamic measurements, surface wind from SFMR, and storm-scale dynamics from radar, we will have a unique dataset to study air-sea interactions and ABL processes.

The data collection should continue during transits to/from storms to not only characterize storm scale inflow structure, but also to improve the initial state of the HWRF model and to validate the boundary layer structures represented in the model.

CRL will collect data continuously during P-3 research and operational missions to provide real-time fine-scale environment variations in TC, which are hard to detect with satellite measurements or airborne passive sensors alone. With the current small laser, we expect CRL water vapor and temperature measurements to be limited within 2 km below aircraft altitude without extensive spatial averaging. The instrument can obtain surface aerosol measurements and surface wave structure when the P-3 flies within 3–4-km altitude and is clear of clouds. Such measurements are still valuable to characterize thermodynamics structure and aerosol variations within TC. For example, flights between the eyewall and rainbands can measure the inflow structure within the inner core. CRL also provides aerosol depolarization measurements, which can be used to effectively identify dust aerosols associated with the Saharan air layer (SAL).

### *8.5 Analysis Strategy*

The CRL will provide an unprecedented fine-scale water vapor, temperature, and aerosol structures in and around a TC. Using the CRL data together with other measurements from the P-3, the following basic analyses will be produced to study:

- 1) The TC ABL structures across different scales: Key questions we seek to answer are:
  - a. How does the ABL evolve from the outer rainbands to the inner core?
  - b. Does deepening of the ABL coincide with TC intensification?
  - c. What is the dominant scale of horizontal ABL inhomogeneity?
- 2) Ocean wave structure and sea spray under different wind regimes: The spectrum analyses of ocean wave heights will be performed to study the variations of transition wave scales between the energy injection spectrum and the inertial spectrum under different near surface wind speeds. Sea spray has been recognized as a key part of air-sea interactions under high wind conditions, but challenging to observe. CRL near surface aerosol structure will be used to study sea spray productions and their impacts on near-surface water vapor and temperature structures, which control sensible and latent heat fluxes from ocean.
- 3) The variations of environmental thermodynamic properties within the lower free troposphere under different TC conditions: The key initial analysis is to understand the interactions of the lower free troposphere and ABL. The vertical distributions of aerosol, water vapor and temperature will be used to determine ABL top heights and vertical mixing across them. Other than the entrainment/mixing processes across the

INSTRUMENT DESCRIPTIONS

---

ABL top, the exchange of the free troposphere and ABL can occur through different scale circulations, especially around the convective rainband. The fine-scale 2-D structures of water vapor, temperature, and aerosol will allow us to identify such processes.

- 4) The observed fine-scale ABL structure and evaluate high-resolution hurricane model simulations against those observations (e.g., Zhang et al. 2015): The ultimate goal of improved TC ABL observations is to advance our understanding of ABL processes in the TC environment and to improve their simulations in weather forecast models. As the first step to achieve the goal, we will use observations to evaluate TC ABL structures simulated by high-resolution HWRF focusing on how HWRF capturing ABL structure variations between the inner core and the outer rainband and under different TC intensities.

8.6 References

- Barnes, G. M., 2008: Atypical thermodynamic profiles in hurricanes. *Mon. Wea. Rev.*, **136**, 631–643.
- Bender, M. A., I. Ginis, R. Tuleya, B. Thomas, and T. Marchok, 2007: The operational GFDL hurricane-ocean prediction system and a summary of its performance. *Mon. Wea. Rev.*, **135**, 3965–3989.
- Cione, J. J., E. A. Kalina, E. W. Uhlhorn, A. M. Farber, and A. B. Damiano, 2016: *Coyote unmanned aircraft system observations in Hurricane Edouard (2014)*. *Earth and Space Science*, **3**, 370–380, doi:10.1002/2016EA000187.
- Davis, C., and Coauthors, 2008: Prediction of landfalling hurricanes with the Advanced Hurricane WRF model. *Mon. Wea. Rev.*, **136**, 1990–2005.
- Franklin, J. L., M. L. Black, and K. Valde, 2003: GPS dropwindsonde wind profiles in hurricanes and their operational implications. *Wea. Forecasting*, **18**, 32–44.
- Liu B., et al. 2014: Compact airborne Raman lidar for profiling aerosol, water vapor and clouds, *Optics express*, 22 (17), 20613–20621.
- Tallapragada, V., C. Kieu, Y. Kwon, S. Trahan, Q. Liu, Z. Zhang, and I. Kwon, 2014: Evaluation of storm structure from the operational HWRF model during 2012 implementation. *Mon. Wea. Rev.*, **142**, 4308–4325.
- Wu, D., et al., 2016: Airborne compact rotational Raman lidar for temperature measurement, *Opt. Express*, **24**, A1210–A1223.
- Zhang, J. A., R. F. Rogers, D. S. Nolan, and F. D. Marks, 2011: On the characteristic height scales of the hurricane boundary layer. *Mon. Wea. Rev.*, **139**, 2523–2535.

## INSTRUMENT DESCRIPTIONS

---

Zhang, J. A., R. F. Rogers, P. Reasor, E. Uhlhorn, and F. D. Marks, 2013: Asymmetric hurricane boundary layer structure from dropsonde composites in relation to the environmental vertical wind shear. *Mon. Wea. Rev.*, **141**, 3968–3984.

Zhang, J. A., D. S. Nolan, R. F. Rogers, and V. Tallapragada, 2015: Evaluating the impact of improvements in the boundary layer parameterization on hurricane intensity and structure forecasts in HWRF, *Mon. Wea. Rev.*, **143**, 3136–3155.

Zhang, J. A., R. F. Rogers, and V. Tallapragada, 2017: Impact of parameterized boundary layer structure on tropical cyclone rapid intensification forecasts in HWRF. *Mon. Wea. Rev.*, doi:10.1175/MWR-D-16-0129.1.

### 9. Imaging Wind and Rain Airborne Profiler (IWRAP) [P-3]

IWRAP, which is also known as the Advanced Wind and Rain Airborne Profile (AWRAP), consists of two dual-polarized, dual-incidence angle radar profilers operating at Ku- and C-bands, and measures profiles of volume reflectivity and Doppler velocity of precipitation, as well as ocean surface backscatter. See the NESDIS OCEAN WINDS portion of the New Observing Systems (NOS) (Science Objective #3) objective in the Mature Stage Experiment for the goals of use of IWRAP for this year's HFP.

### 10. Wide Swath Radar Altimeter (WSRA) [P-3]

The WSRA (developed by ProSensing: <http://www.prosensing.com>) is an instrument that provides for measurements of sea surface topography and rain rate. The WSRA measures the sea surface topography by determining the range to the sea surface in 80 narrow beams spread over  $\pm 30^\circ$  in the cross-track direction (Walsh et al. 2014). Using measurements of sea surface topography and backscattered power, the WSRA offers real-time information on significant wave height, ocean directional wave spectra, the mean square slope of the ocean surface, and rain rate. The mean square slope (i.e., the sea surface small-scale roughness) responds to changes in wind speed, and can be determined by the variation of the radar-backscattered power with incidence angle. Data collected are transmitted to NHC for operational use.

#### *References*

Walsh, E. J., I. PopStefanija, S. Y. Matrosov, E. Uhlhorn, and B. Klotz, 2014: Airborne Rain-rate Measurement with a Wide-Swath Radar Altimeter. *J. Atmos. Oceanic Tech.*, **31**, 860–875.

### 11. Coyote UAS

The Coyote is an electric-powered unmanned aircraft with 1-hour endurance and is built by the Raytheon Company (formerly Sensintel Corporation and British Aerospace Engineering [BAE]). In many ways, this unmanned aerial system (UAS) platform can be considered a 'smart GPS dropsonde system' since it is deployed in similar fashion and currently utilizes a comparable meteorological payload similar to systems currently used on the G-IV and P-3 dropsonde systems. The Coyote can be launched from a P-3 sonobuoy tube in flight, and collects in-situ

**INSTRUMENT DESCRIPTIONS**

---

measurements of temperature, relative humidity, pressure, and remotely senses sea surface temperature. The three-dimensional wind field can be determined using the aircraft's GPS changes in position. Unlike the GPS dropsonde, however, the Coyote UAS can be directed from the P-3 to specific areas within the storm circulation (both in the horizontal and in the vertical). Furthermore, Coyote observations are continuous in nature and give scientists an extended look into important small-scale thermodynamic and kinematic physical processes that regularly occur within the near-surface boundary layer environment. The Coyote, when operated within a hurricane environment, provides a unique observation platform from which the low-level atmospheric boundary layer environment can be diagnosed in great detail.

TAIL DOPPLER RADAR (TDR) EXPERIMENT  
*Science Description*

---

**Investigator(s):** Paul Reasor, John Gamache (Co-PIs)

**Requirements:** Clear air and TCs at any stage

**Science Objectives:**

- 1) Gather airborne Tail Doppler Radar wind measurements that permit an accurate initialization of HWRF, and also provide three-dimensional wind analyses for forecasters [*IFEX Goals 1, 3*]

**Description of Science Objectives:**

**SCIENCE OBJECTIVE #1:** *Gather airborne Tail Doppler Radar wind measurements that permit an accurate initialization of HWRF, and also provide three-dimensional wind analyses for forecasters* [Tail Doppler Radar, TDR, Experiment]

**Motivation:** This experiment is a response to the requirement listed as Core Doppler Radar in Section 5.4.2.9 of the National Hurricane Operations Plan (NHOP). The goal of that particular mission is to gather airborne-Doppler wind measurements that permit an accurate initialization of the Hurricane Weather Research and Forecasting (HWRF) model, and also provide three-dimensional wind analyses for forecasters.

There are five main goals: 1) to provide a comprehensive data set for the initialization (including data assimilation) and validation of numerical hurricane simulations (in particular HWRF), 2) to improve understanding of the factors leading to TC intensity and structure changes by examining as much of the life cycle as possible, 3) to improve and evaluate technologies for observing TCs, 4) to develop rapid real-time communication of these observations to NCEP, and 5) to contribute to a growing tropical-cyclone database that permits the analysis of statistics of quantities within tropical cyclones of varying intensity.

**Background:** The real-time analysis of tail Doppler radar data was made possible by an automated quality control process (Gamache 2005) and variational wind synthesis method (Gamache 1997; Reasor et al. 2009).

**Hypotheses:**

1. Improving representation of a storm's inner core in the HWRF initial conditions through assimilation of P-3 and G-IV TDR data leads to reduced error in short-term structure and intensity forecasts.

TAIL DOPPLER RADAR (TDR) EXPERIMENT  
*Science Description*

---

**Aircraft Pattern/Module Descriptions:**

**P-3 Pattern #1: TDR**

**P-3 Pattern #2: TDR (Clear Air)**

NOAA will conduct a set of flights during several consecutive days, encompassing as much of a particular storm life cycle as possible. This would entail using P-3s on back-to-back flights on a 12-h schedule when the system is at depression, tropical storm, or hurricane strength.

The ultimate requirement for EMC is to obtain the three-dimensional wind field of Atlantic TCs from airborne Doppler data every 6 h to provide an initialization of HWRF through assimilation every 6 h. The maximum possible rotation of missions is two per day or every 12 h. A “poor man’s” version of the 6-h data collection is to collect data in the last half of one 6-h observing period, and in the first half of the next 6-h observing period.

At times when more than one system could be flown, one may take precedence over others depending on factors such as storm strength and location, operational tasking, and aircraft availability. All other things being equal, the target will be an organizing tropical depression or weak tropical storm, to increase the observations available in these systems. One scenario could likely occur that illustrates how the mission planning is determined: an incipient TC, at depression or weak tropical storm stage is within range of an operational base and is expected to develop and remain within range of operational bases for a period of several days. Here, the highest priority would be to start the set of flights, with single-P-3 missions, while the TC is below hurricane strength (preferably starting at depression stage), with continued single-P-3 missions at 12-h intervals until the system is out of range or makes landfall. During the tropical depression or tropical-storm portion of the vortex lifetime, higher azimuthal resolution of the wind field is preferred over radial extent of observations, while in the hurricane portion, the flight plan would be designed to get wavenumber-0 and -1 coverage of the hurricane out to the largest radius possible, rather than the highest temporal resolution of the eyewall. In all cases adequate spatial coverage is preferred over increased temporal resolution during one sortie.

The highest vertical resolution is needed in the boundary and outflow layers. This is assumed to be where the most vertical resolution is needed in observations to verify the initialization and model. For this reason it is desirable that *if sufficient dropwindsondes are available*, they should be deployed in the radial penetrations to verify that the boundary layer and surface wind forecasts produced by HWRF resemble those in observations. These observations will also supplement airborne Doppler observations, particularly in sectors of the storm without sufficient precipitation for radar reflectivity. *If sufficient dropwindsondes are not available*, a combination of SFMR and airborne Doppler data will be used for verification.



TAIL DOPPLER RADAR (TDR) EXPERIMENT  
*Science Description*

---

**G-IV Pattern #1: TDR**

**G-IV Pattern #2: TDR (Clear Air)**

The ultimate requirement for EMC is to obtain the three-dimensional wind field of Atlantic TCs from airborne Doppler data every 6 h to provide an initialization of HWRF through assimilation every 6 h. The maximum possible rotation of missions is two per day or every 12 h. The TDR on the G-IV will be considered operational; therefore velocity data will be transmitted in real-time to EMC. We recommend storm overflight whenever possible during synoptic surveillance missions. The most effective pattern, fulfilling the needs for inner-core assimilation and the current operational requirement for synoptic measurement, will be refined through experiments using the Hurricane Ensemble Data Assimilation System (HEDAS) and consultation with NHC and EMC.

Beyond operationally-tasked G-IV missions, among some specific scenarios in which this experiment would be carried out are as follows: 1) at the conclusion of NHC tasking for a landfalling TC, likely coordinated with the P-3 aircraft; 2) prior to NHC tasking for a TC of interest to EMC (priority is coordination with P-3 aircraft); 3) a recurving TC (priority is coordination with P-3 aircraft). Since coordination with the P-3 aircraft is an early requirement, this experiment would have to be weighed against other experiments, which stagger the P-3 and G-IV flight times. This initial coordination is necessary for 1) comparing and synthesizing storm structure derived from the two radar platforms and 2) the most thorough testing of HEDAS with this new data source. Subsequent flights may relax this requirement for P-3 coordination as the quality of the G-IV data is established and G-IV overflight of systems becomes more routine.

**Analysis Strategy:** The emphasis here is on "real-time" products. Quality-controlled, thinned Doppler radials are output, packaged and transmitted to NCEP Central Operations (NCO) for assimilation into the operational HWRF model. Similarly, Doppler radial superobs are transmitted for use by research groups. Three-dimensional and vertical profile analyses of wind and reflectivity are also produced. Plan-view images derived from the analyses are transmitted to a location where NHC hurricane specialists can view them. Additional products include composite analysis images with dropwindsonde winds overlaid and, most recently, wind and reflectivity structure images for real-time mission planning and viewing by NHC specialists.

**References:**

Gamache, J. F., 1997: Evaluation of a fully three-dimensional variational Doppler analysis technique. Preprints, *28th Conf. on Radar Meteorology*, Austin, TX, Amer. Meteor. Soc., 422–423.

## 2018 NOAA/AOML/HRD Hurricane Field Program - IFEX

### TAIL DOPPLER RADAR (TDR) EXPERIMENT

#### *Science Description*

---

Gamache, J. F., 2005: Real-time dissemination of hurricane wind fields determined from airborne Doppler radar data. National Hurricane Center, 38 pp. [Available online at [http://www.nhc.noaa.gov/jht/2003-2005reports/DOPLRgamache\\_JHTfinalreport.pdf](http://www.nhc.noaa.gov/jht/2003-2005reports/DOPLRgamache_JHTfinalreport.pdf).]

Reasor, P. D., M. Eastin, and J. F. Gamache, 2009: Rapidly intensifying Hurricane Guillermo (1997). Part I: Low-wavenumber structure and evolution. *Mon. Wea. Rev.*, **137**, 603–631.

**SFMR EXPERIMENT**  
*Science Description*

---

**Investigator(s):** Heather Holbach (PI, FSU/NGI, AOML/HRD) and Mark Bourassa (FSU)

**Requirements:** *High-Incidence Angle:* wind speeds  $\geq 15 \text{ m s}^{-1}$ ; *G-IV SFMR:* TS or Hurricane

**Science Objectives:**

- 1) Collect high-incidence angle (off-nadir) SFMR data in regions with different wind speeds ( $\geq 15 \text{ m s}^{-1}$ ), rain rates, storm relative quadrants, and radii from the storm center [*IFEX Goal 2*]
- 2) Sample the wind speed and rain rate from the G-IV SFMR in coordination with the P-3 SFMR [*IFEX Goal 2*]

**Description of Science Objectives:**

**SCIENCE OBJECTIVE #1:** *Collect high-incidence angle (off-nadir) SFMR data in regions with different wind speeds ( $\geq 15 \text{ m s}^{-1}$ ), rain rates, storm relative quadrants, and radii from the storm center* [SFMR High Incidence Angle Measurements, HiSFMR]

**Motivation:** Surface winds in a tropical cyclone are essential for determining its intensity. Currently, the Stepped-Frequency Microwave Radiometer (SFMR) is used for obtaining surface wind measurements at nadir. Due to poor knowledge about sea surface microwave emission at large incidence angles and high wind speeds, SFMR winds are only retrieved when the antenna is pointed directly downward from the aircraft during level flight. Understanding the relationship between the SFMR measured brightness temperatures, surface wind speed, wind direction, and the ocean surface wave field at off-nadir incidence angles would potentially allow for the retrieval of wind speed measurements when the aircraft is not flying level. It is hypothesized that at off-nadir incidence angles the distribution of foam on the ocean surface from breaking waves impacts the SFMR measurements differently than at nadir and is dependent on polarization. Therefore, by analyzing the excess brightness temperature at various wind speeds and locations within the tropical cyclone environment at various off-nadir incidence angles, the relationship between the ocean surface characteristics and the SFMR measurements will be quantified as a function of wind direction relative to the SFMR look angle and polarization.

**Background:** Currently, if the aircraft pitch or roll angle exceeds a threshold of  $\pm 5^\circ$ , wind speeds are not reported for the SFMR. These thresholds result in wind speeds not being provided when the aircraft turns or if the aircraft exceeds the pitch threshold while flying a constant pressure surface through the eyewall where the highest wind speeds are usually measured. By improving our understanding of the physics of the air-sea interaction between the wind and sea surface in the extreme environment of tropical cyclones, it will be possible to develop corrections for the SFMR algorithm to obtain wind speed measurements when the aircraft is not flying level.

**SFMR EXPERIMENT**  
*Science Description*

---

**Hypothesis:** Collecting high-incidence angle SFMR data will allow for quantification of the changes in the SFMR brightness temperature at off-nadir incidence angles that are related to the wind direction relative to the SFMR look angle and polarization.

**Aircraft Pattern/Module Descriptions:**

**P-3 Module #1: HiSFMR**

Two down-looking SFMRs should be mounted on the P-3 aircraft. The operational wing-pod mounted SFMR should be operating as usual. A second SFMR is to be mounted parallel to the latitudinal axis of the airframe (rotated 90° from the operational position).

When the aircraft rolls, the operational SFMR will be collecting off-nadir data at H-pol and the second SFMR will be collecting off-nadir data at V-pol, simulating the data that the SFMR would collect when the aircraft pitches. The high-incidence angle modules can be flown during any mission with any flight pattern and are designed to obtain SFMR measurements in various locations of the tropical cyclone environment at several different wind speeds during constant banked aircraft turns at several different roll angles, specified below. A full pattern for each module consists of three complete circles for each specified roll angle (Figure SF-1). It is important to maintain as constant of a roll angle, pitch angle, and altitude as possible. A dropsonde and AXBT pair should be released at the beginning of the pattern. The wide swath radar altimeter (WSRA), if available, should also be obtaining measurements during the pattern for analysis of the ocean surface characteristics. The wave spectra obtained by the WSRA will allow for a more accurate investigation of the sensitivity of the SFMR to the surface wave characteristics. It is ideal to fly these modules in rain-free areas as to reduce the impact of the atmospheric emission on the SFMR measurements and to obtain measurements in regions of moderate to heavy precipitation, as deemed safe by the aircraft pilots, in order to understand the impact of varying the path length of the precipitation.

**SFMR EXPERIMENT**  
*Science Description*

---

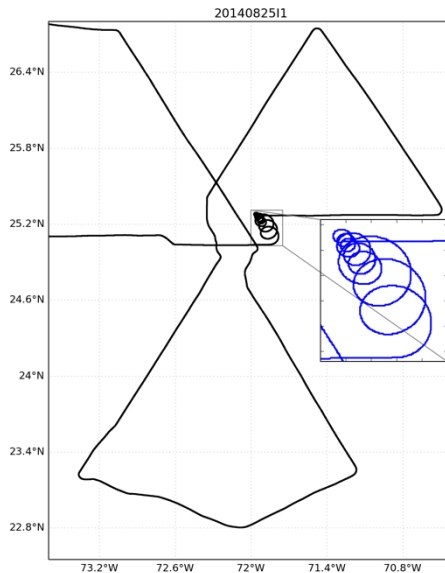


**Figure SF-1:** Example flight path (black) with SFMR high-incidence angle module. The inset zoomed in portion with the blue track displays the SFMR module in more detail.

Module Options:

1. Zero wind, high incidence angle response
  - This module is designed to determine the antenna pattern corrections and possible impacts of sun glint
  - Fly circles at roll angles of 15, 30, 45, and 60 degrees
2. Moderate wind response ( $\sim 15 \text{ m s}^{-1}$ , 30 kts)
  - This module is designed to understand the mixed “phase” (i.e., foam vs roughness contributions to brightness temperature)
  - Fly circles at roll angles of 15, 30, and 45 degrees
3. Moderate winds ( $\sim 15 \text{ m s}^{-1}$ , 30 kts) and substantial swell or varying fetch length response
  - This module is designed to determine the sensitivity to stress
  - This can be performed on the way to the storm or in different sectors of the storm
  - Fly circles at roll angles of 15, 30, and 45 degrees
4. Strong wind response ( $>30 \text{ m s}^{-1}$ , 60 kts)
  - This module should be flown in multiple storm quadrants (motion relative)
  - Fly circles at roll angles of 15, 30, and 45 degrees

**SFMR EXPERIMENT**  
*Science Description*

Thus far, measurements have been obtained in all storm-relative quadrants except for the rear left quadrant (Figure SF-2). To develop a more complete composite picture, *we are particularly interested in obtaining measurements in the rear left quadrant* of storms (motion relative) this season. We would also like to focus on regions with wind speeds greater than  $20 \text{ m s}^{-1}$  and regions of stratiform precipitation.

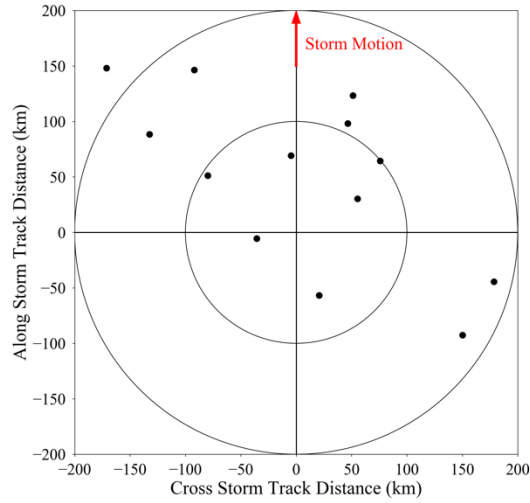


**Figure SF-2:** Storm-relative locations of high-incidence angle SFMR observations obtained in previous seasons.

**Analysis Strategy:** The SFMR data from these flights will be analyzed to quantify the double harmonic oscillation that is evident in high-incidence angle SFMR data collected during previous seasons. The WSRA data will then be used to analyze the differences in the ocean surface characteristics to reveal any possible relationships between the double harmonic oscillation found in the SFMR measurements and the ocean surface characteristics. The surface wind direction from the dropsondes will be used to compute the relative look angle of the SFMR to the surface wind direction. Wind speed from the dropsondes will be used to quantify the differences in the SFMR brightness temperatures expected at nadir with the high-incidence angle measurements. SST from the AXBTs will be used as input to the brightness temperature algorithm.

**SFMR EXPERIMENT**  
*Science Description*

---

**SCIENCE OBJECTIVE #2:** *Sample the wind speed and rain rate from the G-IV SFMR in coordination with the P-3 SFMR [G-IV SFMR Validation]*

**Motivation:** The SFMR on the P-3 has a proven track record for providing surface wind data in tropical cyclones (Uhlhorn et al. 2007, Klotz and Uhlhorn 2014). However, there is no documentation of the G-IV SFMR data and its usefulness under the current specifications of the G-IV flight patterns. To our knowledge no data from the G-IV SFMR has been released or used in any research or operational capacity. This data could potentially provide important information about the tropical cyclone wind radii as well as for mapping the environmental surface winds. The goal of this module is to validate the G-IV SFMR data with reliable, coincident P-3 SFMR data in the full spectrum of wind speeds and rain rates.

**Background:** Historically, the SFMR has primarily served as a research instrument that measured surface wind speeds and rain rates in hurricanes. As early as 1980, data were collected to estimate surface wind speeds from the breaking waves on the sea surface, but they were used in a limited capacity due to various errors. Beginning in 1998–1999, SFMR data were regularly collected on the P-3 aircraft with reasonable estimates of wind speeds, but an algorithm upgrade in the mid-2000s significantly improved the data. The SFMR still struggled at the low wind regime and within rainy conditions, which prompted a second algorithm update that became operational in 2015.

An SFMR was also installed on the G-IV, but it has several additional factors with which to contend. Because of the aircraft altitude, the footprint size is ~4–5 times larger than the SFMR on the P-3. The SFMR on the P-3 was designed to only interpret rain below the melting level because the P-3 normally operates at those altitudes. The G-IV must not only interpret rain, but also ice particles in the column between the flight-level and melting level. The combined factors call into question the G-IV SFMR ability to produce reasonable wind speeds (and rain rates) along the flight track.

A third SFMR (upward looking) was installed on the P-3 (NOAA42) to take measurements of the air column above the aircraft. This data has not been used in any research or operational capacity either, but could prove very useful for this module. Figure SF-3 provides a schematic of the footprint size and coverage for the three SFMR instruments based on standard flight altitudes of 42,000 ft and 10,000 ft for the G-IV and P-3, respectively. Note that this schematic is not to scale.

**SFMR EXPERIMENT**  
*Science Description*

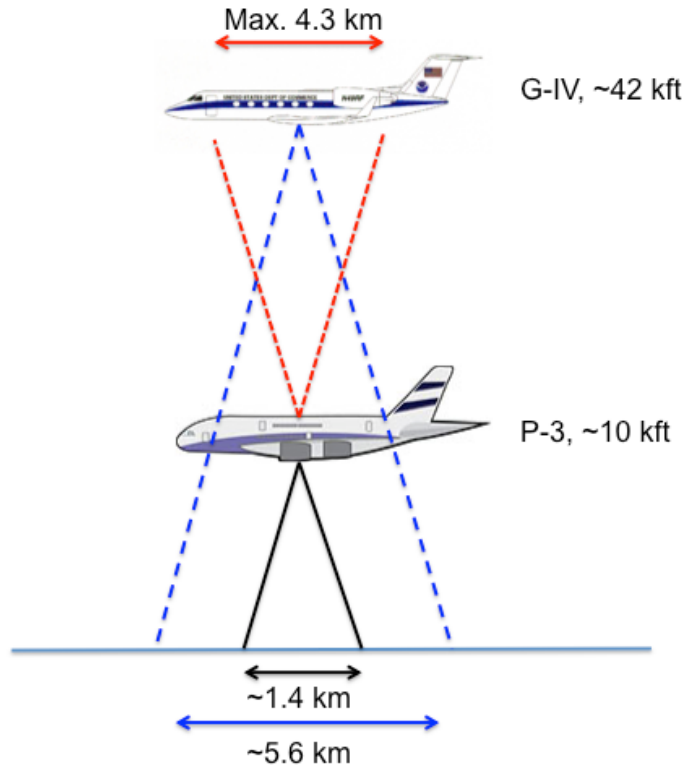


**Figure SF-3.** A schematic figure of the footprint coverage for the various SFMR instruments is provided. Also indicated are the normal operating altitudes of each aircraft. This schematic is not to scale.

**Hypothesis:** Comparison with P-3 SFMR data will necessitate modifications to the G-IV SFMR processing and/or algorithm to account for the additional impacts on the received signal. It is expected that if the G-IV uses the P-3 processing algorithm, there will be noticeable deficiencies in the returned values.

**Aircraft Pattern/Module Descriptions:**

**P-3 Module #1: G-IV SFMR Validation**

**G-IV Module #1: G-IV SFMR Validation**

The premise behind this module is fairly simple: coordinate small sections of overlapping flight tracks between the G-IV and P-3. It is expected that this module should fit into a larger experiment so as not to interrupt the overall goals of said mission. Because the G-IV and P-3 often fly very different patterns, the best way to have the aircraft overlap is using the circumnavigation pattern. This flight option would coordinate along the inner circumnavigation (G-IV), targeting an area that is experiencing intermittent but occasionally moderate to heavy rain. This flight strategy allows for comparison of similar strength wind speeds



**SFMR EXPERIMENT**  
*Science Description*

(consistent radius) with a large variety of rain rates. If the G-IV can fly a radial pass in conjunction with the P-3 (maybe possible for a tropical storm), this would allow evaluation over a variety of wind speeds and rain rates. A third option would be to complete this module on a downwind leg of a P-3 TDR mission.

The two aircraft operate at different air speeds (~325 kt for the P-3 and ~440 kt for the G-IV), which limits the amount of time the aircraft will have reasonable coverage over the same portion of the ocean surface. Therefore, this module needs to be operated from the perspective of a preselected meeting point or midpoint of the pattern, which ensures both SFMR are observing the same portion of the ocean. The aircraft should be flying along the same heading during this coordinated overlap. For about 3–4 minutes prior to and after this midpoint, the two SFMR will have varying overlap in their footprints with the least overlap at the beginning and end of the module. A reasonable estimate of the duration of this module is ~8 minutes. Figure SF-4 is a schematic of the footprint coverage as a function time within the module centered on the preselected midpoint. As confirmation of the wind speeds observed at the midpoint, a dropsonde should be launched from the P-3.

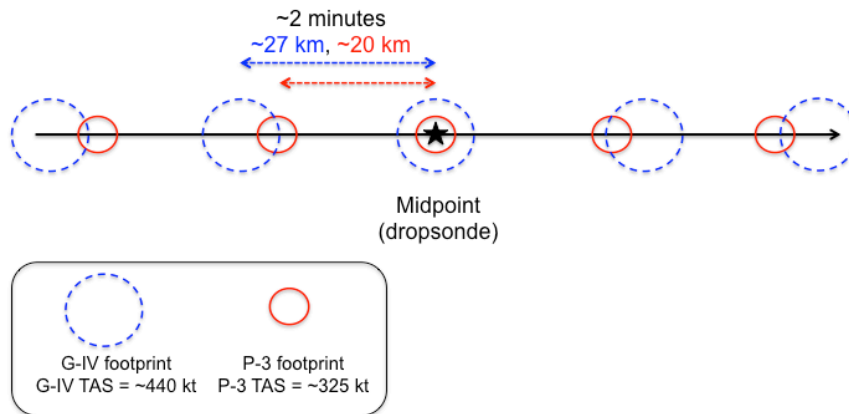


**Figure SF-4.** A schematic diagram of the flight path of the G-IV and P-3 aircraft during the module is provided. The red and blue circles indicate the P-3 and G-IV SFMR footprint size, respectively. The timing between successive locations in the figure is ~2 minutes with the distance covered by each aircraft noted. This figure is not to scale as the footprint size is emphasized for visibility.

**Analysis Strategy:** Data that are collected during this module will first be post-processed and quality-controlled. The two downward looking SFMR will be compared and statistically evaluated depending on the overlapping footprint coverage and distance from the midpoint. From this perspective, differences can be determined based on coverage, wind speed, and rain rate. A surface-adjusted wind speed from the dropsonde will serve as the truth to validate both SFMR. A determination of the additional impacts of the air

**SFMR EXPERIMENT**  
*Science Description*

---

column above the P-3 on the G-IV SFMR results could prompt further investigation into changes for the G-IV processing or algorithm. Comparison of the upward looking P-3 SFMR will serve as an independent measure of the above aircraft air column and will help confirm any impacts the G-IV SFMR encounters.

**References:**

Klotz, B. W., and E. W. Uhlhorn, 2014: Improved Stepped Frequency Microwave Radiometer tropical cyclone surface winds in heavy precipitation. *J. Atmos. Oceanic Technol.*, 31, 2392–2408.

Uhlhorn, E. W., P. G. Black, J. L. Franklin, M. Goodberlet, J. Carswell, and A. S. Goldstein, 2007: Hurricane Surface Wind Measurements from an Operational Stepped Frequency Microwave Radiometer. *Mon. Wea. Rev.*, 135, 3070–

GENESIS STAGE EXPERIMENT  
*Science Description*

---

**Investigator(s):** Ghassan Alaka, Jon Zawislak (Co-PIs), Paul Reasor, Jason Dunion, Alan Brammer (SUNY Albany), Chris Thorncroft (SUNY Albany), Mark Boothe (Naval Postgraduate School, NPS), Michael Montgomery (NPS), Tim Dunkerton (Northwest Research Associates, NWRA), Blake Rutherford (NWRA) (Co-Is)

**Requirements:** Pre-genesis disturbances (pre-TDs), including NHC-designated “Invests”

**Science Objectives:**

The overarching objective is to investigate if a pre-genesis disturbance has matured into a TC, including the organization of convection and the development of a closed low-level circulation.

- 1) To investigate the precipitation modes that are prevalent during the genesis stage and the response of the vortex to that precipitation organization [*IFEX Goal 3*]
- 2) To investigate the importance of the pouch, including the shear sheath, which tends to indicate a tropical storm, and its relationship to a low-level circulation and organized deep convection within the pouch [*IFEX Goal 3*]
- 3) To investigate the favorability in both dynamics (e.g., vertical wind shear) and thermodynamics (e.g., moisture) for tropical cyclogenesis in the environment near a pre-TD, especially the downstream environment [*IFEX Goal 3*]

**Description of Science Objectives:**

**SCIENCE OBJECTIVE #1:** *To investigate the precipitation modes that are prevalent during the genesis stage and the response of the vortex to that precipitation organization*  
[Precipitation Mode, PMODE]

**Motivation:** One of the fundamental requirements to achieve a more accurate prediction, and understanding, of tropical cyclogenesis events is an improved knowledge of the precipitation organization and the developing vortex response, in the context of environmental forcing, during the formation process.

While true that the favorable environmental conditions for tropical cyclogenesis have been well accepted for decades, those conditions also frequently exist in nondeveloping disturbances. An understanding of the sequence of events, and thus more informed prediction, of tropical cyclogenesis is still very much constrained by our inability to describe the relative contributions of precipitation organization (e.g., deep convection vs. stratiform rain), in the context of the environmental properties, to the evolution of the developing incipient vortex. Numerical models are a convenient platform to study tropical cyclogenesis events, and are often able to reproduce them, but the processes — particularly the relative roles of various precipitation modes involved — that contribute to genesis have generally been unobserved. Satellites are a convenient tool for identifying

GENESIS STAGE EXPERIMENT  
*Science Description*

---

precipitation properties, particularly with the availability of the Dual-frequency Precipitation Radar (DPR) on the core satellite of the Global Precipitation Measuring Mission (GPM) and multiple higher resolution passive microwave sensors (AMSR2, GMI, SSMIS), but the vortex itself is not well observed; thus the co-evolution of precipitation and vortex cannot be described using satellites alone. Dedicated aircraft missions (outside of the GRIP-PREDICT-IFEX, tri-agency field program effort in 2010) have historically been too few.

**Background:** Results from previous observational case studies suggest that convergence (spin-up) is initially maximized in the midtroposphere, and as genesis nears the troposphere moistens (humidity increases to saturation) and stabilizes (warming at upper levels and cooling near the surface) (Raymond and Sessions 2007; Davis and Ahijevych 2012; Komaromi 2013; Zawislak and Zipser 2014a). The stabilization apparently coincides with a lowering of the peak in the vertical mass flux profile, and thus a more bottom-heavy mass flux profile whereby convergence and spin-up is maximized at low levels (Raymond and López Carillo 2011; Raymond et al. 2011). Upper-level warming, either through compensating subsidence from deep convection or latent heating, also favors surface pressure falls and enhanced low-level convergence (Zhang and Zhu 2012), which is required to overcome surface divergence that would otherwise persist from mesoscale downdrafts (Komaromi 2013). Research using observations from developing cases (Karl, Matthew, and Fiona) and nondeveloping cases (ex-Gaston, PREDICT/GRIP/IFEX -27, -30) in 2010 (Davis and Ahijevych 2013; Zawislak and Zipser 2014b), suggest that (at least initially) contributions from the larger, more persistent stratiform raining areas could initially be more influential during the genesis stage, particularly since the Rossby radius of deformation is large. Once the troposphere stabilizes and the Rossby radius is reduced, the role of deep convection becomes more influential. Another pathway to genesis has emerged from modeling studies (e.g., Montgomery et al. 2010; Wang et al. 2010a; Wang 2012), and suggest a greater influence from intense deep convection throughout the genesis process.

Using Tropical Rainfall Measuring Mission (TRMM) Precipitation Radar (PR) data, Fritz et al. (2016) identified the evolution of various precipitation modes (i.e., shallow, mid-level, and deep convection, as well as stratiform rain) during the genesis stage. Their conclusion was that multiple precipitation modes are responsible for tropical cyclogenesis. Although stratiform rain accounted for 80% of the raining area, convective precipitation made a nearly equal contribution to overall rainfall, given the larger rain rate. While they did not discount the important role of deep convection, they highlighted the potentially larger and unique role of mid-level convection, which was to moisten the lower to middle troposphere and spin up the surface circulation.

The goal of this objective is, thus, to obtain observations on the distributions of various precipitation modes and the environmental characteristics that govern those modes. Then, through a sequence of missions, measure the time evolution of those modes and the vortex kinematic and thermodynamic responses.

GENESIS STAGE EXPERIMENT  
*Science Description*

---

**Hypotheses:**

1. A low-level center can develop rapidly as a result of deep convective bursts in a region of anomalously high vorticity.
2. Mid-tropospheric moistening through stratiform and/or moderately deep convection precipitation enhances the mid-tropospheric circulation, reduces downdrafts through saturation, and favors lower-tropospheric convergence prior to tropical cyclogenesis.
3. Persistent latent heating in the middle-to-upper troposphere focuses convergence in the lower troposphere.
4. The presence of a mid-level circulation, either pre-existing (e.g., African easterly waves, upper-level lows) or developed in situ in response to convection, is a necessary condition for a TC to develop.

**Aircraft Pattern/Module Descriptions:**

**P-3 Pattern #1: PMODE**

This pattern ideally uses a repeated, standard (repeated) single Figure-4 or a standard Rotated Figure-4 pattern to maximize coverage of the pre-TC disturbance and convective features of interest. The pattern should be centered on either: a) the convective burst center (or in close proximity to it) for larger, more organized mesoscale convective systems (MCSs) or b) the estimated mid-level circulation center, which can be determined from a model analysis or satellite imagery. The pattern should translate with the phase speed of disturbance (circulation) center, as determined by satellite or model analysis. This pattern is ideally flown with a coinciding G-IV mission in the environment (consistent with other Genesis Stage objectives and their flight patterns).

**G-IV Pattern #1: PMODE**

*P-3 Pattern #1: PMODE* may be adapted for the G-IV, while ensuring hazard avoidance around the convective areas. The G-IV mission will only be necessary if the P-3 is unavailable, and is not otherwise chosen to fly other objectives in the Genesis Stage Experiment.

**Analysis Strategy:** Three-dimensional analyses of wind and reflectivity from the TDR will facilitate an analysis of the precipitation structure (i.e., mode) within precipitation areas of the disturbance, and the identification of low- and mid-tropospheric circulation centers. If possible, repeated sampling of a convective burst area over multiple missions (every 12 h) will allow us to identify the relationship between low- and mid-level circulations and the precipitation mode evolution (e.g., stratiform v. deep, moderately-deep, and shallow convective fractions). Dropsonde observations (ideally from both the G-IV and P-3) provide key measures of the thermodynamic (e.g., moisture, relative humidity) properties in, and around, the burst and mid-level circulation centers. They will

GENESIS STAGE EXPERIMENT  
*Science Description*

---

allow us to identify if (when) the low and middle troposphere become nearly saturated, the timing and vertical location of the formation of the warm anomaly, and whether there is a relationship with the observed precipitation evolution.

**References:**

- Davis, C. A., and D. A. Ahijevych, 2012: Mesoscale structural evolution of three tropical weather systems observed during PREDICT. *J. Atmos. Sci.*, **69**, 1284–1305.
- Fritz, C., Z. Wang, S. W. Nesbitt, and T. J. Dunkerton, 2016: Vertical structure and contribution of different types of precipitation during Atlantic tropical cyclone formation as revealed by TRMM PR. *Geophys. Res. Lett.*, **43**, 894–901, L067122.
- Komaromi, W. A., 2013: An investigation of composite dropsonde profiles for developing and nondeveloping tropical waves during the 2010 PREDICT field campaign. *J. Atmos. Sci.*, **70**, 542–558.
- Montgomery, M. T., Z. Wang, and T. J. Dunkerton, 2010: Coarse, intermediate, and high resolution numerical simulations of the transition of a tropical wave critical layer to a tropical storm. *Atmos. Chem. Phys.*, **10**, 10803–10827.
- Raymond, D. J., and S. L. Sessions, 2007: Evolution of convection during tropical cyclogenesis. *Geophys. Res. Lett.*, **34**, L06811, 5 pp.
- \_\_\_\_\_, and C. López Carrillo, 2011: The vorticity budget of developing Typhoon Nuri (2008). *Atmos. Chem. Phys.*, **11**, 147–163.
- \_\_\_\_\_, S. L. Sessions, and C. López Carrillo, 2011: Thermodynamics of tropical cyclogenesis in the northwest Pacific. *J. of Geophys. Res.*, **116**, D18101, 18 pp.
- Wang, Z., M. T. Montgomery, and T. J. Dunkerton, 2010a: Genesis of pre-Hurricane Felix (2007). Part I: The role of the easterly wave critical layer. *J. Atmos. Sci.*, **67**, 1711–1729.
- \_\_\_\_\_, 2012: Thermodynamic aspects of tropical cyclone formation. *J. Atmos. Sci.*, **69**, 2433–2451.
- Zawislak, J., and E. J. Zipser, 2014a: Analysis of the thermodynamic properties of developing and nondeveloping tropical disturbances using a comprehensive dropsonde dataset. *Mon. Wea. Rev.*, **142**, 1250–1264.
- \_\_\_\_\_, \_\_\_\_\_, 2014b: A multisatellite investigation of the convective properties of developing and nondeveloping tropical disturbances. *Mon. Wea. Rev.*, **142**, 4624–4645.
- Zhang, D.-L., and L. Zhu, 2012: Roles of upper-level processes in tropical cyclogenesis. *Geophys. Res. Lett.*, **39**, L17804, doi:10.1029/2012GL053140.

GENESIS STAGE EXPERIMENT  
*Science Description*

---

**SCIENCE OBJECTIVE #2:** *To investigate the importance of the pouch, including the shear sheath, which tends to indicate a tropical storm, and its relationship to a low-level circulation and organized deep convection within the pouch [Pouch]*

**Motivation:** A longstanding challenge for hurricane forecasters, theoreticians, and numerical weather forecast systems is to distinguish tropical waves that will develop into hurricanes from tropical waves that will not develop. The Naval Postgraduate School (NPS) Montgomery Research Group (MRG) has been tracking pouches in the Atlantic since 2008 in numerical models. Airborne observations provide much-needed data for analysis of processes critical for TC genesis, as well as an opportunity to compare our much-used numerical models with reality.

**Background:** The scientific basis for the methodology is given in Dunkerton et al. (2009), which describes how to view genesis in the semi-Lagrangian frame co-moving with a parent wave. Recent years have seen several field campaigns aimed at understanding the science of tropical cyclogenesis and new lessons have emerged from these experiments, as summarized by Montgomery et al. (2012), Smith and Montgomery (2012), Wang (2012) and Rutherford and Montgomery (2012). Subsequent work by Rutherford et al. (2015) defined a new key tool, called the Lagrangian Okubo-weiss OW ( $OW_{Lag}$ ) parameter, that shows frame-independent saddles and flow boundaries, along with solid-body vortex cores in a single scalar field. In Rutherford et al. (2017) these principles were applied to six years of ECMWF forecasts to determine objective values for the  $OW_{Lag}$  parameter indicative of TC genesis. Another noteworthy finding from the latter work was the existence of a “shear sheath” of negative  $OW_{Lag}$  at 700 hPa that develops as a protective ring around a pouch at the onset of tropical storm intensity. The new Lagrangian characterization tested extensively during 2017 allows many pouch products to be automated and objectively defined in order to produce more accurate forecast evaluations. These evaluations should provide reliable, consistent targets for research flight operations. The “pouch” is defined as a proto-vortex cyclonic eddy associated with a parent wave’s critical latitude in the lower troposphere that is protected to some degree from lateral intrusion of dry air and impinging vertical wind shear.

**Hypotheses:**

1. The pouch contains a favorable region of cyclonic rotation and weak straining/shearing deformation in which synoptic waves and mesoscale vorticity anomalies, moving westward together, amplify and aggregate on a nearly zero relative mean flow in the lower troposphere.
2. The pouch provides a set of quasi-closed material contours inside of which air is repeatedly moistened by convection.
3. The parent wave is maintained and possibly enhanced by diabatically amplified eddies within the wave (proto-vortices on the mesoscale), a process favored in regions of small intrinsic phase speed.

GENESIS STAGE EXPERIMENT

*Science Description*

---

4. The time at which the protective boundary transforms from one that is determined by the pouch's wave to that of the shear sheath indicates a system that can be self-sustaining without the parent wave (this change can be seen as the Lagrangian manifolds transition from a cat's eye pattern to a circular shear sheath visible in the Lagrangian OW field).

**Aircraft Pattern/Module Descriptions:** Advanced staging in Barbados would most likely be required for pouches tracking westward in the Atlantic main development region (MDR), but flights from Lakeland may be possible for tropical transition cases east of Florida. Patterns discussed below would be centered on the consensus forecast pouch center location based upon all available numerical models used in the pouch-tracking routine.

**P-3 Pattern #1: Pouch**

A lawnmower pattern would be appropriate for an initial flight into a wave-pouch exhibiting scattered convective activity without much organized convective activity near the pouch sweet spot. *The P-3 would need to fly at roughly 20,000 ft.* The proposed pattern is similar to the standard Lawnmower pattern with a few modifications. First, if possible, extend the zonal legs an additional degree longitude. Second, double the number of drops per zonal leg. After extending the legs and adding more drops, each zonal leg would have six drops, for a total of 24 drops in the lawnmower portion of the pattern. Finally, include dropsondes at the same resolution ( $\sim 1^\circ$  latitude/longitude) for three degrees on both the inbound and outbound legs in order to capture a cross-section of the outer boundary of the pouch, resulting in a total of 30 drops.

**P-3 Pattern #2: Pouch**

Observations from the first lawnmower flight, accurate positioning of the pouch center, and indications of some recurrent convective activity near the sweet spot location would allow subsequent flights to utilize the standard square-spiral. Many follow-on flights, with as little temporal gap as possible within operational constraints would be ideal (ideally, once-a-day sampling at approximately the same UTC is optimal). Again, *the P-3 would need to fly relatively high, around 20,000 ft.* Increasing the drop resolution to about  $1^\circ$  latitude/longitude would double the number of drops to 26 in the square, and including three additional drops in each of the inbound/outbound leg would total 32 drops. The sequential combination of the lawnmower and square-spiral patterns, with the suggested number of dropsondes, proved invaluable during the 2010 PREDICT field experiment. These observations proved adequate for sampling the meso-alpha and meso-beta scale flow kinematics and thermodynamics of the targeted wave pouch.



GENESIS STAGE EXPERIMENT  
*Science Description*

---

**G-IV Pattern #1: Pouch**

As with the P-3 lawnmower pattern, a lawnmower pattern would be appropriate for an initial flight into a pouch with scattered convective activity. The G-IV would fly at typical operating altitudes. The proposed pattern is similar to the standard Lawnmower pattern with a couple of modifications. First, if possible, extend the zonal legs an additional degree longitude. Second, double the number of drops per zonal leg. After extending the legs and adding more drops, each zonal leg would have six drops, for a total of 24 drops. Adding three drops to each inbound/outbound leg would result in 30 total drops.

**G-IV Pattern #2: Pouch**

Using observations from the first lawnmower flight, accurate positioning of the pouch center would allow subsequent flights to utilize the standard square-spiral pattern. As many follow-on flights, with as little temporal gap as possible within operational constraints would be ideal. Again, the G-IV would fly at the typical operating altitudes. Increasing the drop resolution to about 1° latitude/longitude would double the number of drops to 26 in the square. Including three additional drops in each of the inbound/outbound leg would total 32 drops.

**Analysis Strategy:** Kinematics of the developing pouches will be revealed by circulation calculations using the wind data from the dropsondes around circuits in the resulting drop pattern. Analyses of observed wind and thermodynamic dropsonde data will provide information about how the protective shear sheath serves as a barrier to lateral mixing. Thermodynamic information from the drops can be partitioned by location and assigned to pouch center, shear sheath, or environment. An example of such analysis is given here in Fig. GN-1 for Cristobal (2014) using model analysis, along with actual research flight data. The results highlight the relatively moist central core, dry outer environment, and details in the profiles of the shear sheath and partial pouch regions, such as relatively moist lower and upper levels but drier midlevels. Fig. GN-1 shows that the core, shear sheath, and environment have different moisture values. The foregoing sampling strategies will help ensure that we are able to capture each of these important regions.

**References:**

- Dunkerton, T. J., M. T. Montgomery and Z. Wang, 2009: Tropical cyclogenesis in a tropical wave critical layer: Easterly waves, *Atmos. Chem. & Phys.*, **9**, 5587–5646.
- Montgomery, et al., 2012: The Pre-Depression Investigation of Cloud Systems in the Tropics (PREDICT) Experiment: Scientific Basis, New Analysis Tools and Some First Results. *Bulletin of the American Meteorological Society*, **93**: 153–172.

**GENESIS STAGE EXPERIMENT**  
*Science Description*

- Rutherford, B. and M. T. Montgomery, 2012: A Lagrangian analysis of a developing and non-developing disturbance observed during the PREDICT experiment. *Atmos. Chem. Phys.*, **12**, 11355–11381.
- Rutherford, B., T. J. Dunkerton and M. T. Montgomery, 2015: Lagrangian vortices in developing tropical disturbances. *Quart. J. Roy. Meteor. Soc.*, **141**, 3344–3354.
- Rutherford, B., M. A. Boothe, T. D. Dunkerton and M. T. Montgomery, 2017. Dynamical properties of developing disturbances using Lagrangian flow topology. *Quart. J. Roy. Meteor. Soc.* DOI:10.1002/qj.3196.
- Smith, R. K. and M. T. Montgomery, 2012: Observations of the convective environment in developing and non-developing tropical disturbances. *Quart. J. Roy. Meteor. Soc.*, **138**, 1721–1739.
- Wang, Z, M. T. Montgomery and C. Fritz, 2012: A first look at the structure of the wave pouch during the 2009 PREDICT-GRIP dry runs over the Atlantic. *Mon. Wea. Rev.*, **140**, 1144–1163.

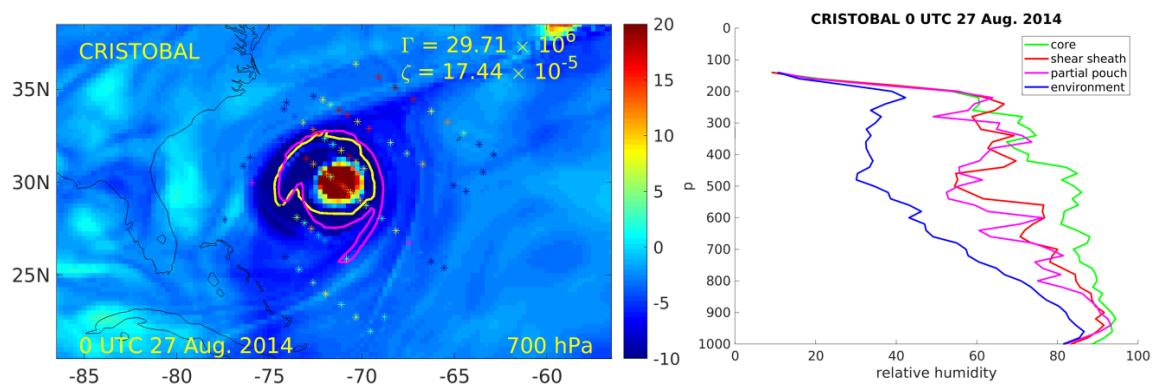


**Figure GN-1.** (Left) GFS 700-hPa  $OW_{Lag}$  field for Hurricane Cristobal at 0000 UTC 27 August 2014.  $OW_{Lag}$  units are dimensionless. Positive values (red) in the center are surrounded by negative values of the shear sheath (blue). The overlaid 700-hPa (yellow) and 850-hPa (magenta) manifolds also indicate pouch boundaries. 700-hPa circulation and relative vorticity values calculated along a circuit corresponding to the 700-hPa manifold are in the upper-right corner. Overlaid drops (\*) are color-coded by their 700-hPa relative humidity values, with darkest red indicating 100% and blue indicating anything less than 40%. (Right) Corresponding composite of the drops in four regions: Inside the core (green), in the shear sheath and either within both manifolds (red) or just one manifold (magenta), and outside of both manifolds (blue).

GENESIS STAGE EXPERIMENT

*Science Description*

---

**SCIENCE OBJECTIVE #3:** *To investigate the favorability in both dynamics (e.g., vertical wind shear) and thermodynamics (e.g., moisture) for tropical cyclogenesis in the environment near a pre-TD, especially the downstream environment [Favorable Air Mass, FAM]*

**Motivation:** The environment near a pre-TD is critical to the favorability for tropical cyclogenesis to occur. The probability of cyclogenesis for a given pre-TD is dependent upon thermodynamics (e.g., moisture) and dynamics (e.g., vertical wind shear) in the adjacent air mass. Increased observations of lower-tropospheric humidity in the near-disturbance environment would shed light upon critical moisture thresholds important (or necessary) for tropical cyclogenesis and would help correct moisture biases in numerical weather prediction models. The downstream environment is most important for cyclogenesis predictions because that is the environment that a pre-TD moves into.

**Background:** As early as the 1930s, westward propagating disturbances in the lower troposphere were identified as seed circulations for most TCs in the North Atlantic Ocean (Dunn 1940). The origins of these pre-genesis disturbances, or pre-tropical depressions (pre-TDs), were traced back to North Africa and are now known as African easterly waves (AEWs; Riehl 1945). About 70% of all TCs and, more impressively, 85% of major hurricanes in the North Atlantic Ocean have been found to initiate from AEWs (Landsea 1993). On average, sixty AEWs exit the West African coast each year. However, determining which of these AEWs will develop into TCs has proven to be a forecasting challenge. For example, over 50% of TC genesis events in the Atlantic main development region predicted by the Global Forecast System (GFS) from 2004–2011 were false alarms (Halperin et al. 2013).

Recent research has shed some light on the relationship between AEWs and TC genesis in the North Atlantic Ocean. The AEW-relative flow around an incipient disturbance has been hypothesized to be an important factor in protecting the disturbance from environmental intrusions, and thus creating or maintaining a favorable environment for TC genesis to occur (Dunkerton et al. 2009). Brammer and Thorncroft (2015) have shown that, as AEWs leave West Africa, the troughs are sensitive to the low-level environment to their west and northwest (Fig. GN-3). Although the vortex at 700 hPa typically has a closed circulation in the wave-relative reference frame, the AEW troughs are still cold-core in the lower troposphere and, therefore, there is relative westerly flow under the vortex and through the lower levels of the trough. In a composite analysis, significant differences in the moisture of the low-level environment to the northwest of the troughs were found between developing and non-developing waves. Favorable developing waves had significantly higher moisture content in the lower troposphere to the northwest of the trough as they exited the West African coast compared to favorable non-developing waves. Trajectory analysis for all the waves revealed that as the AEWs transition over the West African coast the troughs are typically open to the environment ahead and to the northwest of the trough. For developing waves this means that moist air (e.g. moist tropical sounding, Dunion 2011) is ingested into the lower levels of the system, while for non-developing waves dry air (e.g. SAL or mid-latitude dry air

GENESIS STAGE EXPERIMENT  
*Science Description*

---

intrusion soundings) is ingested. At this stage in the AEW life cycle, moisture differences may be fundamental in determining whether a favorable wave will develop or not.

The depth and the integrity of the closed circulation around the pre-genesis disturbance is an important consideration for providing a convectively favorable environment for TC genesis. Freismuth et al. (2016) argue that the vortex of ex-Gaston (2010) was susceptible to dry air above the vortex maxima, which hindered deep convection and led to a weakening of the vortex. In addition, non-developing disturbance (AL90, 2014) encountered lower tropospheric dry air to its west and northwest, which was ingested by the disturbance and was likely a major contributor in the failed genesis (Fig. GN-4). Preliminary results by Brammer (2015) suggest that as AEWs leave the West African coast, these troughs typically possess closed circulations at 700–600 hPa. Yet, these troughs remain open to the environment both above and below the 700–600-hPa layer. As AEWs propagate across the North Atlantic, the troughs are more likely to exhibit closed circulations at low-levels due to either increased vorticity within the trough or the changing background shear profile over the central Atlantic. It was therefore hypothesized that AEWs are especially sensitive to the low-level environment to the west and northwest of the trough during the first three days after leaving the West African coast. Since AEWs typically propagate at  $7.5 \text{ m s}^{-1}$  over the Atlantic (Kiladis et al. 2006), these waves are typically located near  $35^\circ\text{W}$  after three days.

**Hypotheses:**

1. Environmental air downstream from a pre-TD is ingested before the low-level circulation is closed.
2. Environmental relative humidity to the west and northwest of a pre-TD is critical to the development of that disturbance.
3. Environmental vertical wind shear in the vicinity of a pre-TD is critical to the development of that disturbance.
4. Dry air associated with the Saharan Air Layer (SAL) inhibits or delays genesis of pre-TDs.
5. Dynamical models (e.g., GFS) are consistently too moist in the inflow layer to the west of a pre-TD, resulting in genesis false alarms.

**Aircraft Pattern/Module Descriptions:**

**G-IV Pattern #1: FAM**

Sample the *environment* to the west of an easterly wave, especially if dry air is detected in that region. Sample when easterly wave is forecast to develop in reliable computer models or is showing signs of development in observations. Sample when easterly wave is located at or west of  $35^\circ\text{W}$  (to be within range of G-IV). Standard Lawnmower pattern should be used to setup a grid of observations and dropsondes, with drops every 150 n mi (Fig. GN-2). The most likely orientation of the lawnmower pattern will be to the West or Northwest of

**GENESIS STAGE EXPERIMENT**  
*Science Description*

the tropical disturbance/cyclone. Flight level is 40–45 kft. Long legs of pattern should be 600–1000 n mi (depending on flight time and resources) and short legs should be 150 n mi. To maximize the usefulness of the data, a minimum of two boxes should be flown. In some situations, the same box could be flown twice to maximize data coverage in a more specific region.

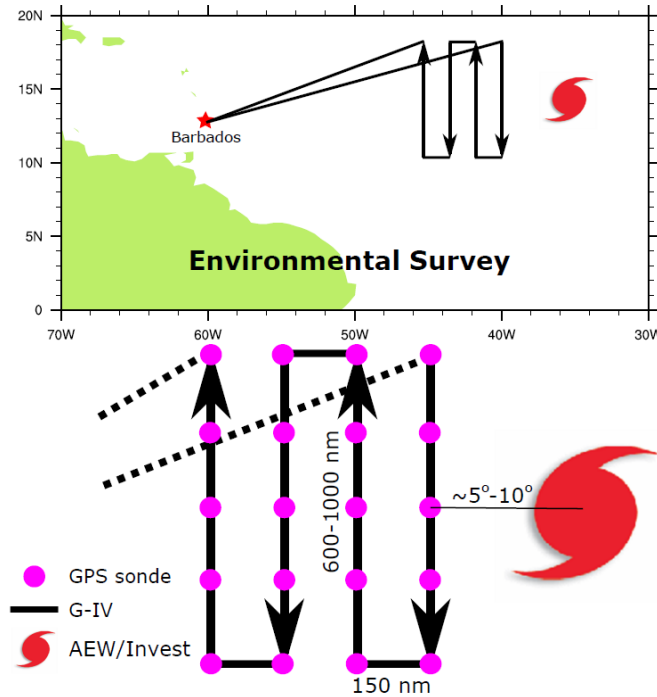


**Figure GN-2.** Example lawnmower pattern to be flown (track in black) by the G-IV, dropsonde locations within the pattern (purple), and the relative location of the AEW/Invest center (hurricane symbol)

**P-3 Pattern #1: FAM**

The Lawnmower pattern described above (and illustrated in Fig. GN-2) can be modified to accommodate the P-3. *Flight level should be 20 kft* to maximize the altitude of dropsonde data. P-3 missions will likely have to start later than G-IV missions since the range of the G-IV is larger, especially if the disturbance is in the Atlantic Main Development Region (east of 50°W)

**Analysis Strategy:** Dropsonde profiles will be evaluated to determine the horizontal gradients and advection of environmental relative humidity. Characteristics of the dry air mass will be scrutinized, including the minimum relative humidity, the height/depth the dry air, and the horizontal extent of the dry air. Wind analyses from dropsondes and TDR will be evaluated to determine the impact of environmental vertical wind shear on the

GENESIS STAGE EXPERIMENT

*Science Description*

---

pre-genesis disturbance. This analysis will go beyond the traditional deep layer vertical wind shear metric, taking into account the hodograph to evaluate vertical wind shear through a number of different levels. The observations collected in this experiment will be crucial to evaluation of dynamics/thermodynamics and the diagnosis of genesis false alarms in numerical weather prediction models (e.g., GFS, HWRF).

**References:**

- Brammer A., (2015): Evolution of African easterly waves and their relationship to tropical cyclogenesis., Ph.D. thesis, SUNY at Albany. url: <http://gradworks.umi.com/37/38/3738908.html>
- Brammer A., and C. D. Thorncroft, 2015: Variability and Evolution of African Easterly Wave Structures and Their Relationship with Tropical Cyclogenesis over the Eastern Atlantic. *Mon. Wea. Rev.* **143**, 4975–4995.
- Dunion, J.P., 2011: Re-writing the climatology of the tropical North Atlantic and Caribbean Sea atmosphere. *J. Climate*, **24**, 893–908.
- Dunkerton, T. J., M. T. Montgomery, and Z. Wang, 2009: Tropical cyclogenesis in a tropical wave critical layer: Easterly waves. *Atmos. Chem. Phys.*, **9**, 5587–5646.
- Dunn, G. E., 1940: Cyclogenesis in the tropical Atlantic. *Bull. Amer. Meteor. Soc.*, **21**, 215–229.
- Freismuth, T. M., Rutherford, B., Boothe, M. A., and Montgomery, M. T., 2016: Why did the storm ex-Gaston (2010) fail to redevelop during the PREDICT experiment?, *Atmos. Chem. Phys.*, **16**, 8511–8519.
- Halperin, D. J., H. E. Fuelberg, R. E. Hart, J. H. Cossuth, P. Sura, and R. J. Pasch, 2013: An evaluation of tropical cyclone genesis forecasts from global numerical models. *Wea. Forecasting*, **28**, 1423–1445, doi:10.1175/WAF-D-13-00008.1
- Landsea, C. W., 1993: A climatology of intense (or major) Atlantic hurricanes. *Mon. Wea. Rev.*, **121**, 1703–1713.
- Riehl, H., 1945: "Waves in the easterlies and the polar front in the tropics" Misc. Rep. No. 17, Department of Meteorology, University of Chicago, 79 pp.

GENESIS STAGE EXPERIMENT  
*Science Description*

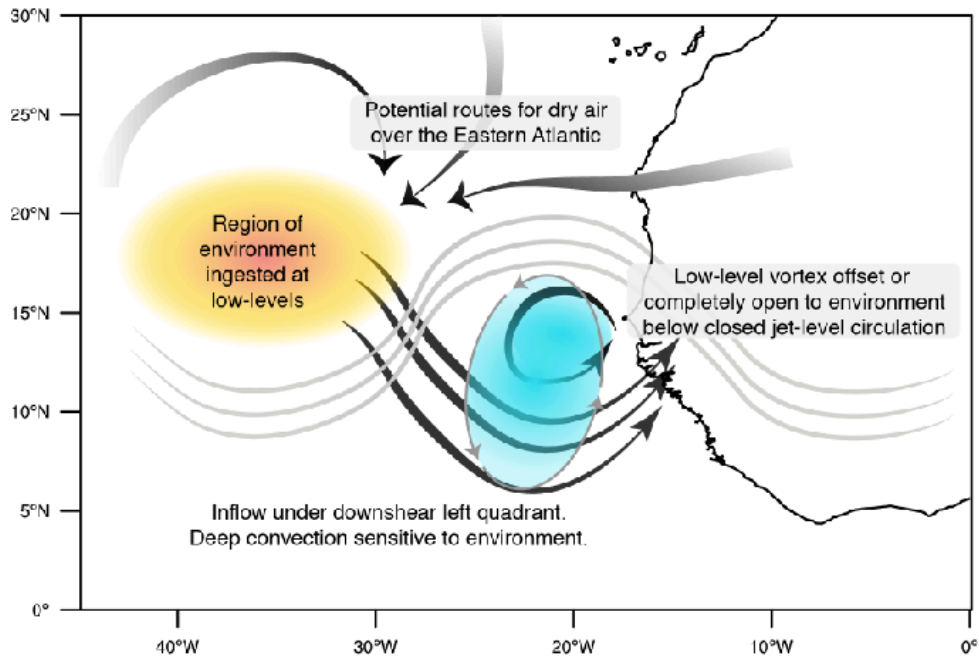


*Figure GN-3. Schematic of the ingestion of dry environmental air by an AEW*

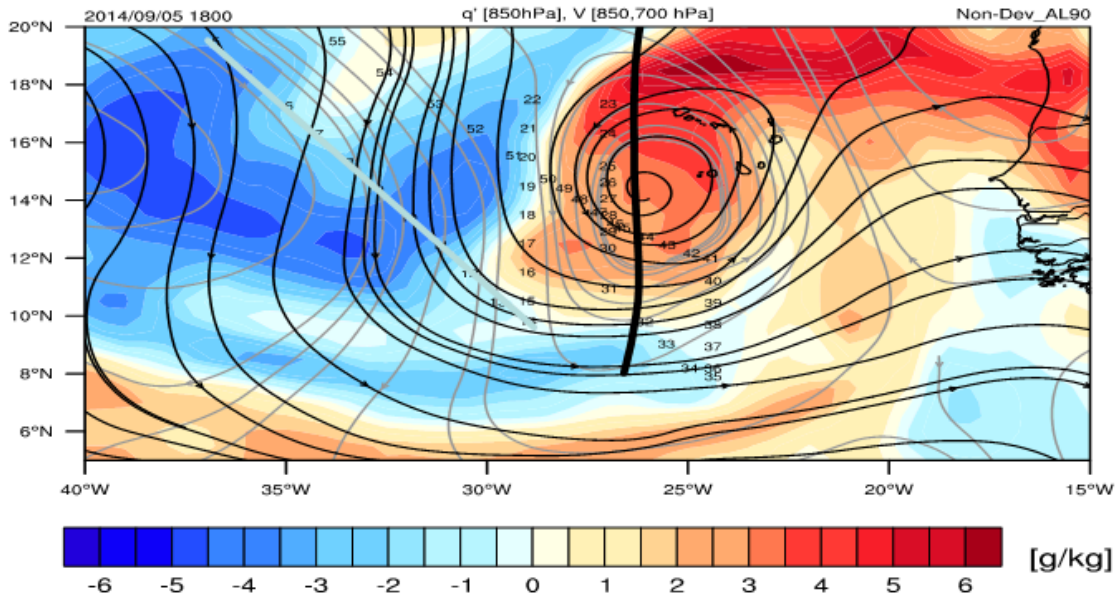


*Figure GN-4. 850-hPa specific humidity anomalies (shading), 850-hPa streamflow (black contours) and 700-hPa streamflow (grey contours) are shown for a non-developing case (AL90) at 1800Z 5 September 2014*

EARLY STAGE EXPERIMENT  
*Science Description*

---

**Investigator(s):** Rob Rogers, Jon Zawislak (Co-PIs), Ghassan Alaka, Jason Dunion, Heather Holbach, Trey Alvey (U. Utah), Josh Wadler (U. Miami/RSMAS) (Co-Is)

**Requirements:** TD, TS, Category 1

**Science Objectives:**

- 1) Collect datasets that can be used to improve the understanding of intensity change processes, as well as the initialization and evaluation of 3-D numerical models, particularly for TCs experiencing moderate vertical wind shear [*IFEX Goals 1, 3*]
- 2) Obtain a quantitative description of the kinematic and thermodynamic structure and evolution of intense convective systems (convective bursts) and the nearby environment to examine their role in TC intensity change [*IFEX Goals 1, 3*]
- 3) Improve our understanding of the physical processes responsible for the formation and evolution of arc clouds, as well as their impacts on TC structure and intensity in the short-term [*IFEX Goals 1, 3*]

**Description of Science Objectives:**

**SCIENCE OBJECTIVE #1:** *Collect datasets that can be used to improve the understanding of intensity change processes, as well as the initialization and evaluation of 3-D numerical models, particularly for TCs experiencing moderate vertical wind shear*  
[Analysis of Intensity Change Processes Experiment, AIPEX]

**Motivation:** While some improvements in operational tropical cyclone (TC) intensity forecasting have been made in recent years (DeMaria et al. 2014), predicting changes in TC intensity (as defined by the 1-min. maximum sustained wind) remains problematic. In particular, the operational prediction of rapid intensification (RI) has proven to be especially difficult (Kaplan et al. 2010). The significant impact of such episodes has prompted the Tropical Prediction Center/National Hurricane Center (TPC/NHC) to declare it as its top forecast priority (Rappaport et al. 2009).

Processes that govern TC intensification span spatial and temporal scales from the environmental to vortex to convective and smaller scales. Recent work has focused on the precipitation distribution and structure to assess regimes associated with TC intensification. Studies using airborne Doppler radar (Rogers et al. 2013) and passive microwave satellite (e.g., Alvey et. al 2015; Tao and Jiang 2015) observations have compared the inner-core structure of intensifying and non-intensifying TCs. Precipitation and deep convection in intensifying cases were found to be more symmetrically distributed and located preferentially inside the radius of maximum wind (RMW) compared to non-intensifying cases. Predictability of the azimuthal and radial distribution of precipitation and deep convection within TCs, however, remains low.



**EARLY STAGE EXPERIMENT**  
*Science Description*

---

Thus, identifying and understanding the environmental and internal (within the inner core) mechanisms that govern the azimuthal and radial distribution of precipitation and deep convection could improve the understanding of the intensification process. Recent studies indicate that these mechanisms may include: the interaction of the vortex with environmental vertical wind shear and dry air, vortex-scale subsidence, surface enthalpy fluxes from the underlying ocean, and precipitation mode (i.e., shallow, moderately deep, and deep convection, as well as stratiform rain).

The goal of this experiment is to collect datasets that can be used to: 1) improve the initialization and evaluation of 3-D numerical models; 2) improve the understanding of intensity change processes across multiple scales, with particular focus on the mechanisms that govern the azimuthal and radial distribution of precipitation and deep convection. TCs that are experiencing moderate vertical wind shear ( $5\text{--}10\text{ m s}^{-1}$ ) over a deep layer (850–200 hPa) are of particular interest, since this range of shear values is often associated with considerable uncertainty with respect to the prospect for TC intensification (Bhatia and Nolan 2013). The overarching goal is to improve the ability to predict the timing and magnitude of intensification, particularly RI, events.

**Background:** Prior studies have found a number of large-scale environmental factors that are generally favorable for TC intensification, including low environmental vertical wind shear, high ocean heat content, and elevated low- to mid-tropospheric humidity. Thus far, statistically-based prediction schemes that employ predictors derived from large-scale environmental fields and GOES infrared satellite imagery have generally been shown to provide the most skillful objective RI guidance (Kaplan et al. 2015). These schemes include the SHIPS rapid intensification index (SHIPS-RII) (Kaplan et al. 2010) and the more recently developed Bayesian and logistic regression RI models (Rozoff and Kossin 2011). Kaplan et al. (2015) showed that these statistical models are capable of explaining roughly 20% of the skill of Atlantic basin RI forecasts at a lead-time of 24 h. The remaining 80% of the skill not explained by the statistical models is assumed to be attributable either to processes not explicitly accounted for by those models or by limitations in the predictability of RI events.

On the vortex-scale, a number of observational studies have found that intensifying TCs have more precipitation and convective bursts occur within the high inertial stability region inside the RMW (e.g., Rogers et al. 2013, 2015, 2016). This configuration is favorable for TC intensification for two hypothesized reasons: 1) in the high inertial stability region, heat energy is much more efficiently converted to kinetic energy (Schubert and Hack 1982; Vigh and Schubert 2009), and 2) diabatic heating within the high inertial stability region enables angular momentum surfaces to be drawn inward at the RMW, resulting in tangential wind spinup (Smith and Montgomery 2016).

Observational studies have also found that intensifying TCs typically have more symmetrically distributed precipitation and deep convection than non-intensifying TCs (e.g., Rogers et al. 2013; Alvey et al. 2015; Tao and Jiang 2015). This is consistent with idealized modeling studies that show that TC intensification is most sensitive to the

## EARLY STAGE EXPERIMENT

### *Science Description*

---

axisymmetric, azimuthal wavenumber-0 component of diabatic heating (e.g., Nolan et al. 2007). One principal environmental factor that can prevent the development of this symmetry is vertical wind shear. The interaction of TCs with environmental vertical wind shear typically results in a wavenumber-1 asymmetry in vertical motion and precipitation, in which upward vertical motion and deep convection is favored in the downshear semicircle, while downward motion and suppression of deep convection is observed in the upshear semicircle (e.g., Marks et al. 1992; Reasor et al. 2013; Rogers et al. 2016; Zawislak et al. 2016). An increase in asymmetry can lead to the decrease in the projection of diabatic heating onto the axisymmetric, azimuthal wavenumber-0 component that has been shown to be important for TC intensification. However, the magnitude of this asymmetry can exhibit considerable variability, particularly within the moderate shear regime ( $5\text{--}10\text{ m s}^{-1}$ ) that has been shown to be problematic for operational intensity forecasts (Bhatia and Nolan 2013). This suggests the importance of understanding what governs the azimuthal distribution of precipitation and deep convection.

Recent studies have used airborne Doppler radar and dropsonde data to examine what hinders the development of precipitation symmetry in sheared TCs (Rogers et al. 2016; Zawislak et al. 2016; Nguyen et al. 2017). These studies show evidence for several potential hindering factors. First, convective downdrafts associated with the downshear convection can cool and stabilize the lower troposphere in the left of shear and upshear quadrants. Second, subsidence in the upshear quadrants can increase the temperature and decrease the relative humidity of the mid-troposphere, effectively capping the lower troposphere. Third, dry air can be transported laterally from the environment into the TC's upshear quadrants. These hindering factors could be mitigated through several potential mechanisms, as listed in the hypotheses below.

**Hypotheses:** The following hypotheses will guide the sampling strategies for TCs that have the potential to undergo (rapid) intensification:

1. Intensification is favored when precipitation and deep convection are distributed symmetrically and located preferentially inside the radius of maximum wind (RMW).
2. The local kinematic (e.g., location and depth of radial inflow, vertical alignment of the vortex) and thermodynamic forcing (e.g., SST, available moisture, and RH) are key in governing whether precipitation (deep convection) is symmetrically distributed and primarily inside the RMW.
3. Symmetry is favored when: (a) the mid-troposphere is moistened upshear due to detrainment from mid-tropospheric congestus, evaporation of falling stratiform rain, or reduced lateral advection of dry air from the environment; (b) the lower troposphere is convectively unstable in the upshear quadrants due to enhanced surface enthalpy fluxes from the underlying ocean and/or reduced convective downdrafts.

EARLY STAGE EXPERIMENT

*Science Description*

---

**Aircraft Pattern/Module Descriptions:** Missions will be targeted for systems that have a reasonable chance of undergoing intensification based on statistical and numerical model forecast guidance. When possible (i.e., subject to range, timing, and other logistical constraints), missions will begin at least 24 h prior to the expected onset of intensification, while the TC is still at tropical depression or tropical storm intensity. This enables the documentation of TC structure during the time leading up to intensification onset (if it indeed occurs). Ideally missions will continue every 12 h, as long as feasible. If either the P-3 or G-IV aircraft cannot fly every 12 h the experiment can still be conducted provided that the gap between missions for any one of the two aircraft does not exceed 24 h. Although all intensification rates are of interest, priority will be given to those with a high potential for RI according to model guidance and/or are forecast to experience at least moderate ( $5\text{--}10\text{ m s}^{-1}$ ) vertical wind shear over a deep layer. There are a few possible configurations for the execution of this experiment, as outlined below:

*1. Both P-3 and G-IV are available*

**P-3 Pattern #1: AIPEX**

**G-IV Pattern #1: AIPEX**

**G-IV Pattern #2: AIPEX**

This is the optimal configuration for this experiment as, under this scenario, the P-3 and G-IV would coordinate operations (i.e., takeoff times would allow both aircraft to sample the TC simultaneously). The P-3 will sample the inner-core with the standard rotated Figure-4 pattern (*P-3 Pattern #1: AIPEX*), while the G-IV will sample the outer environment and near-TC environment (typically around 60 n mi, or 100 km) with either the circumnavigation (*G-IV Pattern #1: AIPEX*) or star (*G-IV Pattern #2: AIPEX*) pattern.

*2. Only P-3 is available*

**P-3 Pattern #1: AIPEX**

**P-3 Pattern #2: AIPEX**

When the G-IV is not available for coordinated operations, either because of operational tasking requirements or aircraft unavailability, P-3 targeted observations in the near environment and inner core can still contribute towards the objectives of the experiment. In this scenario there are two possible strategies for sampling, which depend on whether the precipitation distribution is asymmetric:

(a) TC is highly asymmetric:

This option will be chosen when the precipitation distribution in the targeted TC is expected to be highly asymmetric during the mission. Such an asymmetric configuration would allow for a high-altitude P-3 circumnavigation pattern to at least target the precipitation-free upshear semicircle, and when hazard avoidance is possible the downshear quadrants. Indications of an appropriate magnitude of

EARLY STAGE EXPERIMENT  
*Science Description*

asymmetry may include:

- 1) Visible, infrared, or microwave satellite imagery indicates an exposed or partially exposed low-level circulation center (Fig. ES-1).
- 2) The environmental vertical wind shear, as indicated by SHIPS, is expected to be sufficient ( $> 5 \text{ m s}^{-1}$ ) during the mission to result in an asymmetric precipitation structure.
- 3) High-resolution numerical guidance (i.e. HWRF) forecast a lack of precipitation in the upshear semicircle of the TC during the mission.

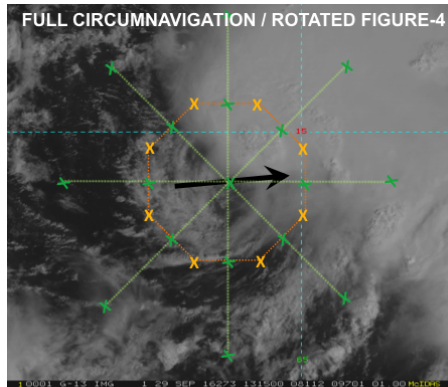


**Figure ES-1.** Figure-4 in green, circumnavigation in orange, shear vector in black, 'X' is a dropsonde location

Given this scenario, the P-3 will sample the near environment and inner core with a pattern that includes a high-altitude circumnavigation and, optimally, a rotated Figure-4 (*P-3 Pattern #2: AIPEX*). If time doesn't permit for a complete rotated Figure-4, then a single Figure-4 can be substituted (Fig. ES-1). The radius of the circumnavigation should be as close to the inner-core precipitation shield as safety allows, as best determined through available visible or infrared satellite, microwave, or radar imagery. The high-altitude circumnavigation allows for increased azimuthal and vertical dropsonde data coverage, particularly in the critical, precipitation-free upshear region that may fill in as intensification commences.

(b) TC is relatively symmetric:

This scenario applies to a targeted TC that has the potential for intensification, but the precipitation is expected to be too symmetric during the mission for the P-3 high-altitude circumnavigation to be conducted safely. Here, the P-3 will sample the inner-core vortex structure with the standard rotated Figure-4 pattern (*P-3 Pattern #1: AIPEX*).

EARLY STAGE EXPERIMENT  
*Science Description*

---

*3. Only G-IV is available:*  
**G-IV Pattern #1: AIPEX**  
**G-IV Pattern #2: AIPEX**

This option is less preferable as targeted observations of the vortex structure are also important towards the objectives of the experiment. This option applies to any targeted TC that has the potential for intensification, regardless of asymmetric structure. Under this option, the G-IV will sample the outer and near environments with either the circumnavigation (*G-IV Pattern #1: AIPEX*) or star (*G-IV Pattern #2: AIPEX*), and requires that hazard avoidance permit the G-IV to obtain measurements within/very near the inner core.

*4. Additional modules*

If the opportunity arises during the execution of AIPEX, fly the Convective Burst and Evolution Module (CBM) or Arc Cloud Module (Arc Cloud) (see accompanying discussion for Science Objectives #2 and #3 of this experiment). The CBM would be optimal for determining the structure and evolution of deep convection within the framework of the broader vortex-scale circulation as it interacts with vertical shear (if appropriate), while the Arc Cloud module would be ideal for documenting locations within the vortex circulation encountering significant low-to mid-level dry air and determining the impact of the associated outflow boundaries on the boundary layer temperature and moisture distribution.

**Analysis Strategy:** The general analysis strategy follows that performed in recent observational studies (Reasor et al. 2013; Zhang et al. 2013; Rogers et al. 2016; Zawislak et al. 2016; Nguyen et al. 2017). The analysis strategy includes assessing and documenting the time evolution of the following:

- *Azimuthal and radial distribution of inner-core precipitation and deep convection* (P-3 TDR/LF, possibly G-IV TDR). The inner-core precipitation asymmetry, and its projection onto the axisymmetric, azimuthal wavenumber-0 component will be assessed quantitatively (assuming sufficient azimuthal coverage). The location of precipitation and convective bursts relative to the RMW will be examined.
- *Precipitation mode, particularly upshear* (P-3 TDR/LF, possibly G-IV TDR). An analysis of the precipitation mode (shallow, moderately deep, deep convection, as well as stratiform rain), using the vertical velocity and reflectivity structure, will allow for an assessment as to whether moistening of the inner core occurs through upscale growth of convection (moistening from convective detrainment at gradually higher altitudes), or from the top-down via stratiform rain as hydrometeors produced downshear are transported azimuthally upshear.

EARLY STAGE EXPERIMENT

*Science Description*

---

- *Low-wavenumber thermodynamic and kinematic structure of the boundary layer* (P-3/G-IV dropsondes, DWL for kinematic only). The thermodynamic focus will be on the boundary layer cooling by convective downdrafts and the subsequent recovery via surface enthalpy fluxes from the underlying ocean in the downstream (upshear-left through downshear-right) quadrants. Surface enthalpy fluxes will be calculated where dropsondes are paired with AXBTs that provide sea surface temperature. The kinematic focus will be on obtaining measurements of the strength and depth of boundary layer inflow and convergence in the boundary layer, both in a symmetric sense and relative to the shear vector (when relevant). Additionally, the gradient and agradient flow in the boundary layer will be calculated.
- *Low-wavenumber thermodynamic and kinematic structure above the boundary layer* (P-3/G-IV dropsondes, P-3/G-IV TDR and DWL for kinematic only). The presence of mid-tropospheric dry air is of particular interest. Assuming mid-tropospheric dry air is present (most likely in the upshear quadrants), the potential sources of this dry air (vortex-scale subsidence or lateral advection from the environment) and how this upshear dry air is removed (i.e., through detrainment from congestus or evaporation of stratiform precipitation) will be assessed.
- *Vortex tilt* (P-3 TDR, possibly G-IV TDR). Assuming sufficient TDR coverage, the vortex tilt will be examined quantitatively by merging TDR analyses from each Figure-4. If the vortex tilt appears to decrease rapidly during a flight, individual TDR analyses can be used to qualitatively examine the time evolution of vortex tilt during the alignment process.
- *Vertical wind shear and upper-level divergence* (G-IV dropsondes). These quantities will be computed and compared with global model analyses. The vertical distribution of shear will also be evaluated, as upper-level shear is hypothesized to be less deleterious than low-level shear.

The overarching hypothesis is that, by performing the above analyses for multiple AIPEX data sets collected during both RI and non-RI events, it will be possible to determine the conditions that are triggers for RI. This analysis strategy can also assist in the evaluation of 3-D numerical models, including the sufficiency (or lack thereof) of the horizontal resolution, and the microphysical and planetary boundary layer parameterization schemes.

**References:**

Alvey, G.R. III, J. Zawislak, and E. Zipser, 2015: Precipitation Properties Observed during Tropical Cyclone Intensity Change. *Mon. Wea. Rev.*, **143**, 4476–4492. doi: 10.1175/MWR-D-15-0065.1.

EARLY STAGE EXPERIMENT

*Science Description*

---

- Bhatia, K. T., and D. S. Nolan, 2013: Relating the skill of tropical cyclone intensity forecasts to the synoptic environment. *Wea. Forecasting*, **28**, 961–980, doi: 10.1175/WAF-D-12-00110.1.
- DeMaria, M., C. R. Sampson, J. A. Knaff, and K. D. Musgrave, 2014: Is tropical cyclone intensity guidance improving? *Bull. Amer. Meteor. Soc.*, **95**, 387–398, doi:10.1175/BAMS-D-12-00240.1.
- Kaplan, J., M. DeMaria, and J. A. Knaff, 2010: A revised tropical cyclone rapid intensification index for the Atlantic and eastern North Pacific basins. *Wea. Forecasting*, **25**, 220–241, doi: 10.1175/2009WAF2222280.1.
- Kaplan, J., and Coauthors, 2015: Evaluating environmental impacts on tropical cyclone rapid intensification predictability utilizing statistical models. *Wea. Forecasting*, **30**, 1374–1396, doi: 10.1175/WAF-D-15-0032.1.
- Marks, F. D., Jr., R. A. Houze Jr., and J. F. Gamache, 1992: Dual-aircraft investigation of the inner core of Hurricane Norbert. Part I: Kinematic structure. *J. Atmos. Sci.*, **49**, 919–942, doi: 10.1175/1520-0469(1992)049<0919:DAIOTI>2.0.CO;2.
- Nguyen, L. T., R. Rogers, and P. Reasor 2017: Thermodynamic and kinematic influences on precipitation symmetry in sheared tropical cyclones: Bertha and Cristobal (2014). *Mon. Wea. Rev.* In review.
- Nolan, D. S., Y. Moon, and D. P. Stern, 2007: Tropical cyclone intensification from asymmetric convection: Energetics and efficiency. *J. Atmos. Sci.*, **64**, 3377–3405, doi: 10.1175/JAS3988.1.
- Rappaport, E. N., and Coauthors, 2009: Advances and Challenges at the National Hurricane Center. *Wea. Forecasting*, **24**, 395–419.
- Reasor, P. D., R. F. Rogers, and S. Lorsolo, 2013: Environmental flow impacts on tropical cyclone structure diagnosed from airborne Doppler radar composites. *Mon. Wea. Rev.*, **141**, 2949–2969, doi: 10.1175/MWR-D-12-00334.1.
- Rogers, R., P. Reasor, and S. Lorsolo, 2013: Airborne Doppler observations of the inner-core structural differences between intensifying and steady-state tropical cyclones. *Mon. Wea. Rev.*, **141**, 2970–2991, doi: 10.1175/MWR-D-12-00357.1.
- Rogers, R. F., P. D. Reasor, and J. A. Zhang, 2015: Multiscale structure and evolution of Hurricane Earl (2010) during rapid intensification. *Mon. Wea. Rev.*, **143**, 536–562, doi: 10.1175/MWR-D-14-00175.1.
- Rogers, R., J. Zhang, J. Zawislak, H. Jiang, G. Alvey, E. Zipser, and S. Stevenson, 2016: Observations of the structure and evolution of Hurricane Edouard (2014) during

EARLY STAGE EXPERIMENT

*Science Description*

---

- intensity change. Part II: Kinematic structure and the distribution of deep convection. *Mon. Wea. Rev.*, **144**, 3355–3376, doi: 10.1175/MWR-D-16-0017.1.
- Rozoff, C. M., and J. P. Kossin, 2011: New probabilistic forecast models for the prediction of tropical cyclone rapid intensification. *Wea. Forecasting*, **26**, 677–689, doi: 10.1175/WAF-D-10-05059.1.
- Schubert, W. H., and J. J. Hack, 1982: Inertial stability and tropical cyclone development. *J. Atmos. Sci.*, **39**, 1687–1697, doi: 10.1175/1520-0469(1982)039<1687:ISATCD>2.0.CO;2.
- Tao, C., and H. Jiang, 2015: Distributions of shallow to very deep precipitation–convection in rapidly intensifying tropical cyclones. *J. Climate*, **28**, 8791–8824, doi: 10.1175/JCLI-D-14-00448.1.
- Vigh, J. L., and W. H. Schubert, 2009: Rapid development of the tropical cyclone warm core. *J. Atmos. Sci.*, **66**, 3335–3350, doi: 10.1175/2009JAS3092.1.
- Zawislak, J., H. Jiang, G. Alvey, E. Zipser, R. Rogers, J. Zhang, and S. Stevenson, 2016: Observations of the structure and evolution of Hurricane Edouard (2014) during intensity change. Part I: Relationship between the thermodynamic structure and precipitation. *Mon. Wea. Rev.*, **144**, 3333–3354, doi: 10.1175/MWR-D-16-0017.1.
- Zhang, J. A., R. F. Rogers, P. Reasor, E. Uhlhorn, and F. D. Marks Jr., 2013: Asymmetric hurricane boundary layer structure from dropsonde composites in relation to the environmental wind shear. *Mon. Wea. Rev.*, **141**, 3968–3984, doi: 10.1175/MWR-D-12-00335.1.



EARLY STAGE EXPERIMENT  
*Science Description*

---

**SCIENCE OBJECTIVE #2:** *Obtain a quantitative description of the kinematic and thermodynamic structure and evolution of intense convective systems (convective bursts) and the nearby environment to examine their role in TC intensity change*

[Convective Burst Structure and Evolution Module, CBM]

**Motivation:** The objectives are to obtain a quantitative description of the kinematic and thermodynamic structure and evolution of intense convective systems (convective bursts) and the nearby environment to examine their role in TC intensity change.

**Background:** It has long been known that deep convection is an integral component of TC structure. What has received greater attention in recent years is the potential role that deep convection, termed here “convective bursts”, or CBs, representing the peak updrafts and highest echo tops, plays in TC evolution, in particular intensity evolution. Various hypotheses attribute their contribution to TC intensification by vortex gradient adjustment to the imposed diabatic heating in the high-inertial stability region inside the RMW (e.g., Shapiro and Willoughby 1982, Schubert and Hack 1982, Hack and Schubert 1986, Nolan and Grasso 2003, Nolan et al. 2007, Vigh and Schubert 2009, Pendergrass and Willoughby 2009, Rogers et al. 2013, 2015, 2016), convergence of angular momentum surfaces in the lower troposphere and boundary layer (Smith and Montgomery 2016), upper-level subsidence warming around the CB periphery (e.g., Heymsfield et al. 2001, Guimond et al. 2010, Rogers 2010, Zhang and Chen 2012, Chen and Zhang 2013, Chen and Gopal 2015), stretching and axisymmetrization in vortical hot towers (Hendricks et al. 2004, Montgomery et al. 2006, Reasor et al. 2009), and vortex alignment/downshear reformation (Reasor et al. 2009, Molinari and Vollaro 2010, Nguyen and Molinari 2012, Reasor and Eastin 2012, Stevenson et al. 2014, Rogers et al. 2015, Nguyen and Molinari 2015). While these studies have emphasized the role of deep convection in TC intensification, other studies have focused on the role of shallow to moderate convection, and even stratiform precipitation, in initiating TC intensification (Kieper and Jiang 2012, Zagrodnik and Jiang 2014, Tao and Jiang 2015, Tao et al. 2017, Nguyen et al. 2017). Common to these and other (e.g., Miyamoto and Takemi 2015) studies, though, is that TC intensification is favored when precipitation, including CBs, are preferentially located inside the RMW with a maximum azimuthal distribution.

Vertical shear is one factor that has been shown to be important in organizing precipitation, including CBs, azimuthally around the TC vortex. This has generally been attributed to the fact that vertical shear tilts the vortex, leading to preferred regions of vortex-scale low-level convergence and upward motion downshear and low-level divergence and subsidence upshear (Jones 1995, Bender 1997, Frank and Ritchie 2001, Black et al. 2002, Corbosiero and Molinari 2003, Rogers et al. 2003, Braun et al. 2006, Wu et al. 2006, Reasor et al. 2009, Reasor and Eastin 2012, Reasor et al. 2013, Dolling and Barnes 2014, DeHart et al. 2014). Recent composite studies of vortices in shear using airborne Doppler radar have shown that the shear-induced circulations are maximized downshear right (DSR) (low-level convergence/upward motion) and upshear left (USL) (low-level divergence/downward motion) (Reasor et al. 2013, DeHart et al.

EARLY STAGE EXPERIMENT

*Science Description*

---

2014). A similar composite methodology has been performed in a CB-relative coordinate system (Wadler et al. 2017). This study found that the peak updraft magnitude and altitude for CBs was minimized DSR, consistent with the notion that this is the quadrant where CBs are initiated. Peak updraft magnitude and altitude increase in the DSL quadrant, as the CBs mature, and they reach their highest and strongest values USL. A similar shear-relative azimuthal relationship was found for echo top height. Significantly, when stratifying TCs by intensity change, it was found that the most significant differences in CB structure between intensifying and non-intensifying TCs were located in the USL quadrant. Intensifying TCs have CBs with stronger peak updrafts, at a higher altitude, with higher echo tops in the USL quadrant than non-intensifying TCs. This relationship suggests that the structure and evolution of CBs, which are to some extent a function of the local environment from which they initiate downshear and mature upshear — including convective available potential energy, midlevel humidity, and subsidence upshear (Zawislak et al. 2016, Rogers et al. 2016, Nguyen et al. 2017) — is an important factor to consider in assessing the potential for a TC to intensify.

It should be noted that the above descriptions presume that CBs do translate downwind, i.e., upshear. However, in some situations, mostly revealed from modeling studies (Munsell et al. 2017, Chen et al. 2017), CBs can remain “trapped” on the downshear side. In fact, cases where the CBs remain downshear were more likely to be associated with non-intensifying periods of TC evolution. This is consistent with the notion of greater azimuthal symmetry of diabatic heating being associated with TC intensification. CBs propagating into the upshear quadrants may also be related to a greater likelihood of vortex alignment, as revealed in the observational analysis of Hurricane Earl (2010; Rogers et al. 2015) and a WRF-ARW ensemble forecast of Edouard (2014; Munsell et al. 2017).

The results described above are valid for composites of many different CBs from many different TCs. They therefore lack the temporal continuity needed to measure the structure of specific individual (or groups of) CBs, and how they evolve in a shear-relative sense. The purpose of this module is to repeatedly sample individual (or groups of) CBs to provide this temporal continuity.

**Hypotheses:** The following hypotheses will guide the sampling strategies for CBs. One set of hypotheses is for CBs that translate downwind/upshear, the other set is for CBs that remain confined downshear:

1. CBs are preferentially initiated in the DSR quadrant; as such, the updraft maxima is likely to be weaker and at a lower altitude in this quadrant;

*For CBs translating downwind/upshear:*

2. Traveling downwind into the DSL quadrant, peak updrafts will strengthen and be located at a higher altitude;

## EARLY STAGE EXPERIMENT

### *Science Description*

---

3. The strength of the CB in the USL quadrant (as measured by strength and height of peak updraft and echo top height relative to the DSL quadrant) will vary depending on the local, vortex-scale environment of the convection. This environment includes midlevel humidity, strength of subsidence upshear, and sea surface temperature (and CAPE) on the downshear side of the TC;
4. If the CB strength USL is higher (lower) than DSL, the TC will intensify (not intensify).

*For CBs remaining confined downshear:*

5. The structural evolution will follow a similar path to those CBs translating downwind/upshear; i.e., updraft peaks beginning in lower to middle troposphere, then ascending with time before becoming dominated by downdrafts and collapse while remaining downshear
6. TC will not intensify

### **Aircraft Pattern/Module Descriptions:**

#### **P-3 Module #1: CBM**

This is a stand-alone module that takes 1–2 h to complete. Execution is dependent on system attributes, aircraft fuel and weight restrictions, and proximity to operations base. It can be flown separately within a mission designed to study local areas of convection or at the end of one of the survey patterns. Once a local area of intense convection is identified, the P-3 will transit at altitude (10–12 kft) to the nearest point just outside of the convective cores and sample the convective area. The sampling pattern will be a series of inbound/outbound radial penetrations or bowtie patterns (when sampling a CB near the RMW of a tropical storm or hurricane). If the CB is at or near the RMW, repeated sampling can allow for a following of the burst around the storm. This is especially useful to sample the structural evolution of the burst as it moves around the storm. If the CB remains confined to the downshear side of the TC rather than translate upshear, the pattern should still be flown.

**Analysis Strategy:** Radar analyses will be performed for each radial pass through the CB, preferentially with a temporal spacing of 30 minutes or less. These analyses will provide high-frequency observations of the structure of the CB, as measured by the peak updraft magnitude and altitude and echo top heights. Additionally, the full spectrum of vertical velocity associated with each radar analysis will be evaluated using contoured frequency by altitude diagrams (CFADs; Yuter and Houze 1995) to obtain a more complete picture of the updraft and downdraft structure and evolution of the CB. Ideally a CB will be flown beginning with its initiation (likely to be downshear) and then followed around the storm as it travels through the downwind quadrants and into the upshear quadrants (or continuously sampled on the downshear side if it remains confined there). Dropsondes released at the starting and ending points of each radial leg will

EARLY STAGE EXPERIMENT  
*Science Description*

---

document the thermodynamic structure of the boundary layer radially bracketing the CB. Optimally, the G-IV will be flying in the storm to provide deep-layer humidity profiles around the storm in addition to the P-3 dropsondes. If the G-IV is not available, the module could still be flown to examine the evolution using the Doppler radar and boundary layer thermodynamics from the P-3 dropsondes.

In addition to the observational analysis described above, the high-resolution data collected in this module is planned to be embedded within the typical Hurricane Ensemble Data Assimilation System (HEDAS; e.g., Aksoy et al. 2013) framework to carry out storm-scale data assimilation that focuses specifically on the high-resolution analysis of the identified intense convective region. With current technology, a smaller domain with 1-km grid spacing will be nested within the HEDAS 3-km analysis domain, where the data will be assimilated for the duration of its collection (1–2 hours, at 5–10 min intervals). This is a typical setup that has been traditionally used in continental storm-scale radar data assimilation applications and has been shown to be effective to obtain realistic storm structures in analyses and short-range forecasts. With such high-resolution analyses, we hope to be able to obtain fully three-dimensional model representations of the observed convective regions for more detailed investigation, as well as investigate their short-range predictability. In an observing system experiment (OSE) mode, various assimilation experiments can also be devised to investigate hypothetical scenarios for how an observed convective region could interact with the surrounding vortex and impact its evolution.

**References:**

- Aksoy, A., S. D. Aberson, T. Vukicevic, K. J. Sellwood, S. Lorsolo, and X. Zhang (2013), Assimilation of high-resolution tropical cyclone observations with an ensemble Kalman filter using NOAA/AOML/HRD's HEDAS: Evaluation of the 2008–11 vortex-scale analyses, *Mon. Wea. Rev.*, **141**, 1842–1865, doi:<http://dx.doi.org/10.1175/MWR-D-12-00194.1>.
- Bender, M. A., 1997: The effect of relative flow on the asymmetric structure in the interior of hurricanes. *J. Atmos. Sci.*, **54**, 703–724, doi:10.1175/1520-0469(1997)054<0703:TEORFO>2.0.CO;2.
- Black, M. L., J. F. Gamache, F. D. Marks, C. E. Samsury, and H. E. Willoughby, 2002: Eastern Pacific Hurricanes Jimena of 1991 and Olivia of 1994: The effect of vertical shear on structure and intensity. *Mon. Wea. Rev.*, **130**, 2291–2312, doi:10.1175/1520-0493(2002)130<2291:EPHJOA>2.0.CO;2.
- Braun, S. A., M. T. Montgomery, and Z. Pu, 2006: High-resolution simulation of Hurricane Bonnie (1998). Part I: The organization of eyewall vertical motion. *J. Atmos. Sci.*, **63**, 19–42, doi:10.1175/JAS3598.1.

EARLY STAGE EXPERIMENT

*Science Description*

---

- Chen, H., and S. G. Gopalakrishnan, 2015: A study on the asymmetric rapid intensification of Hurricane Earl (2010) using the HWRF system. *J. Atmos. Sci.*, **72**, 531–550, doi:10.1175/JAS-D-14-0097.1.
- Chen, H., and D. L. Zhang, 2013: On the rapid intensification of Hurricane Wilma (2005). Part II: Convective bursts and the upper-level warm core. *J. Atmos. Sci.*, **70**, 146–162, doi:10.1175/JAS-D-12-062.1.
- Chen, H., S. Gopalakrishnan, J.A. Zhang, R.F. Rogers, Z. Zhang, and V. Tallapragada, 2017: Use of HWRF ensembles for providing improved understanding of hurricane RI problem: Case study of Hurricane Edouard (2014). *J. Atmos. Sci.*, in review.
- Corbosiero, K. L., and J. Molinari, 2003: The relationship between storm motion, vertical wind shear, and convective asymmetries in tropical cyclones. *J. Atmos. Sci.*, **60**, 366–376, doi:10.1175/1520-0469(2003)060<0366:TRBSMV>2.0.CO;2.
- DeHart, J. C., R. A. Houze Jr., and R. F. Rogers, 2014: Quadrant distribution of tropical cyclone inner-core kinematics in relation to environmental shear. *J. Atmos. Sci.*, **71**, 2713–2732, doi:10.1175/JAS-D-13-0298.1.
- Dolling, K., and G. M. Barnes, 2014: The evolution of Hurricane Humberto (2001). *J. Atmos. Sci.*, **71**, 1276–1291, doi:10.1175/JAS-D-13-0164.1.
- Frank, W. M., and E. A. Ritchie, 2001: Effects of vertical wind shear on the intensity and structure of numerically simulated hurricanes. *Mon. Wea. Rev.*, **129**, 2249–2269, doi:10.1175/1520-0493(2001)129<2249:EOVWSO>2.0.CO;2.
- Guimond, S. R., G. M. Heymsfield, and F. J. Turk, 2010: Multiscale observations of Hurricane Dennis (2005): The effects of hot towers on rapid intensification. *J. Atmos. Sci.*, **67**, 633–654, doi:10.1175/2009JAS3119.1.
- Hack, J. J., and W. H. Schubert, 1986: Nonlinear response of atmospheric vortices to heating by organized cumulus convection. *J. Atmos. Sci.*, **43**, 1559–1573, doi:10.1175/1520-0469(1986)043<1559:NROAVT>2.0.CO;2.
- Hendricks, E. A., M. T. Montgomery, and C. A. Davis, 2004: The role of “vortical” hot towers in the formation of Tropical Cyclone Diana (1984). *J. Atmos. Sci.*, **61**, 1209–1232, doi:10.1175/1520-0469(2004)061<1209:TROVHT>2.0.CO;2.
- Heymsfield, G. M., J. B. Halverson, J. Simpson, L. Tian, and T. P. Bui, 2001: ER-2 Doppler radar investigations of the eyewall of Hurricane Bonnie during the Convection and Moisture Experiment-3. *J. Appl. Meteor.*, **40**, 1310–1330, doi:10.1175/1520-0450(2001)040<1310:EDRIOT>2.0.CO;2.

EARLY STAGE EXPERIMENT  
*Science Description*

---

- Jones, S. C., 1995: The evolution of vortices in vertical shear. I: Initially barotropic vortices. *Quart. J. Roy. Meteor. Soc.*, **121**, 821–851, doi:10.1002/qj.49712152406.
- Kieper, M. E., and H. Jiang, 2012: Predicting tropical cyclone rapid intensification using the 37 GHz ring pattern identified from passive microwave measurements. *Geophys. Res. Lett.*, **39**, L13804, doi:10.1029/2012GL052115.
- Miyamoto, Y., and T. Takemi, 2015: A triggering mechanism for rapid intensification of tropical cyclones. *J. Atmos. Sci.*, **72**, 2666–2681, doi:10.1175/JAS-D-14-0193.1.
- Molinari, J., and D. Vollaro, 2010: Rapid intensification of a sheared tropical storm. *Mon. Wea. Rev.*, **138**, 3869–3885, doi:10.1175/2010MWR3378.1.
- Montgomery, M. T., M. Nicholls, T. Cram, and A. Saunders, 2006: A “vortical” hot tower route to tropical cyclogenesis. *J. Atmos. Sci.*, **63**, 355–386, doi:10.1175/JAS3604.1.
- Munsell, E.B., F. Zhang, J.A. Sippel, S.A. Braun, and Y. Weng, 2017: Dynamics and Predictability of the Intensification of Hurricane Edouard (2014). *J. Atmos. Sci.*, **74**, 573–595, doi: 10.1175/JAS-D-16-0018.1.
- Nguyen, L. T., and J. Molinari, 2012: Rapid intensification of a sheared, fast-moving hurricane over the Gulf Stream. *Mon. Wea. Rev.*, **140**, 3361–3378, doi:10.1175/MWR-D-11-00293.1.
- Nguyen, L. T., and J. Molinari, 2015: Simulation of the downshear reformation of a tropical cyclone. *J. Atmos. Sci.*, **72**, 4529–4551, doi:10.1175/JAS-D-15-0036.1.
- Nguyen, L.T., R.F. Rogers, and P.D. Reasor, 2017: Thermodynamic and kinematic influences on precipitation symmetry in sheared tropical cyclones: Bertha and Cristobal (2014). *Mon. Wea. Rev.*, in review.
- Nolan, D. S., and L. D. Grasso, 2003: Nonhydrostatic, three-dimensional perturbations to balanced, hurricane-like vortices. Part II: Symmetric response and nonlinear simulations. *J. Atmos. Sci.*, **60**, 2717–2745, doi:10.1175/1520-0469(2003)060<2717:NTPTBH>2.0.CO;2.
- Nolan, D. S., Y. Moon, and D. P. Stern, 2007: Tropical cyclone intensification from asymmetric convection: Energetics and efficiency. *J. Atmos. Sci.*, **64**, 3377–3405, doi:10.1175/JAS3988.1.
- Pendergrass, A. G., and H. E. Willoughby, 2009: Diabatically induced secondary flows in tropical cyclones. Part I: Quasi-steady forcing. *Mon. Wea. Rev.*, **137**, 805–821, doi:10.1175/2008MWR2657.1.

EARLY STAGE EXPERIMENT

*Science Description*

---

- Reasor, P. D., and M. D. Eastin, 2012: Rapidly intensifying Hurricane Guillermo (1997). Part II: Resilience in shear. *Mon. Wea. Rev.*, **140**, 425–444, doi:10.1175/MWR-D-11-00080.1.
- Reasor, P. D., M. D. Eastin, and J. F. Gamache, 2009: Rapidly intensifying Hurricane Guillermo (1997). Part I: Low-wavenumber structure and evolution. *Mon. Wea. Rev.*, **137**, 603–631, doi:10.1175/2008MWR2487.1.
- Reasor, P. D., R. F. Rogers, and S. Lorsolo, 2013: Environmental flow impacts on tropical cyclone structure diagnosed from airborne Doppler radar composites. *Mon. Wea. Rev.*, **141**, 2949–2969, doi:10.1175/MWR-D-12-00334.1.
- Rogers, R.F., 2010: Convective-scale structure and evolution during a high-resolution simulation of tropical cyclone rapid intensification. *J. Atmos. Sci.*, **67**, 44–70, doi:10.1175/2009JAS3122.1.
- Rogers, R., S. S. Chen, J. E. Tenerelli, and H. E. Willoughby, 2003: A numerical study of the impact of vertical shear on the distribution of rainfall in Hurricane Bonnie (1998). *Mon. Wea. Rev.*, **131**, 1577–1599, doi:10.1175//2546.1.
- Rogers, R., P. D. Reasor, and S. Lorsolo, 2013: Airborne Doppler observations of the inner-core structural differences between intensifying and steady-state tropical cyclones. *Mon. Wea. Rev.*, **141**, 2970–2991, doi:10.1175/MWR-D-12-00357.1.
- Rogers, R., P. D. Reasor, and J. A. Zhang, 2015: Multiscale structure and evolution of Hurricane Earl (2010) during rapid intensification. *Mon. Wea. Rev.*, **143**, 536–562, doi:10.1175/MWR-D-14-00175.1.
- Rogers, R.F., J.A. Zhang, J. Zawislak, H. Jiang, G.R. Alvey III, E.J. Zipser, and S.N. Stevenson, 2016: Observations of the structure and evolution of Hurricane Edouard (2014) during intensity change. Part II: Kinematic structure and the distribution of deep convection. *Mon. Wea. Rev.*, **144**, 3355–3376.
- Schubert, W. H., and J. J. Hack, 1982: Inertial stability and tropical cyclone development. *J. Atmos. Sci.*, **39**, 1687–1697, doi:10.1175/1520-0469(1982)039<1687:ISATCD>2.0.CO;2.
- Shapiro, L. J., and H. E. Willoughby, 1982: The response of balanced hurricanes to local sources of heat and momentum. *J. Atmos. Sci.*, **39**, 378–394, doi:10.1175/1520-0469(1982)039<0378:TROBHT>2.0.CO;2.
- Smith, R. K., and M. T. Montgomery, 2016: The efficiency of diabatic heating and tropical cyclone intensification. *Quart. J. Roy. Meteor. Soc.*, **142**, 2081–2086, doi:10.1002/qj.2804.

EARLY STAGE EXPERIMENT  
*Science Description*

---

- Stevenson, S. N., K. L. Corbosiero, and J. Molinari, 2014: The convective evolution and rapid intensification of Hurricane Earl (2010). *Mon. Wea. Rev.*, **142**, 4364–4380, doi:10.1175/MWR-D-14-00078.1.
- Tao, C., and H. Jiang, 2015: Distributions of shallow to very deep precipitation–convection in rapidly intensifying tropical cyclones. *J. Climate*, **28**, 8791–8824, doi:10.1175/JCLI-D-14-00448.1.
- Tao, C., H. Jiang, and J. Zawislak, 2017: The Relative Importance of Stratiform and Convective Rainfall in Rapidly Intensifying Tropical Cyclones. *Mon. Wea. Rev.*, **145**, 795–809, doi: 10.1175/MWR-D-16-0316.1.
- Vigh, J. L., and W. H. Schubert, 2009: Rapid development of the tropical cyclone warm core. *J. Atmos. Sci.*, **66**, 3335–3350, doi:10.1175/2009JAS3092.1.
- Wadler, J., R.F. Rogers, and P.D. Reasor, 2017: Radial and azimuthal variations in convective burst structure in tropical cyclones from airborne Doppler observations. *Mon. Wea. Rev.*, manuscript in review.
- Wu, L., S. A. Braun, J. Halverson, and G. Heymsfield, 2006: A numerical study of Hurricane Erin (2001). Part I: Model verification and storm evolution. *J. Atmos. Sci.*, **63**, 65–86, doi:10.1175/JAS3597.1.
- Zagrodnik, J. P., and H. Jiang, 2014: Rainfall, convection, and latent heating distributions in rapidly intensifying tropical cyclones. *J. Atmos. Sci.*, **71**, 2789–2809, doi:10.1175/JAS-D-13-0314.1.
- Zawislak, J., H. Jiang, G. R. Alvey III, E. J. Zipser, R. F. Rogers, J. A. Zhang, and S. N. Stevenson, 2016: Observations of the structure and evolution of Hurricane Edouard (2014) during intensity change. Part I: Relationship between the thermodynamic structure and precipitation. *Mon. Wea. Rev.*, **144**, 3333–3354, doi:10.1175/MWR-D-16-0018.1.
- Zhang, D.-L., and H. Chen, 2012: Importance of the upper level warm core in the rapid intensification of a tropical cyclone. *Geophys. Res. Lett.*, **39**, L02806, doi:10.1029/2012GL052355.
- Yuter, S. E., and R. A. Houze, 1995: Three-dimensional kinematic and microphysical evolution of Florida cumulonimbus. Part II: Frequency distributions of vertical velocity, reflectivity, and differential reflectivity. *Mon. Wea. Rev.*, **123**, 1941–1963, doi:10.1175/1520-0493(1995)123<1941:TDKAME>2.0.CO;2.



EARLY STAGE EXPERIMENT

*Science Description*

---

**SCIENCE OBJECTIVE #3:** *Improve our understanding of the physical processes responsible for the formation and evolution of arc clouds, as well as their impacts on TC structure and intensity in the short-term (Arc Cloud Module)*

**Motivation:** Arc clouds are common features in mid-latitude thunderstorms and mesoscale convective systems. They often denote the presence of a density current that forms when dry mid-level (~600–850 hPa) air has interacted with precipitation. The convectively-driven downdrafts that result reach the surface/near-surface and spread out from the convective core of the thunderstorm. Substantial arc clouds (i.e. >55 n mi (100 km) in length and lasting for several hours) are also common features in the tropics (Fig. ES-2), particularly on the periphery of African easterly waves (AEWs) and TCs. However, the physical processes responsible for such tropical arc clouds as well as their impacts on the short-term evolution of their parent disturbances are not well understood.

**Background:** Large low-level thunderstorm outflow boundaries emanating from TCs have been previously documented and have been hypothesized to occur when high vertical wind shear promotes the intrusion of dry mid-level air toward the TC eyewall (Knaff and Weaver 2000). However, the mid-level moisture found in the *moist tropical* North Atlantic sounding described by Dunion (2011) is hypothesized to be insufficiently dry to generate extensive near-surface density currents around an AEW or TC. However, Dunion (2011) also described two additional air masses that are frequently found in the tropical North Atlantic and Caribbean during the summer months and could effectively initiate the formation of large arc clouds: (1) the Saharan Air Layer (SAL) and (2) *mid-latitude dry air intrusions*. Both of these air masses were found to contain substantially dry air (~50% less moisture than the *moist tropical* sounding) in the mid-levels that could support convectively-driven downdrafts and large density currents. Furthermore, outward-propagating arc clouds on the periphery of AEWs or TCs could be enhanced by near-surface super-gradient winds induced by the downward transport of high momentum air. Since most developing tropical disturbances in the North Atlantic are associated with a mid-level jet and/or mesoscale convective vortex near a state of gradient balance, any convectively-driven downdrafts would inject high momentum air into a near-surface environment that often contains a weaker horizontal pressure gradient. In such cases, density currents may be temporarily enhanced during local adjustments to gradient balance. Finally, tropical arc clouds may be further enhanced by outward-propagating diurnal pulses that originate from the convective core of the tropical disturbance (see TC Diurnal Cycle objective in the Mature Stage Experiment). New GOES IR TC diurnal cycle imagery indicates that arc clouds tend to form along the leading edge of outwardly propagating diurnal pulses that are associated with the TC diurnal cycle. The diurnal pulses reach peripheral radii where low to mid-level dry air is often located (e.g. R=300–500 km) at remarkably predictable times of day (e.g. 400 km at ~1200–1500 LST). Therefore, UW-CIMSS real-time TC diurnal cycle and visible satellite imagery, as well as P-3 LF radar data (where TC diurnal pulses are denoted by 25+ dBZ semi-circular convective bands propagating away from the storm) will be used to monitor the diurnal pulse propagation throughout the local morning hours and signs of arc cloud formation.

## EARLY STAGE EXPERIMENT

### *Science Description*

As arc clouds propagate away from the tropical disturbance, they visibly emerge from underneath the central dense overcast that can obscure them from visible and infrared satellite view. Therefore, when arc clouds are identified using satellites, they are often in the middle to later stages of their lifecycles. Hence, the mechanism of enhanced low-level outflow is likely occurring at the time of satellite identification, while the mechanism of cooling/drying of the boundary layer has already occurred (though the effects may still be observable by aircraft flight-level, GPS dropsonde, and satellite data). This necessitates that the arc clouds be identified and sampled as early in their lifecycle as possible using available aircraft observations (e.g. flight-level, GPS dropsonde and P-3 LF radar, and P-3/G-IV Doppler radar data) and satellite imagery (e.g. TC diurnal cycle infrared, visible, infrared, and microwave).

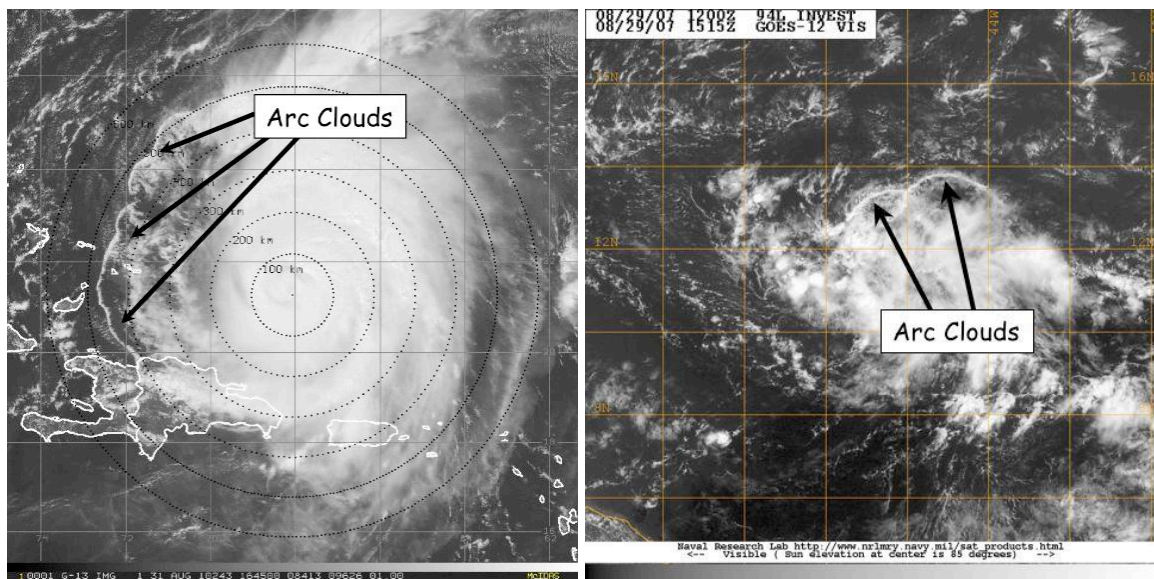


**Figure ES-2:** GOES visible satellite imagery showing arc clouds racing away from the convective cores of (left) 2003 Hurricane Isabel and (right) 2007 Pre-Tropical Depression Felix.

**Hypotheses:** Arc clouds form along the leading edge of TC diurnal pulses, are particularly favored to occur at R~105–215 n mi (~200–400 km) in areas with mid-level (~600–800 hPa) dry air ( $\leq 45$  mm total precipitable water [TPW]), and can act to temporarily stabilize the TC environment.

EARLY STAGE EXPERIMENT  
*Science Description*

---

**Aircraft Pattern/Module Descriptions:**

**P-3 Module #1: Arc Cloud**

**G-IV Module #1: Arc Cloud**

When arc clouds emanating from the periphery of the TC convective core are identified using satellite imagery and/or P-3 LF radar, perform this break-away pattern by transecting orthogonally across to these outwardly propagating features.

**Analysis Strategy:** This experiment seeks to collect observations across arc cloud features in the periphery of mature TCs using aircraft flight-level, GPS dropsonde, and TDR data to improve our understanding of the physical processes responsible for their formation and evolution, as well as how these features may affect TC structure and intensity in the short-term. Flight-level and GPS dropsonde data will be used to calculate changes in static stability and possible impacts on surface fluxes both ahead of and behind the arc cloud (e.g. enhanced stability/reduced surface fluxes behind the arc cloud leading edge). TDR data will be used to define the vertical structure of the kinematics ahead of, across and behind the arc cloud. Finally, kinematics and thermodynamics associated with arc cloud events will be compared to corresponding locations in model analysis fields (e.g. GFS and HWRF).

**References:**

- Dunion, J.P., 2011: Rewriting the climatology of the tropical North Atlantic and Caribbean Sea atmosphere. *J. Climate*, **24**, 893–908.
- Knaff, J.A., and J.F. Weaver, 2010: A mesoscale low-level thunderstorm outflow boundary associated with Hurricane Luis. *Mon. Wea. Rev.*, **128**, 3352–3355.

**MATURE STAGE EXPERIMENT**  
*Science Description*

---

**Investigator(s):** Paul Reasor, Jason Dunion (Co-PIs), Sim Aberson, Hui Christophersen, Paul Chang, Joe Cione, John Gamache, Heather Holbach, Ghassan Alaka, Kelly Ryan, Paul Leighton, Robert Rogers, Zorana Jelenak, Jun Zhang (Co-Is)

**Requirements:** Categories 2–5

**Science Objectives:**

- 1) Collect observations targeted at better understanding internal processes contributing to mature hurricane structure and intensity change. These processes include mixing between the eye and eyewall, secondary eyewall formation, the TC diurnal cycle, and gravity waves that emanate from the TC inner core [*IFEX Goal 3*]
- 2) Collect observations targeted at better understanding the response of mature hurricanes to their changing environment, including changes in vertical wind shear and underlying oceanic conditions [*IFEX Goal 3*]
- 3) Test new (or improved) technologies with the potential to fill gaps, both spatially and temporally, in the existing suite of airborne measurements in mature hurricanes. These measurements include improved three-dimensional representation of the hurricane wind field, more spatially dense thermodynamic sampling of the boundary layer, and more accurate measurements of ocean surface winds [*IFEX Goal 2*]

**Description of Science Objectives:**

**SCIENCE OBJECTIVE #1:** *Collect observations targeted at better understanding internal processes contributing to mature hurricane structure and intensity change. These processes include mixing between the eye and eyewall, secondary eyewall formation, the TC diurnal cycle, and gravity waves that emanate from the TC inner core*  
[Internal Processes]

TC DIURNAL CYCLE

**Motivation (TC Diurnal Cycle):** Numerous studies have documented the existence of diurnal maxima and minima associated with tropical convection. However, predicting the timing and extent of this variability remains a difficult challenge. Recent research using GOES satellite imagery has identified a robust TC diurnal cycle (TCDC) signal in mature storms that includes regularly occurring TC diurnal pulses. TC diurnal pulses can be tracked using new GOES infrared satellite image differencing that reveals a “cool ring” (i.e., diurnal pulse) in the infrared that begins forming near the storm’s inner core around local sunset each day. The TC diurnal pulse continues to propagate away from the storm overnight, reaching areas several hundred km from the storm center by the following afternoon. There appear to be significant structural changes to TCs (as indicated by GOES infrared and microwave (37 and 85 GHz) satellite imagery and P-3 LF radar data)

MATURE STAGE EXPERIMENT

*Science Description*

---

as TC diurnal pulses move out from the inner core each day and the timing of their radial propagation is remarkably predictable. Although the relationships between the TCDC and TC structure and intensity are unclear at this time, this phenomenon may be an important and fundamental TC process.

**Background (TC Diurnal Cycle):** Although numerous studies have documented the existence of diurnal maxima and minima associated with tropical oceanic convection and the TC upper-level cirrus canopy, we lack a thorough understanding of the nature and causes of these variations and especially the extent to which these variations are important for TCs. It is well known that the coherent diurnal cycle of deep cumulus convection and associated rainfall is different over the land and ocean (Gray and Jacobson 1977; Yang and Slingo 2001). While over the land it tends to peak in the late afternoon/early evening due to daytime boundary layer heating, over the ocean it peaks in the early morning. In addition, Gray and Jacobson (1977), Mapes and Houze (1993), and Liu and Moncrieff (1998) found that the oceanic peak was more prominent when the preexisting convection was more intense and associated with an organized weather system such as an African easterly wave or mesoscale convective system. Numerous studies have also highlighted diurnal changes in the cirrus anvils of tropical deep convection and TCs. Weikmann et al. (1977) noted that anvils emanating from large cumulonimbus clouds tended to grow preferably between 2200 and 0300 local standard time (LST). Browner et al. (1977) found that the areal extent of the TC cirrus canopy was a minimum at 0300 LST and a maximum at 1700 LST and suggested that this diurnal oscillation might be important for the TC. More recently, Kossin (2002) used storm-centered GOES infrared imagery to calculate azimuthally averaged brightness temperatures and create Hovmöller-type diagrams of brightness temperature diurnal oscillations over time. That study concluded that although a clear diurnal oscillation of the TC cirrus canopy was present at larger radii (e.g., 300 km), few storms exhibited diurnal oscillation signals in their innermost 100 km. It was hypothesized that different processes might be forcing periodic oscillations in the TC deep inner-core convection and the TC cirrus canopy.

Dunion et al. (2014) examined all North Atlantic major hurricanes from 2001 to 2010 and documented a phenomenon they referred to as the TC diurnal cycle and associated diurnal pulses in mature TCs. They found an intriguing diurnal pulsing pattern that appears to occur with remarkable regularity through a relatively deep layer of the TC. Storm-centered GOES and Meteosat infrared imagery were used to create 6-h brightness temperature difference fields of the storm's inner core and its surrounding environment (Radius,  $R$ , 5 100–600 km). The imagery reveals periodic oscillations of cooling and warming in the IR brightness temperature field over time. One prominent characteristic of these oscillations is a cold ring (i.e., local cooling of the brightness temperatures with time) that begins forming in the storm's inner core ( $R \leq 150$  km; Rogers et al. 2012) near the time of sunset each day. This cold ring feature (that they referred to as a TC diurnal pulse) continues to move away from the storm overnight, reaching areas several hundred kilometers from the circulation center by the following afternoon and is well-predicted by a TC diurnal clock that they developed (Fig. MA-1). A marked warming of the cloud tops

**MATURE STAGE EXPERIMENT**  
*Science Description*

occurs behind this propagating feature and structural changes in the storm are noted as it moves away from the inner core. This systematic variation of cloud-top temperatures suggests that TC diurnal pulses are a distinguishing characteristic of the TCDC and may have implications for TC intensity change and structure.

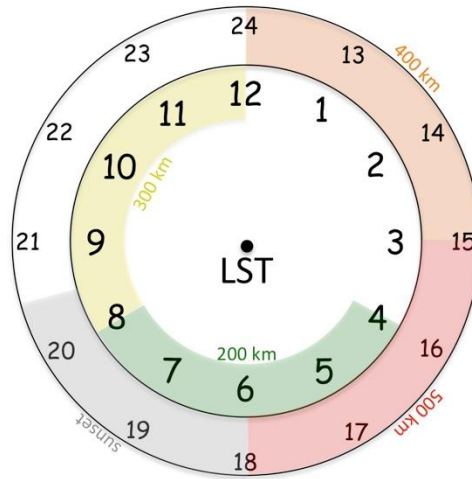


**Figure MA-1.** Conceptual 24-hr TCDC clock that estimates the radial location of TC diurnal pulses propagating away from storm. TC diurnal pulses typically form around local sunset (~1800–2030 LST, gray shading) and begin to propagate away from the inner core, passing 200 km radius at ~0400–0800 LST (green shading) the following morning. They reach 400 km radius at ~1200–1500 LST (orange shading) in the early to middle afternoon.

**Hypotheses (TC Diurnal Cycle):** The TC diurnal cycle and associated TC diurnal pulses manifest as semi-circular rings of enhanced convection that radially propagate away from the storm each day and are associated with periods of enhanced upper-level outflow and lower-level inflow that extend through a relatively deep layer of the troposphere.

**Aircraft Pattern/Module Descriptions:**

**P-3 Pattern #1: Internal Processes (TC Diurnal Cycle)**

For TCs exhibiting TC diurnal cycle signals, perform any standard pattern that provides symmetric coverage (e.g. Rotated Figure-4, Figure-4, Butterfly).

**G-IV Pattern #1: Internal Processes (TC Diurnal Cycle)**

For TCs exhibiting TC diurnal cycle signals, perform a standard G-IV Star with circumnavigation (optimal) or star (minimal) pattern.

**MATURE STAGE EXPERIMENT**  
*Science Description*

---

**Analysis Strategy (TC Diurnal Cycle):** This objective seeks to observe the formation and evolution of the TC diurnal cycle and associated TC diurnal pulses. GPS dropsonde and radar observations will be used to analyze both the inner-core and environmental kinematics and thermodynamics that may lead to the formation of TC diurnal pulses and to document the kinematics, thermodynamics, and precipitation patterns that are associated with radially propagating TC diurnal pulses at various stages of their evolution.

**References (TC Diurnal Cycle):**

- Browner, S. P., W. L. Woodley, and C. G. Griffith, 1977: Diurnal oscillation of cloudiness associated with tropical storms. *Mon. Wea. Rev.*, **105**, 856–864.
- Dunion, J.P., C.D. Thorncroft, and C.S. Velden, 2014: The tropical cyclone diurnal cycle of mature hurricanes. *Mon. Wea. Rev.*, **142**, 3900–3919.
- Gray, W. M., and R. W. Jacobson, 1977: Diurnal variation of deep cumulus convection. *Mon. Wea. Rev.*, **105**, 1171–1188.
- Kossin, J. P., 2002: Daily hurricane variability inferred from GOES infrared imagery. *Mon. Wea. Rev.*, **130**, 2260–2270.
- Liu, C., and M. W. Moncrieff, 1998: A numerical study of the diurnal cycle of tropical oceanic convection. *J. Atmos. Sci.*, **55**, 2329–2344.
- Mapes, B. E., and R. A. Houze Jr., 1993: Cloud clusters and superclusters over the oceanic warm pool. *Mon. Wea. Rev.*, **121**, 1398–1415.
- Rogers, R. F., S. Lorsolo, P. Reasor, J. Gamache, and F. Marks, 2012: Multiscale analysis of tropical cyclone kinematic structure from airborne Doppler radar composites. *Mon. Wea. Rev.*, **140**, 77–99.
- Weickmann, H. K., A. B. Long, and L. R. Hoxit, 1977: Some examples of rapidly growing oceanic cumulonimbus clouds. *Mon. Wea. Rev.*, **105**, 469–476.
- Yang, G., and J. Slingo, 2001: The diurnal cycle in the tropics. *Mon. Wea. Rev.*, **129**, 784–801.

**MATURE STAGE EXPERIMENT**  
*Science Description*

---

GRAVITY WAVE

**Motivation (Gravity Wave):** Internal gravity waves are ubiquitous in the atmosphere and are continuously generated by deep moist convection around the globe. Gravity waves play a critical role in the dynamical adjustment processes that keep the atmosphere close to hydrostatic and geostrophic wind balance, by redistributing localized heating over larger distances. Numerical simulations showed gravity waves radiating from the eyewall region to the outer core in TCs. TC convection produces gravity waves that propagate both upward and outward. This module is designed to observe smaller scale gravity waves, with radial wavelengths of 2 to 20 km, that radiate outward from the TC core with phase speeds of 20 to 30 m s<sup>-1</sup>. The goal is to quantify how the characteristics of these waves are tied to TC intensity and intensity change.

**Background (Gravity Wave):** Gravity waves exist due to the natural restoring force associated with the static stability of the atmosphere (Markowski and Richardson 2010; Sutherland 2010). Most gravity wave generation is associated with three processes: 1) the interaction of the atmospheric flow with topography, 2) rapidly evolving imbalances of the large-scale flow, and 3) disruptions to the atmosphere by moist convection. Visual evidence for these waves existing in TCs was documented in the early study by Black (1983), who analyzed features in cloud tops using stereoscopic analysis of photographs taken from hand-held cameras on the Skylab space station. Simulations with mesoscale atmospheric models have reproduced these features, which generally have wavelengths of tens to hundreds of km (Kim et al. 2009). These waves propagate long distances and their influences on the atmospheric boundary layer have also been observed (Niranjan-Kumar et al. 2014).

These waves can be observed by research aircraft and surface instruments (Nolan and Zhang 2017). The flight-level data reveal waves with radial wavelengths of 2–10 km, and by compositing the data from inbound and outbound flight legs separately, an outward phase speed of 20–25 m s<sup>-1</sup> can be inferred. Data from a research buoy in the Pacific also show evidence for the effects of the gravity waves on surface pressure and wind speed, with periods around 1000 s and 2000 s. Numerical simulations reproduce these waves and indicate distinct vertical structures for the dominant modes, with peaks in amplitude of vertical velocity near the tropopause and in the lower troposphere (Nolan and Zhang 2017). The simulations also indicate that TC intensity can be correlated with the amplitudes of these wave signals. Thus, analysis of atmospheric gravity waves may be a more direct approach for remote monitoring of TC intensity.

**Hypotheses (Gravity Wave):** Gravity waves radiating from the TCs inner core are prevalent in TCs and their wave amplitudes correlate with TC intensity.

**Aircraft Pattern/Module Descriptions:**

**P-3 Module #1: Internal Processes (Gravity Wave)**



**MATURE STAGE EXPERIMENT**  
*Science Description*

---

For mature stage TCs, after completing Figure-4 pattern, at the end of the last leg, continue outward to distance of 160 n mi from the center, or further, if possible. Then turn P-3 back to the eye. This module ideally should be conducted in quadrant with the least rainband activity, typically the upshear right or right-real quadrant.

**Analysis Strategy (Gravity Wave):** This module seeks to observe the characteristics of the TC gravity waves. Flight-level wind observations will be used to analyze the wavelengths and amplitudes of these waves. The vertical velocity will be quality controlled by correcting the attack angle and dynamical pressure using specially designed modules conducted by calibration flights before each hurricane season (Zhang 2010; Zhang and Drennan 2012). To avoid the contamination of the spectra by convection near the eyewall, only data from at least 100 km away from the storm center are used. The power spectrum will be computed using a fast Fourier Transform (FFT) algorithm to estimate the peak wavelengths of these waves.

**References (Gravity Wave):**

- Black, P. G., (1983), Tropical storm structure revealed by stereoscopic photographs from Skylab. *Adv. Space Res.*, **2**, No. 6, 115–124.
- Kim, S.-Y., H.-Y. Chun, and D. L. Wu (2009), A study on stratospheric gravity waves generated by Typhoon Ewiniar: Numerical simulations and satellite observations. *J. Geophys. Res.*, **114**, D22104.
- Markowski, P., and Y. Richardson (2010), *Mesoscale meteorology in mid-latitudes*. Wiley-Blackwell, Hoboken, New Jersey, 430 pp.
- Niranjan Kumar, K., Ch. Kanaka Rao, A. Sandeep, and T. N. Rao (2014), SODAR observations of inertia-gravity waves in the atmospheric boundary layer during the passage of tropical cyclone. *Atmos. Sci. Lett.*, **15**, 120–126.
- Nolan, D.S., and J.A. Zhang, 2017: Spiral gravity waves radiating from tropical cyclones. *Geophysical Research Letters*, **44**(8):3924–3931, doi:10.1002/2017GL073572.
- Sutherland, B. R., *Internal Gravity Waves* (2010). Cambridge University Press, New York, 377 pp.
- Zhang, J. A., (2010), Spectral characteristics of turbulence in the hurricane boundary layer over the ocean between the outer rainbands. *Quart. J. Roy. Meteorol. Soc.*, **136**, 918–926.
- Zhang, J. A., and W. M. Drennan (2012), An observational study of vertical eddy diffusivity in the hurricane boundary layer. *J. Atmos. Sci.*, **69**, 3223–3236.

**MATURE STAGE EXPERIMENT**  
*Science Description*

---

SECONDARY EYEWALL FORMATION (SEF)

**Motivation (SEF):** Secondary eyewall formation (SEF) and eyewall replacement cycles (ERCs) frequently occur during the mature phase of the TC lifecycle. These processes typically result in a halting of the intensification of a TC, and occasionally lead to a temporary weakening as the secondary eyewall becomes the dominant eyewall (Sitkowski et al. 2011). Additionally, they typically lead to a significant broadening of the wind field, increasing the total kinetic energy of the storm and thus the risks from storm surge. Statistical analysis of a 10-year (1997–2007) dataset shows that 77% of major hurricanes (120 knots or higher) in the Atlantic Ocean, 56% in the eastern Pacific, 81% in the western Pacific, and 50% in the Southern Hemisphere underwent at least one ERC (Hawkins and Helveston 2008). Despite the relative frequency of their occurrence, operational forecasting of SEF/ERCs remains a great challenge, partly since there is no consensus on the mechanisms responsible for SEF or ERC.

**Background (SEF):** There are a wide variety of studies that aim to understand SEF and ERC with different emphases on the internal dynamics and external environmental forcing. The axisymmetric balanced flow, constrained by heat and tangential momentum forcing, generally satisfies gradient wind and hydrostatic balance above the boundary layer (BL) (Abarca and Montgomery 2013). From the perspective of diabatic forcing, Rozoff et al. (2012) proposed that a sustained azimuthal-mean latent heating outside of the primary eyewall could lead to SEF. This hypothesis was supported by the numerical simulations given by Zhu and Zhu (2014). In a similar sense, diabatic heating/cooling associated with rainbands plays an important role in the structure and intensity change of the storm (Wang 2009; Li et al. 2014; Moon and Nolan 2010; Didlake and Houze 2013a, b) and thus they may also contribute to the SEF/ERC. Didlake and Houze (2013a) proposed that there exists a critical zone where sufficiently high vertical shear of the radial wind can limit the altitude of the convectively induced supergradient flow, leading to low-level convergence in this radial zone and allowing the convection to develop into a secondary eyewall. Corbosiero and Torn (2016) proposed a hypothesis that an increase of convergence induced by the cold pool that formed from convectively-driven downdrafts and low-level radial inflow could enhance rainband convection and lead to SEF. The roles of convective and stratiform heating profiles in rainbands in modifying hurricane structure and intensity, and potentially SEF, is an area of ongoing research.

Montgomery and Kallenbach (1997) proposed that vortex Rossby wave (VRW) interaction with the mean flow may contribute to SEF. VRWs, supported by the radial vorticity gradient outside of the radius of the maximum wind (RMW), propagate from the primary eyewall radially outward until they reach their stagnation radius. At this stagnation radius, inward-moving cyclonic eddy momentum may contribute to SEF. The role of VRWs in SEF is further examined in high-resolution hurricane simulations by Abarca and Corbosiero (2011). Judt and Chen (2010), by contrast, downplayed the importance of VRWs, and instead attributed the large accumulation of convectively generated PV through eddy heating in the rainband region as an essential factor for SEF.

**MATURE STAGE EXPERIMENT**

*Science Description*

---

In contrast to the balanced arguments discussed above, unbalanced dynamics in the BL have also been recognized as an important element in SEF. In this framework, the axisymmetric flow in the BL does not satisfy gradient wind and thermal wind balance. Several studies (Wu et al. 2011; Huang et al. 2012; Abarca and Montgomery 2013) have pointed out that the precursors of SEF include the broadening of the tangential wind field and the intensification of inflow in the BL, followed by development of supergradient winds and an enhanced horizontal convergence. In-situ observations also demonstrated this existence of supergradient flow (Didlake and Houze 2011; Bell et al. 2012). Kepert (2013) specifically examined the role of the BL in a balanced vortex framework. He proposed that the BL contributed to the SEF and ERC through a positive feedback mechanism that involves a local enhancement of the radial gradient of vorticity, frictionally forced updraft and convection. Moon et al. (2010) attributed the local vorticity enhancement from processes such as rainband convection.

To test the varying mechanisms proposed to explain SEF and ERC, it is important to obtain kinematic and thermodynamic observations near the eyewall and rainbands. In particular, since most previous analyses focus on azimuthally averaged quantities, it is important to obtain adequate azimuthal and radial sampling both near the primary eyewall and a potentially-developing secondary eyewall. For example, Abarca et al. (2016) pointed out the lack of data particularly at radial distance between 120–200 km in Hurricane Edouard (2014). Additionally, some measure of kinematic and thermodynamic structures along a rainband/developing secondary eyewall can be used to evaluate the along-band structures (Wang 2009; Moon and Nolan 2010; Didlake and Houze 2011, 2013a,b). Observations sampled through this module can be used to evaluate the different proposed mechanisms of SEF and ERC. Data-impact studies on TC analyses and forecasts can also be conducted using the OSSE approach to find optimal sampling strategies for the prediction of SEF/ERC. If this module is flown every 12 h (e.g., in conjunction with the TDR experiment), then the temporal resolution will provide an opportunity to evaluate the importance of the various proposed mechanisms at different stages in the evolution of the secondary eyewall. The dataset from this module eventually will benefit our understanding of the dynamic and physical processes that are responsible for SEF/ERC.

*The main objectives of the SEF/ERC module are:*

- Perform analyses with sampled observations to examine key factors that are responsible for SEF/ERCs;
- Validate key features linked with different hypotheses of SEF/ERCs using observations;
- Conduct OSE/OSSE studies to optimize sampling strategies for improving SEF/ERC predictions;
- Improve understanding of the dynamic and physical processes of SEF/ERCs.

**Hypotheses (SEF):** Secondary eyewall formation could be attributed from an unbalanced boundary layer spin-up paradigm. The precursors of SEF include the broadening of the

**MATURE STAGE EXPERIMENT**  
*Science Description*

---

tangential wind field and the intensification of inflow in the boundary layer, followed by development of supergradient winds and an enhanced horizontal convergence.

**Aircraft Pattern/Module Descriptions:**

**P-3 Module #2: Internal Processes (Pre-SEF)**

**P-3 Module #3: Internal Processes (Post-SEF)**

**G-IV Module #1: Internal Processes (SEF)**

This module focuses on mature hurricanes (e.g., category 2 or stronger) with a well-defined eye as seen in visible, infrared, and microwave satellite imagery. Sampling can be achieved in combination with the P-3 Doppler Wind Lidar, Coyote UAS, P-3 and G-IV dropsondes. This module can generally be flown in conjunction with TDR Experiment survey patterns, with the addition of either a spiral pattern (Pre-SEF) or moat circumnavigation (Post-SEF) added onto the survey. The module can also be flown for the TC Diurnal Cycle objective.

**Analysis Strategy (SEF):** Data collected by the pre-SEF module can be used to diagnose different roles in SEF. Specifically, gradient wind (and departures thereof) within and above the BL can be calculated from dropsondes; tangential winds and vorticity can be calculated from dropsonde, Doppler radar, flight-level, and DWL measurements; and moist static energy calculation, can be calculated from dropsondes. Observations that are collected can also be used to conduct data impact studies as well as provide insights for OSSE studies. Data measured by the post-SEF module would be useful to diagnose the formation and characteristics of the moat region and its role in ERC. Azimuthal coverage of the data would be particularly important to carry out analysis to validate different hypotheses of SEF/ERC.

**References (SEF):**

- Abarca, S. F., and K. L. Corbosiero, 2011: Secondary eyewall formation in WRF simulations of Hurricanes Rita and Katrina (2005). *Geophys. Res. Lett.*, **38**, 1–5.
- Abarca, S. F., and M. T. Montgomery, 2013: Essential Dynamics of Secondary Eyewall Formation. *J. Atmos. Sci.*, **70**, 3216–3230.
- Abarca, S. F., M. T. Montgomery, S. Braun, and J. Dunion, 2016: Secondary Eyewall Dynamics as Captured by an Unprecedented Array of GPS Dropsondes Deployed into Edouard 2014, 32nd Conf. on Hurricanes and Tropical Meteorology, San Juan, PR.
- Bell, M. M., M. T. Montgomery, and W.-C. Lee, 2012: An Axisymmetric View of Concentric Eyewall Evolution in Hurricane Rita (2005). *J. Atmos. Sci.*, **69**, 2414–2432.

MATURE STAGE EXPERIMENT

*Science Description*

---

- Corbosiero K. L., and R. D. Torn, 2016: Diagnosis of Secondary Eyewall Formation Mechanisms in Hurricane Igor (2010), 32nd Conf. on Hurricanes and Tropical Meteorology, San Juan, PR.
- Didlake Jr., A. C., and R. A. Houze, 2011: Kinematics of the Secondary Eyewall Observed in Hurricane Rita (2005). *J. Atmos. Sci.*, **68**, 1620–1636.
- Didlake, Jr., A. C., and R. A. Houze, 2013a: Convective-Scale Variations in the Inner-Core Rainbands of a Tropical Cyclone. *J. Atmos. Sci.*, **70**, 504–523.
- Didlake, A. C., and R. A. Houze, 2013b: Dynamics of the Stratiform Sector of a Tropical Cyclone Rainband. *J. Atmos. Sci.*, **70**, 1891–1911.
- Hawkins, J. D., and M. Helveston, 2008: Tropical cyclone multiple eyewall characteristics. Preprints, 28th Conf. on Hurricanes and Tropical Meteorology, Amer. Meteor. Soc., Orlando, FL.
- Huang, Y.-H., M. T. Montgomery, and C.-C. Wu, 2012: Concentric Eyewall Formation in Typhoon Sinlaku (2008). Part II: Axisymmetric Dynamical Processes. *J. Atmos. Sci.*, **69**, 662–674.
- Judt, F., and S. S. Chen, 2010: Convectively Generated Potential Vorticity in Rainbands and Formation of the Secondary Eyewall in Hurricane Rita of 2005. *J. Atmos. Sci.*, **67**, 3581–3599.
- Kepert, J. D., 2013: How does the boundary layer contribute to eyewall replacement cycles in axisymmetric tropical cyclones? *J. Atmos. Sci.*, **70**, 2808–2830.
- Li, Q., Y. Wang, and Y. Duan, 2014: Effects of Diabatic Heating and Cooling in the Rapid Filamentation Zone on Structure and Intensity of a Simulated Tropical Cyclone. *J. Atmos. Sci.*, **71**, 3144–3163.
- Montgomery, M. T., and R. J. Kallenbach, 1997: A theory for vortex Rossby-waves and its application to spiral bands and intensity changes in hurricanes. *Quart. J. Roy. Meteor. Soc.*, **123**, 435–465.
- Moon, Y., and D. S. Nolan, 2010: The Dynamic Response of the Hurricane Wind Field to Spiral Rainband Heating. *J. Atmos. Sci.*, **67**, 1779–1805.
- Moon, Y., D. S. Nolan, and M. Iskandarani, 2010: On the Use of Two-Dimensional Incompressible Flow to Study Secondary Eyewall Formation in Tropical Cyclones. *J. Atmos. Sci.*, **67**, 3765–3773.

MATURE STAGE EXPERIMENT

*Science Description*

---

- Rozoff, C. M., D. S. Nolan, J. P. Kossin, F. Zhang, and J. Fang, 2012: The Roles of an Expanding Wind Field and Inertial Stability in Tropical Cyclone Secondary Eyewall Formation. *J. Atmos. Sci.*, 69, 2621–2643.
- Sitkowski, M., J. P. Kossin, and C. M. Rozoff, 2011: Intensity and Structure Changes during Hurricane Eyewall Replacement Cycles. *Mon. Wea. Rev.*, 139, 3829–3847.
- Wang, Y., 2009: How Do Outer Spiral Rainbands Affect Tropical Cyclone Structure and Intensity?. *J. Atmos. Sci.*, 66, 1250–1273.
- Wu, C.-C., Y.-H. Huang, and G.-Y. Lien, 2012: Concentric Eyewall Formation in Typhoon Sinlaku (2008). Part I: Assimilation of T-PARC Data Based on the Ensemble Kalman Filter (EnKF). *Mon. Wea. Rev.*, 140, 506–527.
- Zhu, Z.-D., and P. Zhu, 2014: The role of outer rainband convection in governing the eyewall replacement cycle in numerical simulations of tropical cyclones, *J. Geophys. Res. Atmos.*, 119, 8049–8072.

EYE-EYEWALL MIXING

**Motivation and Background (Eye-Eyewall Mixing):** Eyewall mesovortices have been hypothesized to mix high-entropy air from the eye into the eyewall, thus increasing the amount of energy available to the hurricane. Signatures of such mesovortices have been seen in cloud formations within the eyes of strong TCs, in radar reflectivity signatures (Hurricane Fabian), and from above during aircraft penetrations (Hurricanes Hugo and Felix). Doppler radar was able to sample such features in Hurricanes Hugo and Felix, though interpretation with sparse observations through the small features has been difficult. Dropwindsondes released in very intense tropical cyclones, in conjunction with large-eddy simulations, have provided some thermodynamic data. However, the kinematic and thermodynamic structures of these features have never been directly observed. Observations within the eye near or below the inversion can allow for the study of the these mesovortices and improve knowledge of small-scale features and intensity changes in very strong TCs.

**Hypotheses (Eye-Eyewall Mixing):** Eyewall mesovortices play an important role in TC intensity change.

**Aircraft Pattern/Module Descriptions:**

**P-3 Module #4: Internal Processes (Eye-Eyewall Mixing)**

This is a break-away pattern that is compatible with any standard pattern with an eye passage (all P-3 patterns except the Square spiral or Lawnmower). The P-3 will penetrate the eyewall at the standard-pattern altitude. Once inside the eye, the

MATURE STAGE EXPERIMENT

*Science Description*

---

P-3 will descend to a safe altitude below the inversion while performing a Figure-4 pattern. The leg lengths will be determined by the eye diameter, with the ends of the legs at least 2 n mi from the edge of the eyewall. Upon completion of the descent, the P-3 will circumnavigate the eye about 2 n mi from the edge of the eyewall in the shape of a pentagon or hexagon. Time permitting; another Figure-4 will be performed during ascent to the original flight level. Depending upon the size of the eye, this pattern should take between 0.5 and 1 h. The module need only be done once and will then be evaluated for the future.

**Analysis Strategy (Eye-Eyewall Mixing):** The data will be examined to look for meso- or miso-scale vortices at the eye-eyewall interface. Analyses with an advanced data assimilation system will also be conducted.

**References (Eye-Eyewall Mixing):**

Aberson, S. D., J. A. Zhang, and K. Nunez-Ocasio, 2017: An extreme event in the eyewall of Hurricane Felix on 2 September 2007. *Mon. Wea. Rev.*, in press.

Aberson, S. D., J. P. Dunion, and F. D. Marks, 2006: A photograph of a wavenumber-2 asymmetry in the eye of Hurricane Erin. *J. Atmos. Sci.*, **63**, 387–391.

Aberson, S. D., M. T. Montgomery, M. M. Bell, and M. L. Black. 2006: Hurricane Isabel (2003): New insights into the physics of intense storms. Part II: Extreme localized wind. *Bull. Amer. Met. Soc.*, **87**, 1349–1354.

Marks, F.D., P.G. Black, M.T. Montgomery, and R.W. Burpee. Structure of the eye and eyewall of Hurricane Hugo (1989). *Mon. Wea. Rev.*, **136**, 1237–1259.

Rogers, R. F., S. Aberson, M. M. Bell, D. J. Cecil, J. D. Doyle, T. B. Kimberlain, J. Morgerman, L. K. Shay, and C. Velden, 2017: Re-writing the tropical record books: The extraordinary intensification of Hurricane Patricia (2015). *Bull. Amer. Met. Soc.*, in press.

Stern, D. P., G. H. Bryan, and S. D. Aberson, 2016: Extreme low-level updrafts and wind speeds measured by dropsondes in tropical cyclones. *Mon. Wea. Rev.*, **144**, 2177–2204.

MATURE STAGE EXPERIMENT  
*Science Description*

---

**SCIENCE OBJECTIVE #2:** *Collect observations targeted at better understanding the response of mature hurricanes to their changing environment, including changes in vertical wind shear and underlying oceanic conditions [Environment Interaction]*

TC IN SHEAR

**Motivation (TC in Shear):** Although most TCs in HRD's data archive experience some degree of vertical wind shear (VWS), the timing of flights with respect to the shear evolution and the spatial sampling of kinematic and thermodynamic variables have not always been carried out in an optimal way for testing hypotheses regarding shear-induced modifications of TC structure and their impact on intensity change (see below). This objective will sample the TC at distinct phases of its interaction with VWS and measure kinematic and thermodynamic fields with the azimuthal and radial coverage necessary to test existing hypotheses.

**Background (TC in Shear):** Recently, Riemer et al. (2010) and Riemer et al. (2013) have proposed an intensity modification mechanism rooted in a balance-dynamics framework. They argue that balanced vorticity asymmetry at low levels, generated outside the core through shear forcing, organizes convection outside the eyewall into a wavenumber-1 pattern through frictional convergence. Downdrafts associated with this vortex-scale convective asymmetry arise as precipitation generated by the convective updrafts falls into unsaturated air below. In their simulations, the downdrafts led to a vortex-scale transport of low equivalent potential temperature ( $\theta_e$ ) air into the inflow layer and disruption of the TC heat engine (Emanuel 1986, 1991). If particularly low  $\theta_e$  air at lower to middle levels of the environment is able to reach the core region where convective enhancement occurs, the thermodynamic impacts of the downward transport of low  $\theta_e$  air would be enhanced. Riemer and Montgomery (2011) proposed a simple kinematic model for this environmental interaction, quantifying the shear-induced distortion of the "moist envelope" surrounding the TC core as a function of shear strength, vortex size, and vortex intensity.

In the simulations of Riemer et al. (2010), the TC core region developed vertical tilt following its initial encounter with VWS, but then realigned, i.e., the vortex was resilient. The problem of dynamic resilience focuses on the ability of the TC to maintain a vertically-coherent vortex structure as it experiences vertical shearing. Jones (1995) found that coupling between vertical layers, and the tendency for the upper- and lower-level potential vorticity (PV) of the cyclonic core to precess upshear, restricts the development of vertical tilt that would otherwise occur through differential advection. For small-amplitude tilt, Reasor et al. (2004) developed a balance theory for the shear forcing of vortex tilt in which the tilt asymmetry behaves as a vortex-Rossby wave. In this vortex-Rossby wave framework, they developed a heuristic model for the TC in shear, which predicts a left-of-shear tilt equilibrium. Furthermore, they demonstrated that the evolution towards this equilibrium tilt state depends not only on intrinsic scales of the flow (e.g., Rossby number and Rossby deformation radius), but also on the radial



MATURE STAGE EXPERIMENT

*Science Description*

---

distribution of (potential) vorticity in the core region. Reasor and Montgomery (2015) have recently evaluated this heuristic model. The model is capable of predicting the enhancement of resilience that arises as the PV gradient outside the core increases. Even when moist neutral conditions exist within the eyewall, the model still describes the long-time evolution of the tilt asymmetry outside the eyewall.

**Hypotheses (TC in Shear):** Vertical wind shear inhibits TC intensification through the downward transport of low-entropy air into the inflow layer outside the eyewall, brought on by vortex-tilt-induced organization of convection there.

**Aircraft Pattern/Module Descriptions:**

**P-3 Pattern #1: Environment Interaction (TC in Shear)**

Prior to an increase in vertical wind shear, perform a Figure-4 pattern (orientation chosen for efficiency) with TDR to obtain the TC core structure. As time permits, the aircraft executes a second, rotated Figure-4 pattern.

**P-3 Pattern #2: Environment Interaction (TC in Shear)**

Following an increase in vertical wind shear (~12 h after *P-3 Pattern #1: Environment Interaction*), perform a single Figure-4 pattern with TDR to obtain the TC core-region structure. Then travel downwind to set up a rotated Figure-4 pattern with truncated radial legs. The radial legs should extend just outside the primary mesoscale region of convection radially beyond (~15–30 n mi) the eyewall. Dropsondes should be launched within and downwind of the convective region outside the eyewall in such a way as to sample low-entropy air spiraling into the eyewall within the boundary layer. Repeat every 12 h.

**G-IV Pattern #1: Environment Interaction (TC in Shear)**

Perform storm-relative environmental TDR and dropsonde sampling through clockwise circumnavigation, starting at 150 n mi, moving inward to 90 n mi, and finishing at 60 n mi. This pattern should be coordinated with *P-3 Pattern #1: Environment Interaction (TC in Shear)* during the pre-shear stage and then 24 h later with *P-3 Pattern #2: Environment Interaction (TC in Shear)*. A primary objective of the coordinated P-3 and G-IV dropsonde sampling is to document the evolution of the moist envelope surrounding the core.

**Analysis Strategy (TC in Shear):** The basic analysis follows that presented in recent observational studies of the vertically sheared TC (Reasor et al. 2009; Reasor and Eastin 2012; Reasor et al. 2013; Rogers et al. 2013; Zhang et al. 2013). The analysis includes: low-wavenumber kinematic structure of the core region above the boundary layer, vortex tilt, and local VWS derived from airborne Doppler radar observations; low-wavenumber kinematic structure of the boundary layer derived from SFMR and dropsonde

MATURE STAGE EXPERIMENT

*Science Description*

---

measurements; low-wavenumber thermodynamic structure within and above the boundary layer derived from dropsondes and flight-level measurements; and convective burst statistics derived from Doppler radar observations. New elements of the analysis will include: 3-D kinematic structure out to at least 4–5xRMW using radar observations; low-wavenumber kinematic, thermodynamic, and moisture structures out to 150 n mi using G-IV radar and dropsonde observations; high azimuthal and radial representation of the inflow structure downwind of the mesoscale-organized convection radially outside the eyewall.

**References (TC in Shear):**

- Emanuel, K. A., 1986: An air-sea interaction theory for tropical cyclones. Part I: Steady-state maintenance. *J. Atmos. Sci.*, **43**, 585–605.
- Emanuel, K. A., 1991: The theory of hurricanes. *Annu. Rev. Fluid Mech.*, **23**, 179–196.
- Jones, S. C., 1995: The evolution of vortices in vertical shear. I: Initially barotropic vortices. *Quart. J. Roy. Meteor. Soc.*, **121**, 821–851.
- Reasor, P. D., M. T. Montgomery, and L. D. Grasso, 2004: A new look at the problem of tropical cyclones in vertical shear flow: Vortex resiliency. *J. Atmos. Sci.*, **61**, 3–22.
- Reasor, P. D., M. Eastin, and J. F. Gamache, 2009: Rapidly intensifying Hurricane Guillermo (1997). Part I: Low-wavenumber structure and evolution. *Mon. Wea. Rev.*, **137**, 603–631.
- Reasor, P. D., and M. D. Eastin, 2012: Rapidly intensifying Hurricane Guillermo (1997). Part II: Resilience in shear. *Mon. Wea. Rev.*, **140**, 425–444.
- Reasor, P. D., R. Rogers, and S. Lorsolo, 2013: Environmental flow impacts on tropical cyclone structure diagnosed from airborne Doppler radar composites. *Mon. Wea. Rev.*, **141**, 2949–2969.
- Reasor, P. D., and M. T. Montgomery, 2015: Evaluation of a heuristic model for tropical cyclone resilience. *J. Atmos. Sci.*, **72**, 1765–1782.
- Riemer, M., M. T. Montgomery, and M. E. Nicholls, 2010: A new paradigm for intensity modification of tropical cyclones: thermodynamic impact of vertical wind shear on the inflow layer. *Atmos. Chem. Phys.*, **10**, 3163–3188.
- Riemer, M., and M. T. Montgomery, 2011: Simple kinematic models for the environmental interaction of tropical cyclones in vertical wind shear. *Atmos. Chem. Phys.*, **11**, 9395–9414.

MATURE STAGE EXPERIMENT

*Science Description*

---

Riemer, M., M. T. Montgomery, and M. E. Nicholls, 2013: Further examination of the thermodynamic modification of the inflow layer of tropical cyclones by vertical wind shear. *Atmos. Chem. Phys.*, **13**, 327–346.

Rogers, R., P. Reasor, and S. Lorsolo, 2013: Airborne Doppler observations of the inner-core structural differences between intensifying and steady-state tropical cyclones. *Mon. Wea. Rev.*, **141**, 2970–2971.

Zhang, J. A., R. F. Rogers, P. D. Reasor, E. W. Uhlhorn, and F. D. Marks Jr., 2013: Asymmetric hurricane boundary layer structure in relation to the environmental vertical wind shear from dropsonde composites. *Mon. Wea. Rev.*, **141**, 3968–3984.

ARC CLOUD

**Motivation (Arc Cloud):** Arc clouds are common features in mid-latitude thunderstorms and mesoscale convective systems. They often denote the presence of a density current that forms when dry mid-level (~600–850 hPa) air has interacted with precipitation. The convectively-driven downdrafts that result reach the surface/near-surface and spread out from the convective core of the thunderstorm. Substantial arc clouds (i.e. >55 n mi (100 km) in length and lasting for several hours) are also common features in the tropics (Fig. MA-2), particularly on the periphery of African easterly waves (AEWs) and TCs. However, the physical processes responsible for such tropical arc clouds as well as their impacts on the short-term evolution of their parent disturbances are not well understood.

**Background (Arc Cloud):** Large low-level thunderstorm outflow boundaries emanating from TCs have been previously documented and have been hypothesized to occur when high vertical wind shear promotes the intrusion of dry mid-level air toward the TC eyewall (Knaff and Weaver 2000). However, the mid-level moisture found in the *moist tropical* North Atlantic sounding described by Dunion (2011) is hypothesized to be insufficiently dry to generate extensive near-surface density currents around an AEW or TC. However, Dunion (2011) also described two additional air masses that are frequently found in the tropical North Atlantic and Caribbean during the summer months and could effectively initiate the formation of large arc clouds: (1) the Saharan Air Layer (*SAL*) and (2) *mid-latitude dry air intrusions*. Both of these air masses were found to contain substantially dry air (~50% less moisture than the *moist tropical* sounding) in the mid-levels that could support convectively-driven downdrafts and large density currents. Furthermore, outward-propagating arc clouds on the periphery of AEWs or TCs could be enhanced by near-surface super-gradient winds induced by the downward transport of high momentum air. Since most developing tropical disturbances in the North Atlantic are associated with a mid-level jet and/or mesoscale convective vortex near a state of gradient balance, any convectively-driven downdrafts would inject high momentum air into a near-surface environment that often contains a weaker horizontal pressure gradient. In such cases, density currents may be temporarily enhanced during local adjustments to gradient balance. Finally, tropical arc clouds may be further

## MATURE STAGE EXPERIMENT

### *Science Description*

enhanced by outward-propagating diurnal pulses that originate from the convective core of the tropical disturbance (see the TC Diurnal Cycle objective). New GOES IR TC diurnal cycle imagery indicates that arc clouds tend to form along the leading edge of outwardly propagating diurnal pulses that are associated with the TC diurnal cycle. The diurnal pulses reach peripheral radii where low to mid-level dry air is often located (e.g. Radius, R, 300–500 km) at remarkably predictable times of day (e.g. 400 km at ~1200–1500 LST). Therefore, UW-CIMSS real-time TC diurnal cycle and visible satellite imagery, as well as P-3 LF radar data (where TC diurnal pulses are denoted by 25+ dBZ semi-circular convective bands propagating away from the storm) will be used to monitor the diurnal pulse propagation throughout the local morning hours and signs of arc cloud formation.

As arc clouds propagate away from the tropical disturbance, they visibly emerge from underneath the central dense overcast that can obscure them from visible and infrared satellite view. Therefore, when arc clouds are identified using satellites, they are often in the middle to later stages of their lifecycles. Hence, the mechanism of enhanced low-level outflow is likely occurring at the time of satellite identification, while the mechanism of cooling/drying of the boundary layer has already occurred (though the effects may still be observable by aircraft flight-level, GPS dropsonde, and satellite data). This necessitates that the arc clouds be identified and sampled as early in their lifecycle as possible using available aircraft observations (e.g. flight-level, GPS dropsonde and P-3 LF radar, and P-3/G-IV Doppler radar data) and satellite imagery (e.g. TC diurnal cycle infrared, visible, infrared, and microwave).

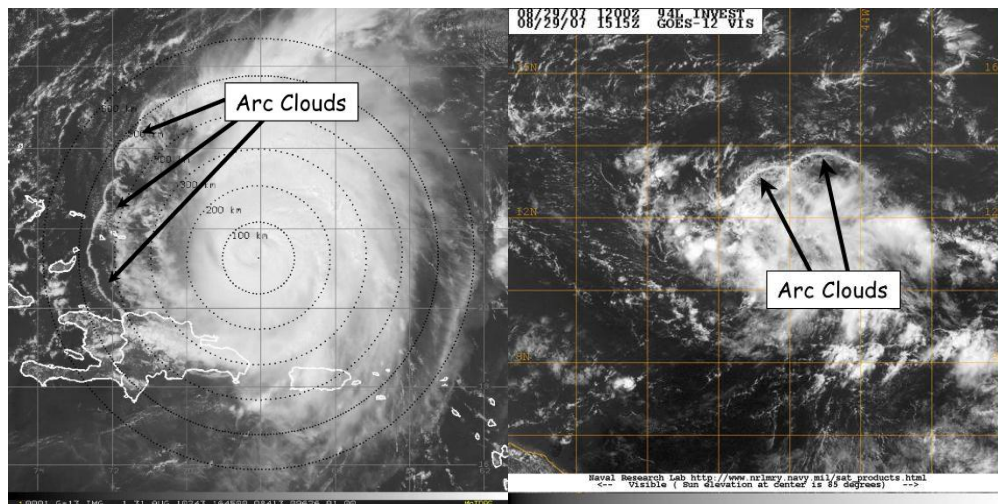


**Figure MA-2.** GOES visible satellite imagery showing arc clouds racing away from the convective cores of (left) 2003 Hurricane Isabel and (right) 2007 Pre-Tropical Depression Felix.

**MATURE STAGE EXPERIMENT**

*Science Description*

---

**Hypotheses (Arc Cloud):** Arc clouds form along the leading edge of TC diurnal pulses, are particularly favored to occur at R~105–215 n mi (~200–400 km) in areas with mid-level (~600–800-hPa) dry air ( $\leq 45$  mm total precipitable water [TPW]), and can act to temporarily stabilize the TC environment.

**Aircraft Pattern/Module Descriptions:**

**P-3 Module #1: Environment Interaction (Arc Cloud)**

**G-IV Module #1: Environment Interaction (Arc Cloud)**

When arc clouds emanating from the periphery of the TC convective core are identified using satellite imagery and/or P-3 LF radar, perform this break-away pattern by transecting orthogonally across to these outwardly propagating features.

**Analysis Strategy (Arc Cloud):** This experiment seeks to collect observations across arc cloud features in the periphery of mature TCs using aircraft flight-level, GPS dropsonde, and TDR data to improve our understanding of the physical processes responsible for their formation and evolution, as well as how these features may affect TC structure and intensity in the short-term. Flight-level and GPS dropsonde data will be used to calculate changes in static stability and possible impacts on surface fluxes both ahead of and behind the arc cloud (e.g. enhanced stability/reduced surface fluxes behind the arc cloud leading edge). TDR data will be used to define the vertical structure of the kinematics ahead of, across and behind the arc cloud. Finally, kinematics and thermodynamics associated with arc cloud events will be compared to corresponding locations in model analysis fields (e.g. GFS and HWRF).

**References (Arc Cloud):**

Dunion, J.P., 2011: Rewriting the climatology of the tropical North Atlantic and Caribbean Sea atmosphere. *J. Climate*, **24**, 893-908.

Knaff, J.A., and J.F. Weaver, 2010: A mesoscale low-level thunderstorm outflow boundary associated with Hurricane Luis. *Mon. Wea. Rev.*, **128**, 3352-3355.

MATURE STAGE EXPERIMENT

*Science Description*

---

**SCIENCE OBJECTIVE #3:** *Test new (or improved) technologies with the potential to fill gaps, both spatially and temporally, in the existing suite of airborne measurements in mature hurricanes. These measurements include improved three-dimensional representation of the hurricane wind field, more spatially dense thermodynamic sampling of the boundary layer, and more accurate measurements of ocean surface winds*

[New Observing Systems (NOS)]

COYOTE

**Motivation (Coyote):** Reducing the uncertainty associated with TC intensity forecasts remains a top priority of NWS/NHC. In addition to NOAA's operational requirements (sampling surface wind and thermodynamic structure), developing the capability to regularly fly low altitude unmanned aerial system (UAS) into TCs helps to advance NOAA research by allowing scientists to sample and analyze a region of the storm that would otherwise be impossible to observe in detail (due to the severe safety risks associated with manned reconnaissance). It is believed that such improvements in basic understanding are likely to improve future numerical forecasts of TC intensity change. Over time, projects such as this, which explore the utilization of unconventional and innovative technologies in order to more effectively sample critical regions of the storm environment should help reduce this inherent uncertainty.

**Background (Coyote):** Coyote is an electric-powered unmanned aircraft with 1-hour endurance and is built by the Raytheon Company (formerly Sensintel Corporation and British Aerospace Engineering [BAE]). In many ways, this UAS platform can be considered a 'smart GPS dropsonde system' since it is deployed in similar fashion and currently utilizes a comparable meteorological payload similar to systems currently used by NOAA on the GIV and P-3 dropsonde systems. The Coyote can be launched from a P-3 sonobuoy tube in flight, and collects in-situ measurements of temperature, relative humidity, pressure, and remotely senses sea surface temperature. The three-dimensional wind field can be determined using the aircraft's GPS changes in position. Unlike the GPS dropsonde, however, the Coyote UAS can be directed from the NOAA P-3 to specific areas within the storm circulation (both in the horizontal and in the vertical). Furthermore, Coyote observations are continuous in nature and give scientists an extended look into important small-scale thermodynamic and kinematic physical processes that regularly occur within the near-surface boundary layer environment. The Coyote, when operated within a hurricane environment, provides a unique observation platform from which the low-level atmospheric boundary layer environment can be diagnosed in great detail.

**Hypotheses (Coyote):** 360-degree depictions of hurricane boundary layer RMW and Vmax are possible by conducting UAS eyewall orbit missions that continually synchronize the prevailing wind direction with UAS heading.

**MATURE STAGE EXPERIMENT**  
*Science Description*

---

**Aircraft Pattern/Module Descriptions:**

**P-3 Module #1: NOS (Coyote, Eyewall A)**

**P-3 Module #2: NOS (Coyote Eyewall B)**

For Coyote Eyewall module: “Sun Pattern” or “Pizza Slice” Pattern

**P-3 Module #3: NOS (Coyote, Inflow)**

For Coyote Inflow module: modified Lawnmower pattern

**Analysis Strategy (Coyote):** The analysis of these data includes two components: understanding hurricane boundary layer structure and potential improvements to hurricane prediction that UAS observations provide. Three Coyote working groups analyze existing Coyote data and are focused on three main areas: boundary layer thermodynamics, boundary layer turbulence, and observing system experiments. The understanding of boundary layer physics (both kinematic and thermodynamic processes) uses observations to understand the smaller scale features captured using Coyote data and evaluates the representation of the boundary layer in various model physics schemes using data assimilation (DA) and other statistical techniques. Multiple models and DA schemes will continue to be used for these analyses. Observing system experiments (OSEs) and observing system simulation experiments (OSSEs) can quantify the impact of Coyote observations and allow help optimize Coyote resources by comparing observing strategies generated from a Nature Run. Multiple Nature Runs exist and will be used for these OSSEs in conjunction with appropriate forecast models and DA schemes. These include but are not limited to HWRF, WRF-ARW, and GFS models; and ensemble-based DA systems such as HRD’s in-house Hurricane Ensemble Data Assimilation System (HEDAS), as well as 3- and 4-dimensional hybrid DA schemes typically used in operations.

**References (Coyote):** N/A

NESDIS OCEAN WINDS

**Motivation (Ocean Winds):** This effort aims to improve our understanding of microwave scatterometer retrievals of the ocean surface wind field and to evaluate new remote sensing techniques/technologies. The NOAA/NESDIS/Center for Satellite Applications and Research in conjunction with the University of Massachusetts (UMASS) Microwave Remote Sensing Laboratory, the NOAA/AOML/Hurricane Research Division, and the NOAA/OMAO/Aircraft Operations Center have been conducting flight experiments during hurricane season for the past several years. The Ocean Winds experiment is part of an ongoing field program whose goal is to further our understanding of microwave scatterometer and radiometer retrievals of the ocean surface winds in high wind speed conditions and in the presence of rain for all wind speeds. This

**MATURE STAGE EXPERIMENT**

*Science Description*

---

knowledge is used to help improve and interpret operational wind retrievals from current and future satellite-based sensors. The hurricane environment provides the adverse atmospheric and ocean surface conditions required.

The Imaging Wind and Rain Airborne Profiler (IWRAP), which is also known as the Advanced Wind and Rain Airborne Profiler (AWRAP), was designed and built by the University of Massachusetts and is the critical sensor for these experiments. IWRAP/AWRAP consists of two dual-polarized, dual-incidence angle radar profilers operating at Ku-band and at C-band, which measure profiles of volume reflectivity and Doppler velocity of precipitation in addition to the ocean surface backscatter. Currently the C-band portion of IWRAP has been installed with the prototype antenna for EUMETSAT's ASCAT follow-on satellite sensor that will be launched on EPS-SG. This antenna, on loan from ESA, is a dual-polarized slotted waveguide antenna which allows us to measure the cross-polarized response of the ocean surface, which is a new capability being implemented for the ASCAT follow-on sensor. The Stepped-Frequency Microwave Radiometer (SFMR) and GPS dropsonde system are also essential instrumentation on the NOAA-P3 aircraft for this effort. The NASA GORE (GNSS reflection) system has also been utilized to collect measurements to support the NASA CYGNSS mission, but future plans call for utilizing an improved GNSS-R receiver being developed by the CYGNSS project at the University of Michigan. A Ka-band radar system is being currently developed to enable finer resolution measurements at the air-sea boundary to help decouple what is happening at the interface in the storm environment.

**Background (Ocean Winds):** The Ocean Winds P-3 flight experiment program has several objectives:

- Calibration and validation of satellite-based ocean surface vector wind (OSVW) sensors such as ASCAT, ScatSat, OceanSat-3 and the new CYGNSS mission that uses GNSS-R techniques to infer the ocean wind speed.
- Product improvement and development for current and planned satellite-based sensors (ASCAT, ScatSat, OceanSat-3, CYGNSS and SCA)
- Testing of new remote sensing technologies for possible future satellite missions (risk reduction) such as the dual-frequency scatterometer concept. A key objective for this year will be the collection of cross-polarized data at C-band to support ESA and EUMETSAT studies for the ASCAT follow-on (SCA), which will be part of their EPS-SG satellite series.
- Advancing our understanding of broader scientific questions such as:
  - Rain processes in tropical cyclones and severe ocean storms: the coincident dual-polarized, dual-frequency, dual-incidence angle measurements would enable us to improve our understanding of precipitation processes in these moderate to extreme rainfall rate events.
  - Atmospheric boundary layer (ABL) wind fields: the conical scanning geometry and the Doppler capabilities of this system provide a unique source of measurements from which the ABL winds can be derived. The advanced digital receivers and data acquisition system recently



## MATURE STAGE EXPERIMENT

### *Science Description*

---

- implemented will enable to potentially retrieve the wind and reflectivity profiles essentially to the surface.
- Analysis of boundary layer rolls: linearly organized coherent structures are prevalent in tropical cyclone boundary layers, consisting of an overturning “roll” circulation in the plane roughly perpendicular to the mean flow direction. IWRAP has been shown to resolve the kilometer-scale roll features, and the vast quantity of data this instrument has already collected offers a unique opportunity to study them.
  - Drag coefficient,  $C_d$ : extending the range of wind speeds for which the drag coefficient is known is of paramount importance to further our understanding of the coupling between the wind and surface waves under strong wind forcing, and has many important implications for hurricane and climate modeling. The advanced digital receivers and data acquisition capability allows us to retrieve wind and reflectivity profiles closer to the ocean surface, which can also be exploited to derive drag coefficients by extrapolating the derived wind profiles down to 0 m altitude.

**Hypotheses (Ocean Winds):** We don’t fully understand what is happening at the air-sea interface in extreme storm conditions but it should be possible to characterize this with the proper instrumentation and data collection methodologies.

### **Aircraft Pattern/Module Descriptions:**

#### **P-3 Pattern #1: NOS (Ocean Winds)**

The sensitivity of the IWRAP/AWRAP system defines the preferred flight altitude to be below 10,000 ft to enable the system to still measure the ocean surface in the presence of rain conditions typical of tropical systems. With the Air Force Reserve typically flying at 10,000 ft pressure altitude, we have typically ended up with an operating altitude of 7,000 ft radar. Operating at a constant radar altitude is desired to minimize changes in range and thus measurement footprint on the ground. Higher altitudes would limit the ability of IWRAP/AWRAP to consistently see the surface during intense precipitation, but these altitudes would still provide useful data, such as measurements through the melting layer, to study some of the broader scientific questions.

#### *Maneuvers:*

Straight and level flight with a nominal pitch offset unique to each P-3 is desired during most flight legs. Constant bank circles of 10–30 degrees have been recently implemented, as a method to obtain measurements at incidence angles greater than the current antenna was configured for. These would be inserted along flight legs where the desired environmental conditions were present. Generally it would be a region of no rain and where we might expect the winds to be consistent over a range of about 6–10 miles, about the diameter of a circle.

**MATURE STAGE EXPERIMENT**  
*Science Description*

---

This would not be something we would want to do in a strong wind gradient region where the conditions would change significantly while circling.

*Patterns:*

Typically an ideal Ocean Winds flight pattern would include a survey pattern (Figure-4 or Butterfly) that extended about 50 n mi from the storm center. The actual distance would be dictated by the storm size and safety of flight considerations. Dependent upon what was observed during the survey pattern radial legs in and out of different sectors of the storm focusing on different wind and/or rain conditions.

*Storm Types:*

The ideal Ocean Winds storm would typically be in a hurricane (category 1 and above) where a large range of wind speeds and rain rates would be found. However, data collected within TDs and TSs would still provide useful observations of rain impacts on the surface observation.

**Analysis Strategy (Ocean Winds): TBD**

**References (Ocean Winds): N/A**

END STAGE EXPERIMENT  
*Science Description*

---

**Investigator(s):** Sim Aberson, John Kaplan (Co-PIs), Peter Dodge, Ghassan Alaka, Heather Holbach, Jun Zhang, and Jason Dunion (Co-Is)

**Requirements:** TC making landfall, undergoing rapid weakening, or extratropical transition

**Science Objectives:**

- 1) Collect observations targeted at better understanding changes TCs undergo at landfall. Objectives include validation of surface wind speed estimates and model forecasts, understanding factors that modulate intensity changes near and after landfall, and to understand processes that lead to tornadoes in outer rainbands. [*IFEX Goals 1, 3*]
- 2) Collect observations targeted at better understanding changes TCs undergo while rapidly weakening over the open ocean or undergo extratropical transition. [*IFEX Goals 1, 3*]

**Description of Science Objectives:**

**SCIENCE OBJECTIVE #1:** *Collect observations targeted at better understanding changes TCs undergo at landfall. Objectives include validation of surface wind speed estimates and model forecasts, understanding factors that modulate intensity changes near and after landfall, and to understand processes that lead to tornadoes in outer rainbands.*

[Landfall]

**Motivation and Background:** The TC lifecycle often ends when it makes landfall and decays as it moves inland. During a landfall threat in the US, an average of 300 n mi (550 km) of coastline is placed under a hurricane warning, which costs approximately \$1 million per n mi. The size of the warned area depends on the forecast track, extent of hurricane- and tropical storm-force winds, and evacuation lead-times. Research has helped reduce uncertainties in track forecasts, so the goal here is to improve the accuracy of the surface wind analyses and forecasts near and after landfall to allow for optimization of warning areas and reduction in preparations costs. In addition, forecasts of decay after landfall and of severe weather in the TC are required to adequately warn populations away from the coastline. Forecasts of severe weather, particularly tornadoes, embedded within a landfalling TC is particularly difficult.

Severe weather, including tornadoes, is often associated with landfalling TCs. The basic dynamic and thermodynamic structures found in TC supercells are not well-understood. While some studies have found that TC tornadoes can be similar to Great Plains tornadoes, some key differences exist, such as the height and amplitude of the vortices. Most TC tornadoes occur in the front-right quadrant of the TC primarily from 12 h prior to 48 h after landfall (Schultz and Cecil 2009). Additionally, the most damaging TC tornadoes occur in rainbands. While TC tornadoes are typically weaker than their Great

## END STAGE EXPERIMENT

### *Science Description*

---

Plains counterparts, they account for at least 10% of all tornadoes from Louisiana to Maryland (Schultz and Cecil 2009). Unlike Great Plains tornadoes, TC tornadoes are typically associated with relatively small values of CAPE, relying instead on friction-induced convergence that accompanies landfalling TCs. The sudden deceleration of the wind as it encounters the rough land surface helps drive vertical motion, which promotes embedded mesovortices and severe weather.

Dropwindsonde data have shown remarkable variations of the wind with height. A common feature is a wind-speed maximum at 300–500 m altitude. Theoretical and numerical modeling of the TC boundary layer suggests that the low-level jets are common features. The height of the jet varies by storm quadrant, and modeling indicates that this variation can be enhanced as a TC crosses land. Many TCs produce over-land wind gusts that exceed values expected based upon observed maximum sustained wind speeds. In addition, uncertainties in deriving surface wind-speed estimates from flight-level and SFMR data collected near the coast remain. Changing bathymetry could alter the breaking-wave field, which could change the roughness length and microwave emissions at high wind speeds. Evaluation of these effects may lead to adjustments to the operational SFMR-derived surface wind-speed algorithms.

Decay over land is also important, and data collected during and shortly after landfall should help refine both operational statistical models (such as the Kaplan/DeMaria decay model) and numerical models.

#### *Objectives:*

- Collect Doppler, flight-level, and SFMR surface wind-speed data both within the core and near storm environment (within about 240 n mi of the TC center) to help improve and validate real-time and post-storm surface wind-speed estimates.
- Document the thermodynamic and kinematic changes in TC structure during and after landfall and improve understanding of the factors that modulate changes in TC intensity near the time of landfall.
- Collect observations to evaluate numerical model forecasts of the three-dimensional structure of TCs during and after landfall.
- Collect kinematic and thermodynamic data in rainbands that have the potential to produce tornadoes.

#### **Hypotheses:**

1. It is possible to improve real-time surface wind-speed estimates for landfalling TCs by obtaining in-situ aircraft data.
2. The above datasets can be used to validate statistical and numerical-model landfall surface wind-speed forecasts.
3. The understanding and ability to forecast changes in the structure and intensity of landfalling TCs can be enhanced utilizing the high-resolution

**END STAGE EXPERIMENT**  
*Science Description*

---

kinematic and thermodynamic data sets collected during the aforementioned landfall research missions.

4. Traditional environmental parameters (e.g., CAPE, vertical shear, helicity) will distinguish sectors of the storm that are most supportive of supercell development. Thus, the areal coverage of Storm Prediction Center issued severe weather watches may be optimized and numerical-model output can be validated.

**Aircraft Pattern/Module Descriptions:**

**P-3 Module #1: Landfall (Offshore Intense Convection)**

A break-away/non-standard pattern in which the P-3 crosses the target rain band 20–25 km downwind of intense convective cells and then proceeds to about 25 km outside the rain band axis. The aircraft turns upwind and proceeds along a straight track parallel to the band axis. When the P-3 is ~20–25 km upwind of the target cells, the aircraft turns and proceeds along a track orthogonal to the band axis until the P-3 is 25 km inside the rain band then turns downwind and flies parallel to the rain band axis.

**P-3 Module #2: Landfall (Coastal Survey)**

A break-away/non-standard pattern in which the P-3 flies parallel, but ~10–15 km offshore so that the SFMR footprint is out of the surf zone. The second pass should be parallel and as close to the coast as safety permits. Finally, a short leg would be flown from the coast spiraling towards the storm center.

**P-3 Module #3: Landfall (Real-time)**

A break-away/non-standard pattern in which the P-3 descends at the initial point and begins a low-level Figure-4 pattern, possibly modifying the legs to fly over buoy or C-MAN sites if possible. If time permits, the P-3 would make one more pass through the eye and then fly the Dual-Doppler option.

**P-3 Module #4: Landfall (SFMR Coastal)**

A break-away/non-standard pattern in which the P-3 flies perpendicular to the coastline, across the bathymetry gradient, in a region with near constant surface winds. After flying away from the coast for about 50 km, the P-3 would turn downwind and then back towards the coast repeating a similar line as the first leg.

**END STAGE EXPERIMENT**  
*Science Description*

---

**Analysis Strategy:**

**Offshore Intense Convection**

Three-dimensional wind-field analyses and vertical profiles will be made from Doppler datasets. Dropwindsonde and flight-level data will be analyzed and combined with any available rawinsonde and surface (e.g. buoys, CMAN, etc.) observations to establish the kinematic and thermodynamic environment of targeted cells. Any available land-based radar will be used to augment airborne observations of cell evolution. Observations of TC supercells will be used to validate numerical models, to assess the ability to predict signatures of tornadic activity, and to compare TC tornadoes with those from mid-latitude supercells.

**Coastal Survey**

Three-dimensional wind-field analyses and vertical profiles will be compared with dropwindsonde, SFMR, IWRAP, and/or LIDAR data to characterize the differences between the onshore and offshore flow.

**Real-time**

Data transmitted from the aircraft in real time will be available for assimilation into numerical models and to validate forecasts of sustained wind speed, wind gusts, and thermodynamic fields such temperature, moisture, and rainfall.

**SFMR Coastal**

By flying this module in a region of nearly constant winds, with the wind speed measured by a dropwindsonde, the effects of bathymetry on SFMR measurements can be identified by comparing the brightness temperature measurements for each frequency along the leg. If the winds are not constant, but multiple dropwindsonde measurements are available along the leg, then any wind-speed change can be accounted for in the comparison. Flying one leg towards the coast and one away will also allow for the impact of wave-breaking direction to be evaluated.

**References:**

Schultz, L. A., and D. J. Cecil, 2009: Tropical cyclone tornadoes, 1950–2007. *Mon. Wea. Rev.*, **137**, 3471–3484.

END STAGE EXPERIMENT  
*Science Description*

---

**SCIENCE OBJECTIVE #2:** *Collect observations targeted at better understanding changes TCs undergo while rapidly weakening over the open ocean or undergo extratropical transition.*  
[Weakening/Extratropical Transition (ET)]

**Motivation and Background:** The poleward movement of a TC initiates complex interactions with the midlatitude environment frequently leading to sharp declines in hemispheric predictive skill. In the Atlantic basin, such interactions frequently result in upstream cyclone development leading to high-impact weather events in the U. S. and Canada, as well as downstream ridge development associated with the TC outflow and the excitation of Rossby waves leading to downstream cyclone development. Such events have been shown to be precursors to extreme events in Europe, the Middle East, and may have led to subsequent TC development in the Pacific and Atlantic basins as the waves progress downstream. During this time, the TC structure begins changing rapidly: the symmetric distributions of winds, clouds, and precipitation concentrated about a mature TC circulation center develop asymmetries that expand. Frontal systems frequently develop, leading to heavy precipitation events, especially along the warm front well ahead of the TC. The asymmetric expansion of areas of high wind speeds and heavy precipitation may cause severe impacts over land without the TC center making landfall. The poleward movement of a TC also may produce large surface wave fields due to the high wind speeds and increased translation speed of the TC that results in a trapped-fetch phenomenon.

During this phase of development, hereafter referred to as extratropical transition (ET), the TC encounters increasing vertical wind shear and decreasing sea surface temperatures, factors that usually lead to weakening of the system. However, transitioning cyclones sometimes undergo explosive cyclogenesis as extratropical cyclones, though this process is poorly forecast. The small scale of the TC and the complex physical processes that occur during the interactions between the TC and the midlatitude environment make it very difficult to forecast the evolution of track, winds, waves, precipitation, and the environment. Due to sparse observations and the inability of numerical models to resolve the structure of the TC undergoing ET, diagnoses of the changes involved in the interaction are often inconclusive without direct observations. Observations obtained during this experiment will be used to assess to what extent improvements to TC structure analyses and the interaction with the midlatitude flow improve numerical forecasts and to develop techniques for forecasting these interactions. Improved understanding of the changes associated with ET will contribute to the development of conceptual and numerical models that will lead to improved warnings associated with these dangerous systems.

*Questions for study:*

- How is the TC vortex maintained in regions of vertical wind shear exceeding  $30 \text{ m s}^{-1}$ ?

## END STAGE EXPERIMENT

### *Science Description*

---

- How is the warm core maintained long after the TC encounters vertical wind shear exceeding  $30 \text{ m s}^{-1}$ ?
- How does vertical shear exceeding  $30 \text{ m s}^{-1}$  alter the distribution of latent heating and rainfall?
- Does vortex resilience depend upon diabatic processes? On subsequent formation of new vortex centers, or by enlisting baroclinic cyclogenesis?
- Does the vertical mass flux increase during ET, as has been shown in numerical simulations?
- Is downstream error growth related to errors in TC structure during ET?  
Is ET sensitive to the sea-surface temperatures?

**Hypotheses:** ET depends upon the survival of the TC as it penetrates into midlatitudes in regions of increasing vertical wind shear.

#### **Aircraft Pattern/Module Descriptions:**

##### **P-3 Pattern #1: Weakening/ET**

##### **G-IV Pattern #1: Weakening/ET**

Two specific targets are to be sampled during each mission, the TC itself, and the interface between the TC and the environmental flow. The systems will be sampled every 12 h from the time it begins the transition to an extratropical cyclone to the time it is out of range of the aircraft, or the system dissipates.

**Analysis Strategy:** Data analysis will occur after the final mission, mainly via case studies based on incorporating the data in a sophisticated data assimilation/model system.

#### **References:**

Evans, C., K. M. Wood, S. D. Aberson, H. M. Archambault, S. M. Milrad, L. F. Bosart, K. L. Corbosiero, C. A. Davis, J. R. Dias Pinto, J. Doyle, C. Fogarty, T. J. Galarneau, Jr., C. M. Grams, K. S. Griffin, J. Gyakum, R. E. Hart, N. Kitabatake, J. S. Lentink, R. McTaggart-Cowan, W. Perrie, J. F. D. Quinting, C. A. Reynolds, J. Riemer, E. Ritchie, Y. Sun, and F. Zhang, 2017: The Extratropical Transition of Tropical Cyclones. Part I: Cyclone Evolution and Direct Impacts. *Mon. Wea. Rev.*, accepted for publication.



SYNOPTIC FLOW EXPERIMENT

*Science Description*

---

**Investigator(s):** Jason Dunion, Sim Aberson (Co-PIs), Kelly Ryan, Jason Sippel, Rob Rogers, Ryan Torn (SUNY Albany), Eric Blake (NWS/NHC), Mike Brennan (NWS/NHC), Chris Landsea (NWS/TAFB) (Co-Is)

**Requirements:** No requirements: flown at any stage of the TC lifecycle

**Science Objectives:**

- 1) Investigate new strategies for optimizing the use of aircraft observations to improve numerical forecasts of TC track, intensity, and structure [*IFEX Goal 1*]

**Description of Science Objectives:**

**SCIENCE OBJECTIVE #1:** *Investigate new strategies for optimizing the use of aircraft observations to improve numerical forecasts of TC track, intensity, and structure*  
(Synoptic Flow)

**Motivation:** Operational G-IV Synoptic Surveillance missions have resulted in average GFS track-forecast improvements of 5–10% and statistically significant intensity improvements through 72 h (Aberson 2007). However, the basic G-IV flight-track design and observational sampling strategies have remained largely unchanged for the past decade while the model, ensemble and data-assimilation systems have been upgraded considerably. The Synoptic Flow Experiment is designed to investigate new strategies for optimizing the use of aircraft observations to improve numerical forecasts of TC track, intensity, and structure.

**Background:** Accurate numerical TC forecasts require the representation of meteorological fields on a variety of scales, and the assimilation of the data into realistic models. Based on this requisite, HRD re-designed a Synoptic Flow Experiment in the 1998 to improve track predictions of TCs during the watch and warning period by targeting dropsonde observations in the storm environment and assimilating those data into numerical models. Optimal sampling was attained using a fully nonlinear technique that employed the breeding method, the operational NCEP ensemble-perturbation technique at the time, in which initially random perturbations in the model were repeatedly evolved and rescaled. This technique helped define the fastest growing modes of the system, where changes to initial conditions due to additional data grow (decay) in regions of large (small) perturbation in the operational NCEP Ensemble Forecasting System. Although this approach provides a good estimate of the locations in which supplemental observations are likely to have the most impact by identifying locations of probable error growth in the model, it does not distinguish those locations which impact the particular TC forecast of interest from those which do not. The G-IV flight track designs and targeting techniques developed from the series of 1996–2006 HRD Synoptic Flow Experiments were transitioned to operations at NOAA NHC and AOC in 2007 and have continued to be an integral part of operations since then. These operational

SYNOPTIC FLOW EXPERIMENT

*Science Description*

---

missions resulted in average GFS track-forecast improvements of 5–10% and statistically significant intensity improvements through 72 h (Aberson 2007).

**Hypotheses:** New, more advanced targeting techniques that optimize aircraft sampling of the TC environment can improve numerical forecasts of TC track, intensity, and structure, and could potentially be transitioned to operations.

**Aircraft Pattern/Module Descriptions:**

**P-3 Pattern #1: Synoptic Flow**

When ensemble prediction systems suggest sensitivity of TC-related forecast metrics (position, intensity and track, etc.) in/near the inner core (i.e.  $R \leq 105$  n mi/ $R \leq 200$  km), fly any standard pattern that provides symmetric coverage (e.g., Figure-4, Rotated Figure-4, Butterfly, P-3 Circumnavigation).

**G-IV Pattern #1: Synoptic Flow**

When ensemble prediction systems suggest sensitivity of TC-related forecast metrics (position, intensity and track, etc.), fly a non-standard pattern that will vary from storm to storm and be defined by regions that are identified using model targeting techniques. These patterns will typically resemble a Lawnmower pattern. The over storm or near storm portion of the pattern could incorporate the following standard patterns: Figure-4, Rotated Figure-4, Butterfly, Lawnmower, Square Spiral, G-IV Circumnavigation, G-IV Star, or G-IV Star with Circumnavigation.

**Analysis Strategy:** Guidance from ensemble prediction systems will be used to compute the sensitivity of TC-related forecast metrics (position, intensity and track, etc.) and will be used to guide GPS dropsonde sampling of the TC and its environment. Retrospective data denial experiments will be conducted post mission to assess the impact of the GPS dropsonde data on model forecasts of TC track, intensity and structure.

**References:**

Aberson, S.D., 2010: 10 years of hurricane synoptic surveillance (1997–2006). *Mon. Wea. Rev.*, **138**, 1536–1549.

Torn, R.D., R. Rios-Berrios, Z. Zhang, and A. Brammer, 2017: Application of ensemble-based sensitivity analysis during SHOUT. *97th AMS Annual Meeting*, Seattle, WA.

Torn, R.D., 2014: The impact of targeted dropwindsonde observations on tropical cyclone intensity forecasts of four weak systems during PREDICT. *Mon. Wea. Rev.*, **142**, 2860–2878.

OCEAN SURVEY EXPERIMENT  
*Science Description*

---

**Investigator(s):** Jun Zhang, Nick Shay (Co-PIs), Rick Lumpkin (NOAA/AOML/Physical Oceanography Division [PhOD]), George Halliwell (NOAA/PhOD), Elizabeth Sanabia (USNA), and Benjamin Jaimes (U. Miami/RSMAS) (Co-Is)

**Requirements:** Categories 1–5

**Science Objectives:**

- 1) Obtain observations on TC-ocean interaction to improve flux parameterizations and to test coupled TC models [*IFEX Goals 1, 3*]

**Description of Science Objectives:**

**SCIENCE OBJECTIVE #1:** *Obtain observations on TC-ocean interaction to improve flux parameterizations and to test coupled TC models* [TC-Ocean Interaction]

**Motivation:** Modeling studies show that the effect of the ocean varies widely depending on storm size and speed and the pre-existing ocean temperature and density structure. The overarching goal of these studies is to provide data on TC-ocean interaction with enough resolution to rigorously test coupled TC models, specifically:

- Measure the two-dimensional SST cooling, air temperature, humidity and wind fields beneath the storm and thereby deduce the effect of the ocean cooling on ocean enthalpy flux to the storm;
- Measure the three-dimensional temperature, salinity and velocity structure of the ocean beneath the storm and use this to deduce the mechanisms and entrainment rates (shear-induced) of ocean cooling;
- Conduct these measurements at several points along the storm evolution therefore investigating the role of pre-existing ocean variability; and,
- Use these data to assess the accuracy of the oceanic component of the coupled model system

Recent improvement in flux parameterizations has led to significant improvements in the accuracy of TC simulations. These parameterizations, however, are based on a relatively small number of direct flux measurements. The overriding goal of these studies is to make additional flux measurements under a sufficiently wide range of conditions to improve flux parameterizations, specifically:

- Measure the air-sea fluxes of enthalpy and momentum using ocean-side budget and covariance measurements and thereby verify and improve parameterizations of these fluxes;

OCEAN SURVEY EXPERIMENT  
*Science Description*

---

- Measure the air-sea fluxes of oxygen and nitrogen using ocean-side budget and covariance measurements and use these to verify newly developed gas flux parameterizations;
- Measure profiles of ocean boundary layer turbulence, its energy, dissipation rate and skewness and use these to investigate the unique properties of hurricane boundary layers;
- Conduct the above flux and turbulence measurements in all four quadrants of a TC so as investigate a wide range of wind and wave conditions

**Hypotheses:** The following hypotheses will guide the sampling strategies for understand the ocean response to TCs and ocean impact of TC intensification:

4. TC intensity is highly sensitive to air-sea fluxes; and ocean heat content
5. Upper ocean properties and dynamics play a key role in determining TC intensity

**Aircraft Pattern/Module Descriptions:** This multi-aircraft experiment is ideally conducted in geographical locales that avoid conflict with other operational requirements, for example, at a forward/eastward-deployed base targeting a storm not imminently threatening the U.S. coastline. As an example, an optimal situation is shown in Fig. OC-1 for missions operating from St. Croix, USVI. A TC of at least minimal hurricane intensity is desired. In this example, the hypothetical storm remains within 600 n mi (a reasonable maximum distance) for four days, and at no time is forecasted to be a threat to land, including the U.S. coast.

**OCEAN SURVEY EXPERIMENT**  
*Science Description*

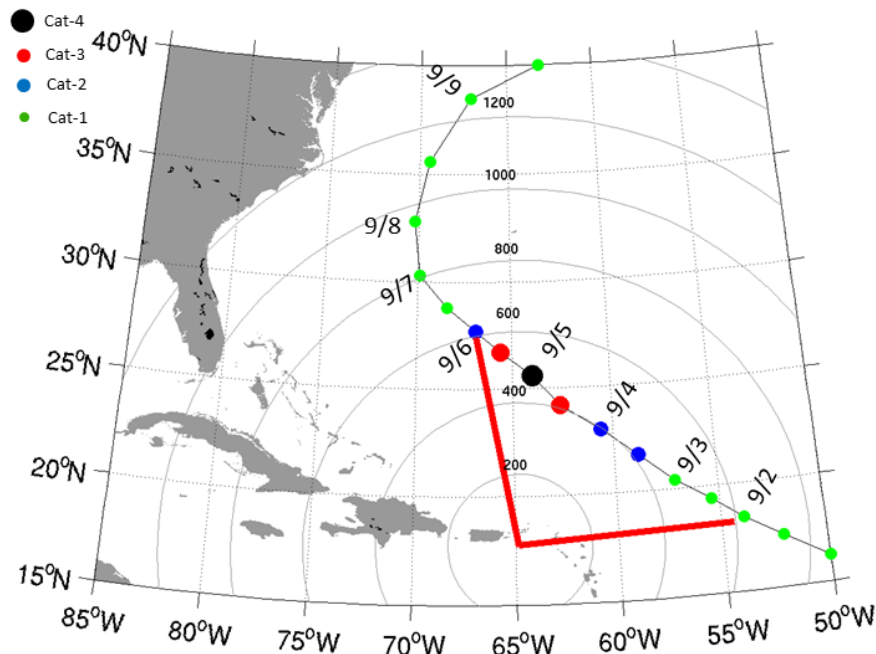


**Figure OC-1:** Storm track with locations plotted every 12 hours. Range rings are 200 n mi relative to forward operating base at St. Croix, USVI (STX/TISX), and red line delineates storm locations within 600 n mi of STX. In this example, the storm center remains within 600 n mi for 4 days.

1. Expendable profiler surveys from P-3 aircraft (Flight Sequence)

**P-3 Pattern #1: Ocean Survey (Pre-storm)**

To establish the pre-storm upper ocean thermal and mass structure prior to a storm's arrival, a pre-storm expendable survey will be conducted. This mission will consist of deploying a large grid of AXCTDs/AXBTS to measure the three-dimensional temperature and salinity fields (Fig. OC-2). This flight would occur **48 hours prior to storm arrival**, based primarily on the forecasted track, and optimally covers the forecast cone-of-error. A total of **50–60 probes** would be deployed, depending on mission duration, and spaced approximate 0.5 deg. apart. The experiment is optimally conducted where horizontal gradients are relatively small, but AXCP probes may be included if significant gradients (and thus currents) are expected to be observed. Either P-3 aircraft (when both available) may be used as long as it is equipped with ocean expendable data acquisition hardware.

**OCEAN SURVEY EXPERIMENT**  
*Science Description*

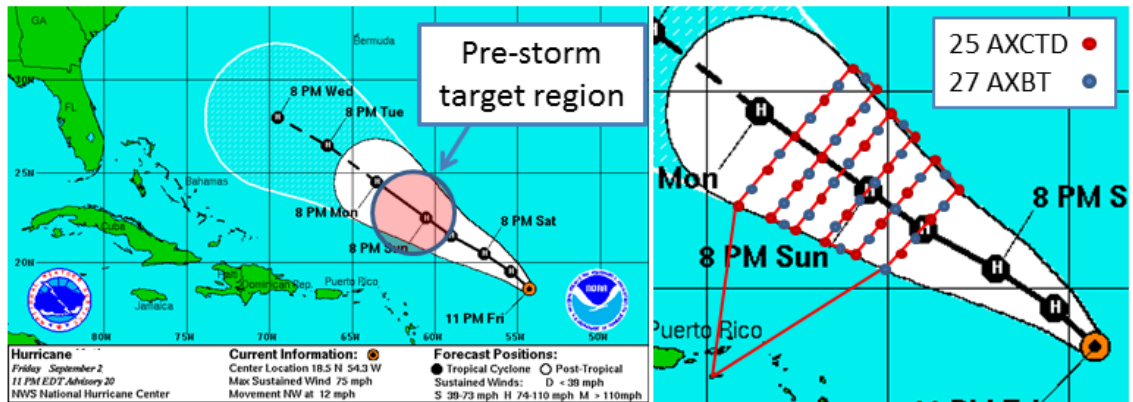


**Figure OC-2:** Left: NHC official forecast track, which pre-storm ocean sampling region highlighted. Target region is centered ~48 hours prior to forecast arrival of storm. Right: P-3 flight track (red line) and ocean sampling pattern consisting of a grid of AXCTD/AXBT probes. Probes are deployed at ~0.5 deg. intervals.

### P-3 Pattern #2: Ocean Survey (In-storm)

Next, a mission is executed within the storm over the ocean location previously sampled (Fig. OC-3). This flight shall be conducted by the **P-3 carrying the Wide-swath Radar Altimeter (WSRA)** for purposes of mapping the two-dimensional wave field. The flight pattern should be a **rotated Figure-4**, and up to **20 AXBTs** should be deployed in combination with GPS dropwindsondes. Note that other experimental goals can and should be addressed during this mission, and a multi-plane mission coordinated with the other P-3, as well as G-IV, is desirable.

OCEAN SURVEY EXPERIMENT  
*Science Description*

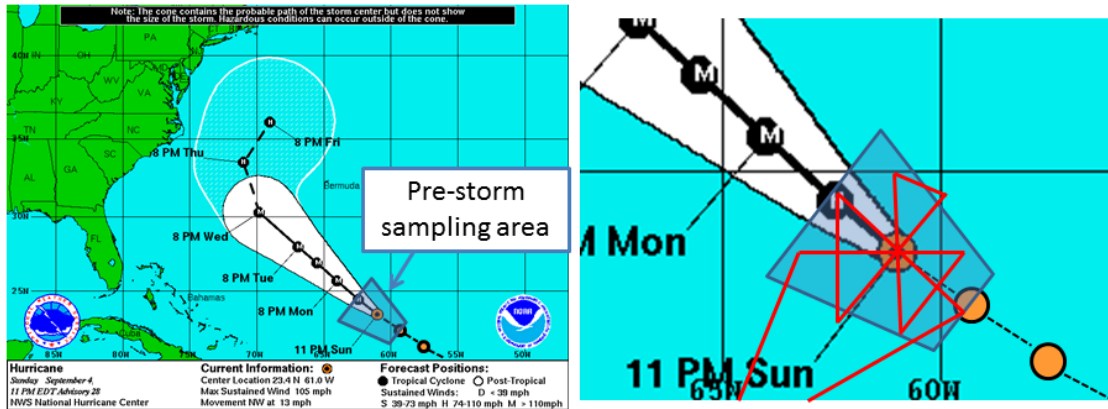


**Figure OC-3:** Left: NHC official forecast track at time of in-storm mission, with pre-storm sampled region highlighted. Right: P-3 in-storm flight pattern centered on storm and over previously sampled ocean area. Typical pattern is expected to be a Rotated Fig-4.

**P-3 Pattern #3: Ocean Survey (Post-storm)**

A post-storm expendable survey shall be conducted over the same geographical location to assess ocean response, with slight pattern adjustments made based on the known storm track (Fig. OC-4). Approximately **60–70 probes** would be deployed (depending on duration limits), consisting mainly of **AXBTs/AXCPs** to map the three-dimensional temperature and currents, ideally 1–2 days after storm passage. In the Fig. OC-4 example, the pattern extends 470 km along the storm track, which in this example is  $\sim 0.75\Lambda$ , where  $\Lambda = 2\pi V/f$  is the inertial wavelength. Ideally, the pattern should extend up to  $1 \Lambda$  to resolve a full ocean response cycle. The storm speed  $V$  and flight duration limits will dictate whether this is possible. As for the pre-storm survey, either P-3 may be used since both of them have been equipped with new data systems as part of the HFP.

**OCEAN SURVEY EXPERIMENT**  
*Science Description*

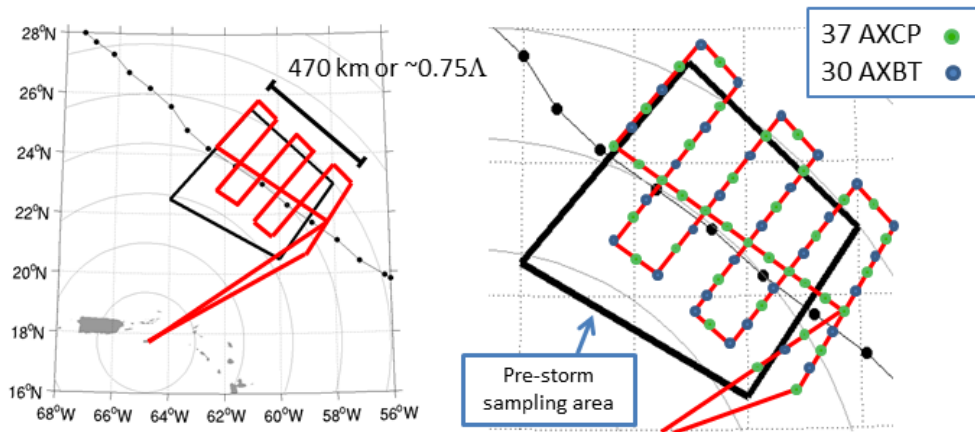


**Figure OC-4:** Left: Post-storm ocean sampling flight pattern (red line), over previously sampled area (black box). In this example, the pattern extends around 470 km in the along-track dimension, or around 0.75 of a near-inertial wavelength. Right: Flight pattern with expendable drop locations, consisting of a combination of AXCP and AXBT probes.

## 2. Coordinated float/drifter deployment by AFRC-130

Measurements will be made using arrays of drifters and E-M Apex (Gulf only) and Alamo (Beth) floats deployed by AFRC WC-130J aircraft in a manner similar to that used in the 2003 and 2004 CBLAST program. Additional deployments have since refined the instruments and the deployment strategies. These measurements provide the rapid time evolution of the response that will be coordinated with the synoptic snapshots of temperatures, salinities, and currents from the P-3 deployments of AXBTs, AXCTDs and AXCPs to obtain a more complete picture of the mesoscale ocean response to storms.

MiniMet drifters measure SST, sea level air pressure and wind velocity. Thermistor chain Autonomous Drifting Ocean Station (ADOS) drifters add ocean temperature measurements to 150 m. All drifter data are reported in real time through the Global Telecommunications System (GTS) of the World Weather Watch. An additional stream of real-time, quality controlled data is also provided by a server located at the Scripps Institution of Oceanography. A few E-M APEX Lagrangian floats will be deployed via the WC-130J that measure temperature, salinity and velocity profiles to as deep as 2000 m. Float profile data will be reported in real time on GTS via iridium. In addition, UM will have ten floats deployed in the northern Gulf of Mexico as part of a funded GoMRI study that measure these physical parameters as well as biogeochemical parameters.



OCEAN SURVEY EXPERIMENT  
*Science Description*

---

(a) Coordination and Communications

Alerts of possible deployments will be sent to the 53rd AWRO up to 5 days before deployment, with a copy to CARCAH, in order to help with preparations. Luca Centuriono (SIO) and Rick Lumpkin (PhOD) will be the primary point of contact for coordination with the 53rd WRS and CARCAH.

(b) Flights

Coordinated drifter deployments would nominally consist of 2 flights, the first deployment mission by AFRC WC-130J and the second overflight by NOAA WP-3D. An option for follow-on missions would depend upon available resources.

*Day 1, WC-130J Float and drifter array deployment:* Figure OC-5 shows a possible nominal deployment pattern for the float and drifter array. It consists of two lines, A and B, set across the storm path with 8 and 4 elements respectively. The line length is chosen to be long enough to span the storm and anticipate the errors in forecast track, and the lines are approximately in the same location as the pre-storm P-3 expendable probe survey. Instrumentation should be deployed 24–48 hours prior to storm arrival. The element spacing is chosen to be approximately the RMW. In case of large uncertainties of the forecast track a single 10 node line is deployed instead. The thermistor chain drifters (ADOS) are deployed near the center of the array to maximize their likelihood of seeing the maximum wind speeds and ocean response. The Minimet drifters are deployed in the outer regions of the storm to obtain a full section of storm pressure and wind speeds. The drifter array is skewed one element to the right of the track in order to sample the stronger ocean response on the right side (cold wake).

*Day 2, P-3 Pattern #2: Ocean Survey (In-storm):* The in-storm mission will be conducted by the P-3 as previously described in *P-3 Pattern #2: Ocean Survey (In-storm)*. Efforts will be made to deploy AXBTs during the mission near the locations of drifters/floats as reported in real time. It is highly desirable that this survey be combined with an WSRA surface wave survey because high quality surface wave measurements are essential to properly interpret and parameterize the air-sea fluxes and boundary layer dynamics, and so that comparisons between the float wave measurements and the SRA wave measurements can be made. In addition, the directional wave measurements from the WSRA, when combined with current measurements from AXCPs or E-M Apex floats, provide structural observations of the effect of surface waves on the oceanic planetary boundary layer processes.

OCEAN SURVEY EXPERIMENT  
*Science Description*

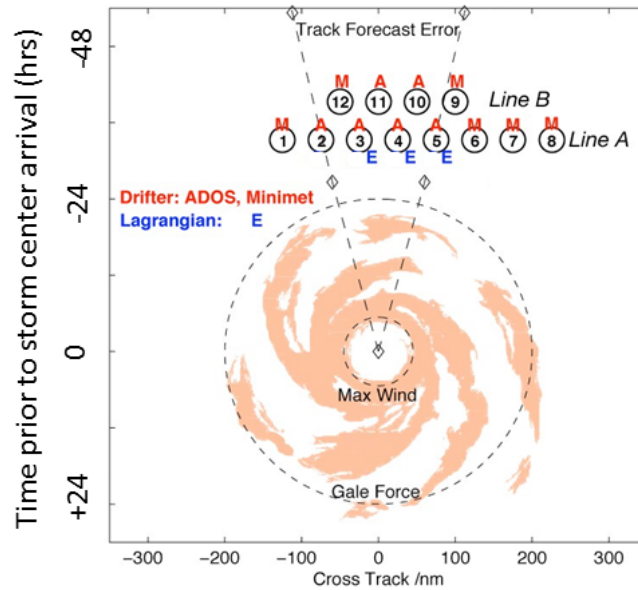


**Figure OC-5:** Drifter array deployed by AFRC WC-130J aircraft. The array is deployed ahead of the storm with the exact array location and spacing determined by the storm speed, size and the uncertainty in the storm track. The array consists of ADOS thermistor chain (A) and minimet (M) drifters, and EM-APEX Lagrangian floats (E). Two items are deployed at locations 3, 4 and 5, and one item elsewhere.

3. AXBT deployments by TROPIC on AFRC C-130

In addition to the P-3 expendable ocean probe deployments described above, additional ocean temperature profiles will be obtained by AFRC WC-130J aircraft as part of the Training and Research in Oceanic and Atmospheric Processes in Tropical Cyclones (TROPIC) program under the direction of CDR Elizabeth Sanabia, Ph.D. (USNA). Several overlapping mission goals have been identified providing an additional opportunity for collaboration and enhancing observational data coverage.

See [www.onr.navy.mil/reports/FY11/mmsanabi.pdf](http://www.onr.navy.mil/reports/FY11/mmsanabi.pdf) for details.

4. Loop Current Experiment

(a) Pre- and post-storm expendable profiler surveys

**P-3 Pattern #4: Ocean Survey (Loop Current, Pre- and Post-storm)**

*Feature-dependent survey.* Each survey consists of deploying 60–80 expendable probes, with takeoff and recovery at AOC. Pre-storm missions are to be flown one to three days prior to the TC’s passage in the LC (Fig. OC-6). Post-storm missions are to be flown one to three days after storm passage, over the same area

## OCEAN SURVEY EXPERIMENT

### *Science Description*

as the pre-storm survey. Since the number of deployed expendables exceeds the number of external sonobuoy launch tubes, profilers must be launched via the free-fall chute inside the cabin. Therefore the flight is conducted un-pressurized at a safe altitude (6–8 kft). In-storm missions, when the TC is passing directly over the observation region, will typically be coordinated with other operational or research missions (e.g. Doppler Winds missions). These flights will require 20–40 aircraft expendables deployed for measuring sea surface temperatures, salinity and currents underneath the storm.

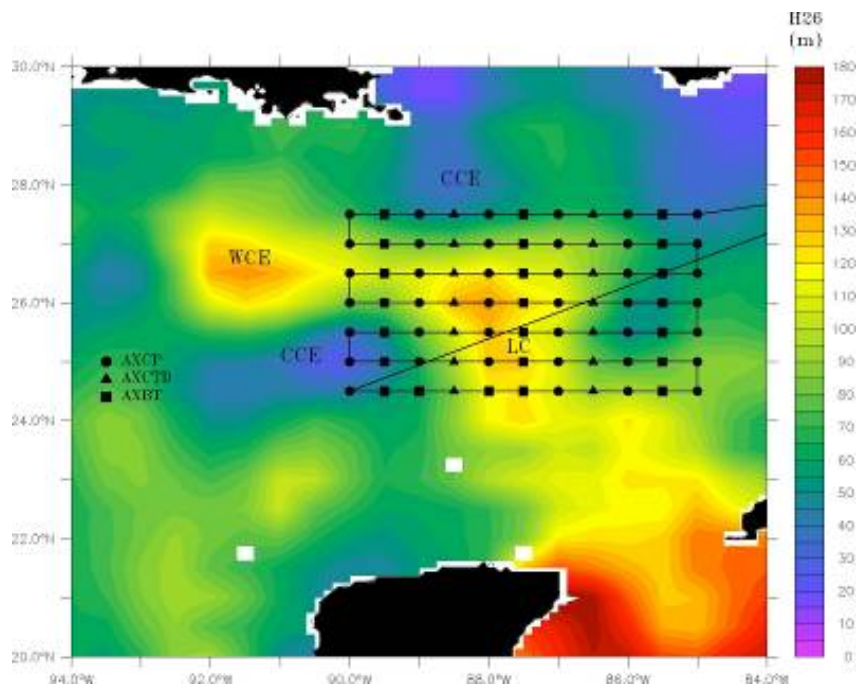


**Figure OC-6:** Typical pre- or post-storm pattern with ocean expendable deployment locations relative to the Loop Current. Specific patterns will be adjusted based on actual and forecasted storm tracks and Loop Current locations. Missions generally are expected to originate and terminate at KMCF.

*Track-dependent survey.* For situations that arise in which a TC is forecast to travel outside of the immediate Loop Current region, a pre- and post-storm ocean survey focused on the official track forecast is necessary. The pre-storm mission consists of deploying AXBTs/AXCTDs on a regularly spaced grid, considering the uncertainty associated with the track forecast. A follow-on post-storm mission would then be executed in the same general area as the pre-storm grid, possibly adjusting for the actual storm motion. Figure OC-7 shows a scenario for a pre-storm survey, centered on the 48-h forecast position. This sampling strategy covers the historical “cone of uncertainty” for this forecast period.

**OCEAN SURVEY EXPERIMENT**  
*Science Description*



**Figure OC-7:** Track-dependent AXBT/AXCTD ocean survey. As for the Loop Current survey, a total of 60–80 probes would be deployed on a grid (blue dots).

(b) Coordinated float/drifter deployment overflights

Measurements will be made using arrays of drifters deployed by AFRC WC-130J aircraft in a manner similar to that used in the 2003 and 2004 CBLAST program. Additional deployments have since refined the instruments and the deployment strategies. MiniMet drifters measure SST, sea level air pressure and wind velocity. Thermistor chain Autonomous Drifting Ocean Station (ADOS) drifters add ocean temperature measurements to 150 m. All drifter data are reported in real time through the Global Telecommunications System (GTS) of the World Weather Watch. An additional stream of real-time, quality controlled data is also provided by a server located at the Scripps Institution of Oceanography.

If resources are available from other Principal Investigators, flux Lagrangian floats will measure temperature, salinity, oxygen and nitrogen profiles to 200 m, boundary layer evolution and covariance fluxes of most of these quantities, wind speed and scalar surface wave spectra, while E-M APEX Lagrangian floats will measure temperature, salinity and velocity profiles to 200 m. Float profile data will be reported in real time on GTS.

This drifter effort is supported by the Global Drifter Program. The HRD contribution consists of coordination with the operational components of the NHC and the 53rd AFRC squadron and P-3 survey flights over the array with SFMR and SRA wave measurements and dropwindsondes. If the deployments occur in the Gulf of Mexico, Loop Current area, this work will be coordinated with P-3 deployments of AXBTs, AXCTDs and AXCPs to obtain a more complete picture of the ocean response to storms in this complex region.

OCEAN SURVEY EXPERIMENT  
*Science Description*

---

(c) Coordination and Communications

Alerts - Alerts of possible deployments will be sent to the 53rd AWRO up to 5 days before deployment, with a copy to CARCAH, in order to help with preparations. Luca Centurioni (SIO) and Rick Lumpkin (PhOD) will be the primary point of contact for coordination with the 53rd WRS and CARCAH.

(d) Flights

Coordinated drifter deployments would nominally consist of 2 flights, the first deployment mission by AFRC WC-130J and the second overflight by NOAA WP-3D. An option for follow-on missions would depend upon available resources.

*Day 1, WC-130J Float and drifter array deployment:* Figure OC-8 shows a possible nominal deployment pattern for the float and drifter array. It consists of two lines, A and B, set across the storm path with 8 and 4 elements respectively. The line length is chosen to be long enough to span the storm and anticipate the errors in forecast track. The element spacing is chosen to be approximately the RMW. In case of large uncertainties of the forecast track a single 10 node line is deployed instead. The thermistor chain drifters (ADOS) are deployed near the center of the array to maximize their likelihood of seeing the maximum wind speeds and ocean response. The Minimet drifters are deployed in the outer regions of the storm to obtain a full section of storm pressure and wind speeds. The drifter array is skewed one element to the right of the track in order to sample the stronger ocean response on the right side (cold wake). Three Lagrangian floats (E-M Apex) will be deployed along the track, 1–2 RMW and 3–4 RMW to measure the rapidly evolving velocity shear and extent of the vertical mixing and cooling of the surface mixed layer.

*Day 2. P-3 Pattern #6: Ocean Survey (Float and Drifter)*

Figure OC-9 shows the nominal P-3 flight path and dropwindsonde locations during the storm passage over the float and drifter array. The survey should ideally be timed so that it occurs as the storm is passing over the drifter array.

The survey includes legs that follow the elements of float/drifter line ‘A’ at the start and near the end. The survey anticipates that the floats and drifters will have moved from their initial position since deployment and will move relative to the storm during the survey. Waypoints 1–6 and 13–18 will therefore be determined from the real-time positions of the array elements. Each line uses 10 dropwindsondes, one at each end of the line; and two at each of the 4 floats, the double deployments are done to increase the odds of getting a 10 m data.

The rest of the survey consists of 8 radial lines from the storm center. Dropwindsondes are deployed at the eye, at half Rmax, at Rmax, at twice Rmax

OCEAN SURVEY EXPERIMENT  
*Science Description*

---

and at the end of the line, for a total of 36 releases. Aircraft expendables are deployed from the sonobuoy launch tubes at the eye, at Rmax and at 2 Rmax. This array is focused at the storm core where the strongest air-sea fluxes occur; the buoy and float array will fill in the SST field in the outer parts of the storm. In this particular example, the final two radials have been moved after the second float survey to avoid upwind transits. For other float drift patterns, this order might be reversed.

It is highly desirable that this survey be combined with an SRA surface wave survey because high quality surface wave measurements are essential to properly interpret and parameterize the air-sea fluxes and boundary layer dynamics, and so that intercomparisons between the float wave measurements and the SRA wave measurements can be made. In addition, the directional wave measurements from the WSRA, when combined with current measurements from AXCPs or E-M Apex floats, provide structural observations of the effect of surface waves on the oceanic planetary boundary layer processes.

(e) Extended Mission Description

If the storm remains strong and its track remains over water, a second or possibly third oceanographic array may be deployed, particularly if the predicted track lies over a warm ocean feature predicted to cause storm intensification. The extended arrays will consist entirely of thermistor chain and Minimet drifters, with 7–10 elements in a single line. As with the main mission, the spacing and length of the line will be set by the size of the storm and the uncertainty in the forecast track.

Mission timing and coordination will be similar to that described above. P-3 overflights would be highly desirable.

**OCEAN SURVEY EXPERIMENT**  
*Science Description*

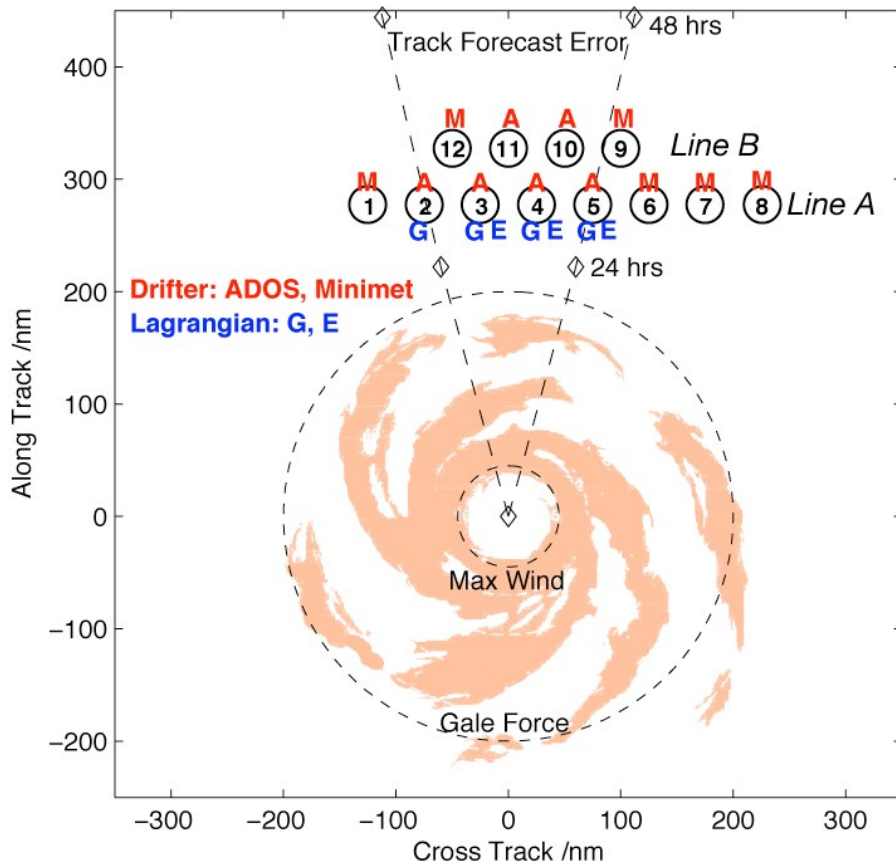


**Figure OC-8:** Drifter array deployed by AFRC WC-130J aircraft. The array is deployed ahead of the storm with the exact array location and spacing determined by the storm speed, size and the uncertainty in the storm track. The array consists of ADOS thermistor chain (A) and minimet (M) drifters. Gas (G) and EM (E) Lagrangian floats could be added if available. Three items are deployed at locations 3, 4 and 5, two items at location 3 and one item elsewhere.

OCEAN SURVEY EXPERIMENT  
*Science Description*

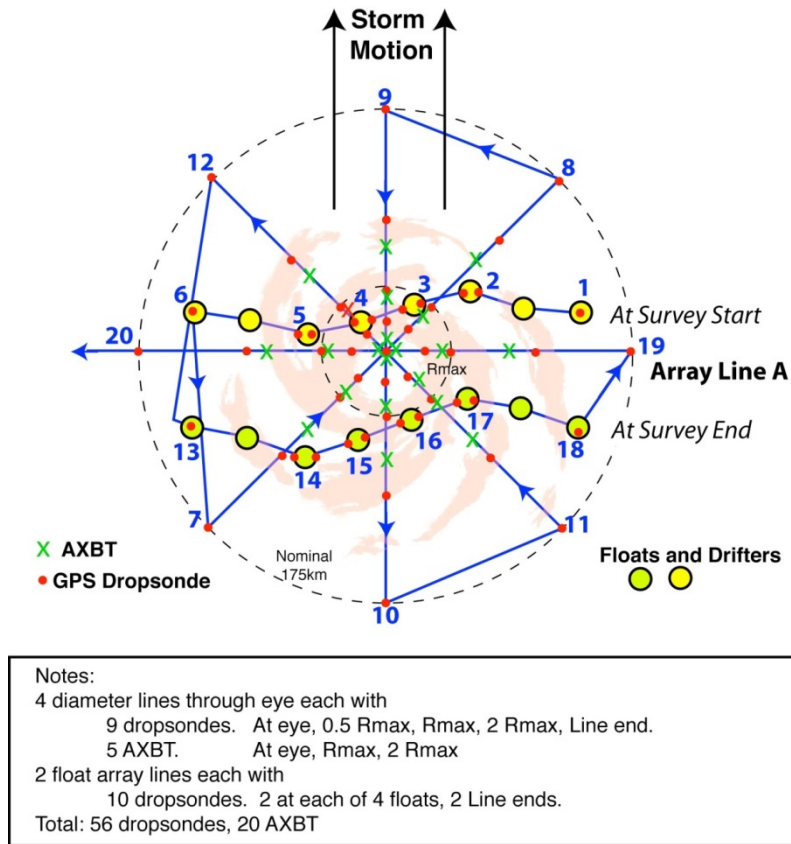


**Figure OC-9:** P-3 pattern over float and drifter array. The array has been distorted since its deployment on the previous day and moves relative to the storm during the survey. The pattern includes two legs along the array (waypoints 1–6 and 13–18) and an 8 radial line survey. Dropwindsondes are deployed along all legs, with double deployments at the floats. AXBTs are deployed in the storm core.



**OCEAN SURVEY EXPERIMENT**  
*Science Description*

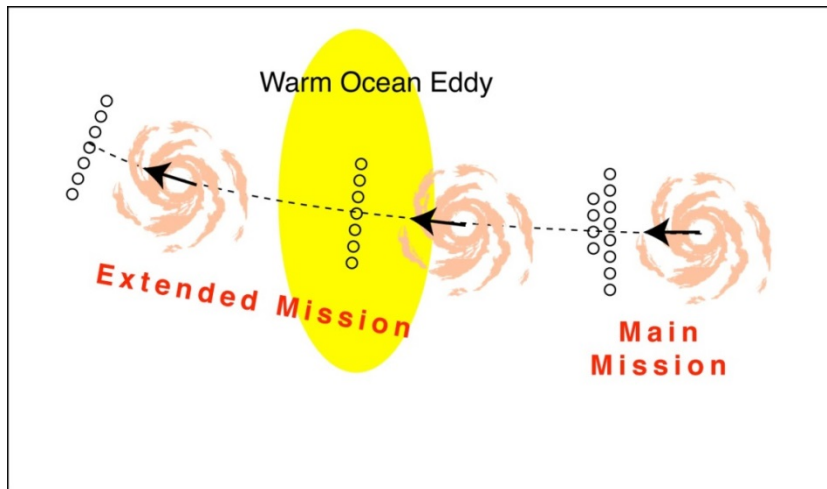


**Figure OC-10:** *Extended Mission.* Two additional drifter arrays will be deployed along the storm track.

**Analysis Strategy:** Upper-ocean three-dimensional thermal, salinity, and current structures will be measured from P-3 aircraft with airborne expendable bathythermographs (AXBT), conductivity–temperature–depth sensors (AXCTD), and current profilers (AXCP). Specifically, AXBT data will be acquired to ~400-m depth, compared to 1000 m and 1500 m for AXCTD and AXCP data, respectively. Additionally, measurements will be made using arrays of profiling and Lagrangian floats (APEX-EM) and drifters deployed by AFRC WC-130J aircraft in a manner similar to that used in the 2003 and 2004 CBLAST program (Black et al. 2007). Additional deployments have since refined the instruments and the deployment strategies. MiniMet drifters will measure SST, surface pressure and wind speed and direction. Thermistor chain Autonomous Drifting Ocean Station (ADOS) drifters add ocean temperature measurements to 150 m. All drifter data is reported in real time through the Global Telecommunications System (GTS). Flux Lagrangian floats will measure temperature, salinity, oxygen and nitrogen profiles to 200 m, boundary layer evolution and covariance fluxes of most of these quantities, windspeed and scalar surface wave spectra. E-M Lagrangian floats will measure temperature, salinity and velocity profiles to 200 m. Profile data will be reported in real time on GTS.

The basic analysis follows that presented in recent observational studies of TC-ocean interaction (Shay et al. 1992; 1994; 2000; Shay and Uhlhorn 2008; Halliwell et al. 2011; Zhang et al. 2011, 2013, 2015; Sanabia et al. 2013; Jaimes et al. 2015; 2016; Lumpkin 2016). These analyses include: estimate of sea surface cooling after the storm; estimate of change in the ocean mixed layer depth and ocean heat content (relative to the 26°C isotherm depth) during and after the storm; computation of surface fluxes using the bulk method; estimate of ocean current change during and after the storm, with emphasis in upwelling processes and vertical shear development; and evaluation of the surface-layer

OCEAN SURVEY EXPERIMENT  
*Science Description*

---

and boundary-layer structure in operational hurricane models using the observational data collected in this experiment.

**References:**

- Halliwell, G., L. K. Shay, J. K. Brewster, and W. J. Teague, 2011: Evaluation and sensitivity analysis to an ocean model to hurricane Ivan. *Mon. Wea. Rev.* **139**, 921-945.
- Lumpkin, R.: Global Characteristics of Coherent Vortices from Surface Drifter Trajectories. *J. Geophys. Res.-Oceans*, **121**, 1306–1321, <http://dx.doi.org/10.1002/2015JC011435>.
- Jaimes, B., L. K. Shay and E. W. Uhlhorn, 2015: Observed enthalpy fluxes during the rapid intensity change of hurricane Earl. *Mon. Wea. Rev.*, **131**, 111–131.
- Jaimes, B., L. K. Shay and J. K. Brewster, 2016: Observed Air-Sea Interactions in Tropical Cyclone Isaac Over Loop Current Mesoscale Eddy Features *Dyn. Atmos. Ocean.*, **76**, 306–324.
- Sanabia, E. R., B. S. Barrett, P. G. Black, S. Chen, and J. A. Cummings, 2013: Real-time upper-ocean temperature observations from aircrafts during operational hurricane reconnaissance: AXBT demonstration project year one results. *Wea. Forecasting*, **28**, 1404–1422
- Shay, L.K., P.G. Black, A.J. Mariano, J.D. Hawkins and R.L. Elsberry, 1992: Upper ocean response to hurricane Gilbert. *J. Geophys. Res.*, **97**, 20,227–20,248.
- Shay, L.K., E.J. Walsh and P.C. Zhang. 1994: Orbital velocities induced by surface waves. *J. Atmos. Ocean. Tech.*, 11(4), Part 2, 1117 –1125.
- Shay, L.K., G.J. Goni and P.G. Black, 2000: Effects of a warm oceanic feature on Hurricane Opal. *Mon. Wea. Rev.*, **125(5)**, 1366–1383.
- Shay, L.K., and E. Uhlhorn, 2008: Loop current response to hurricanes Isidore and Lili, *Mon. Wea. Rev.*, **137**, 3248–3274.
- Uhlhorn, E., and L. K. Shay, 2012: Loop current mixed layer response to Hurricane Lili (2002), Part I: Observations. *J. Phys. Oceanog.*, **42**, 400–419.
- Zhang, J. A., R. F. Rogers, D. S. Nolan, and F. D. Marks, 2011: On the characteristic height scales of the hurricane boundary layer, *Mon. Wea. Rev.*, **139**, 2523–2535.
- Zhang, J. A., R. F. Rogers, P. Reasor, E. Uhlhorn, and F. D. Marks, 2013: Asymmetric hurricane boundary layer structure from dropsonde composites in relation to the environmental vertical wind shear. *Mon. Wea. Rev.*, **141**, 3968–3984.

OCEAN SURVEY EXPERIMENT  
*Science Description*

---

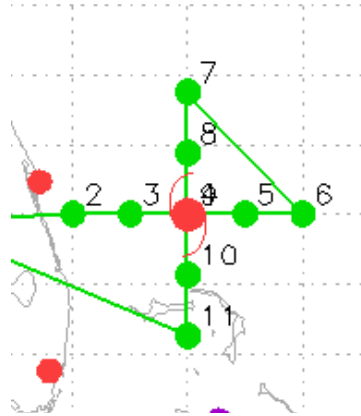
Zhang, J. A., D. S. Nolan, R. F. Rogers, and V. Tallapragada, 2015: Evaluating the impact of improvements in the boundary layer parameterization on hurricane intensity and structure forecasts in HWRF, *Mon. Wea. Rev.*, *143*, 3136–3155.

APPENDIX A  
*Standard Patterns and Expendable Locations*

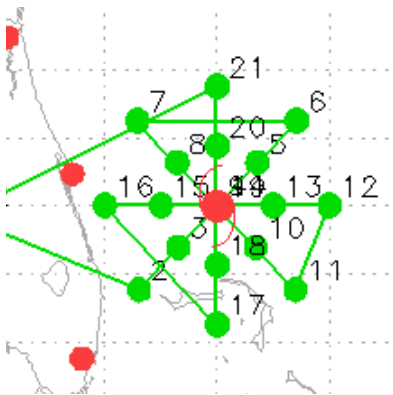
---

CURRENT AS OF FEBRUARY 22, 2018

**Figure-4:** Centers, mid-points and turn points of each leg [10 sondes]  
In-pattern duration (105 n mi legs): ~ 2 h 15 min (P-3), 1 h 20 min (G-IV)



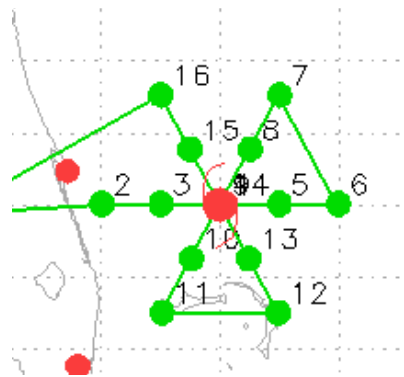
**Rotated Figure-4:** Centers, mid-points and turn points of each leg [20 sondes]  
In-pattern duration (105 n mi legs): ~ 5 h (P-3), 2 h 55 min (G-IV)



APPENDIX A  
*Standard Patterns and Expendable Locations*

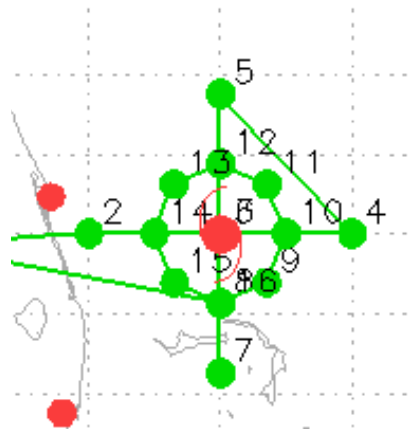
---

**Butterfly:** Centers, mid-points and turn points of each leg [15 sondes]  
In-pattern duration (105 n mi legs): ~ 3 h 25 min (P-3), 2 h (G-IV)



**P-3 Circumnavigation:** Center of first pass, end points of Figure-4 and vertices of octagon [14 sondes]

In-pattern duration (105 n mi legs): ~ 4 h 5 min

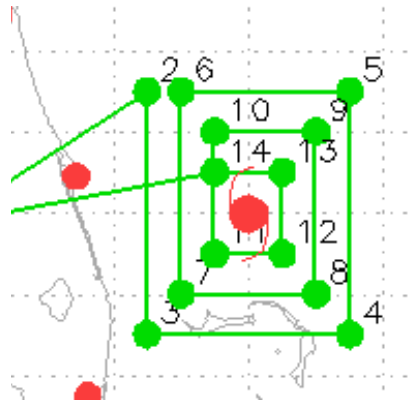


APPENDIX A  
*Standard Patterns and Expendable Locations*

---

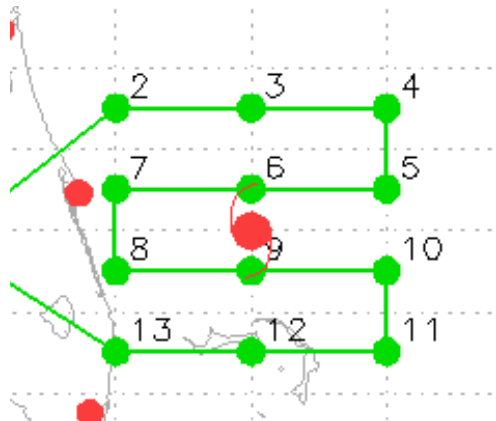
**Square Spiral:** Turn points [13 sondes]

In-pattern duration (180 n mi on a side): ~ 5 h 50 min (P-3), 3 h 20 min (G-IV)



**Lawnmower:** Turn points and mid-points of N-S legs [12 sondes]

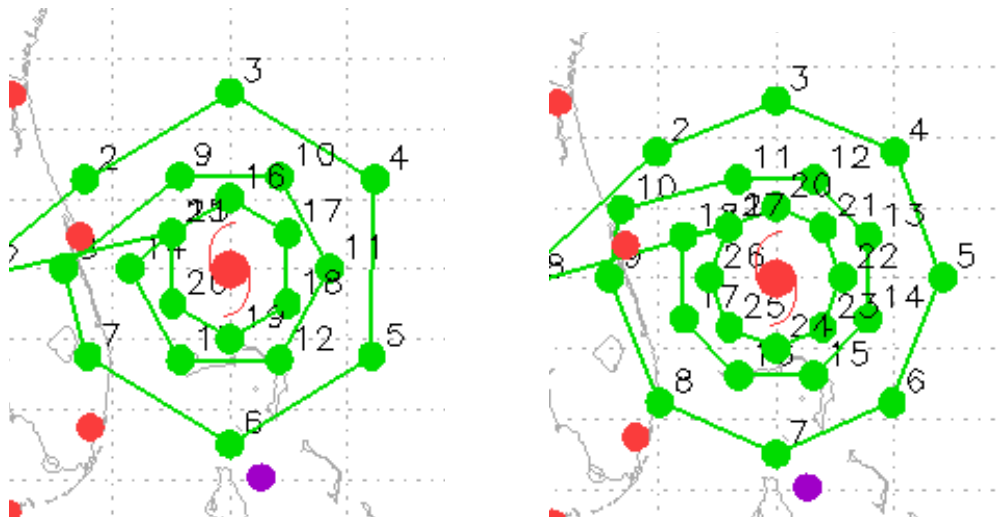
In-pattern duration (240 n mi by 180 n mi): ~ 4 h 20 min (P-3), 2 h 25 min (G-IV)



APPENDIX A  
*Standard Patterns and Expendable Locations*

---

**G-IV Circumnavigation:** Vertices of hexagon (octagon) [18 (24) sondes]  
In-pattern duration (150, 90, 60 n mi): ~ 4 h 25 min (4 h 35 min)



APPENDIX A  
*Standard Patterns and Expendable Locations*

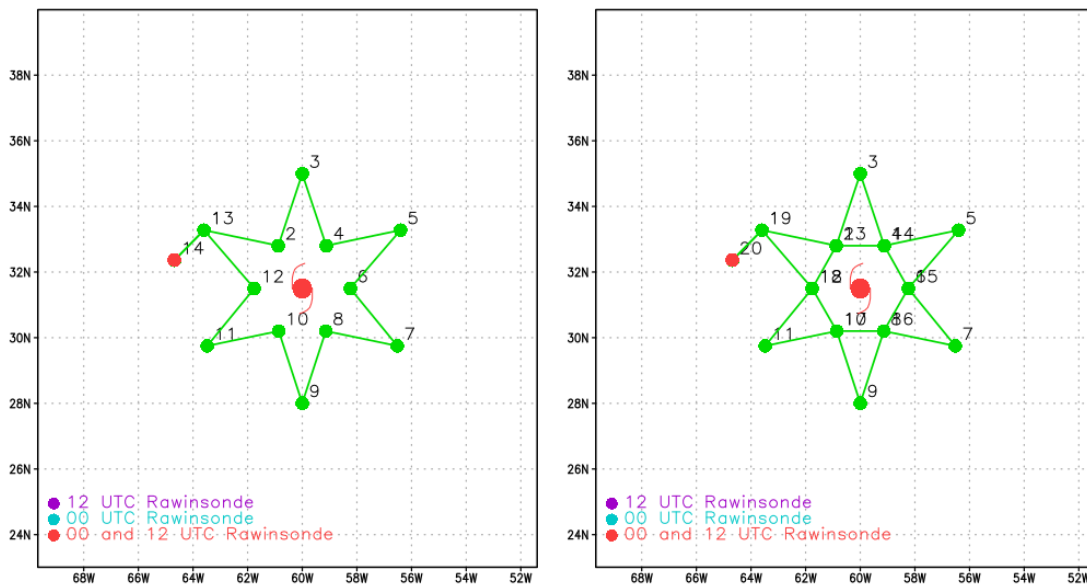
**G-IV Star/Star with Circumnavigation:** Vertices of star [13/19 sondes with hexagonal circumnavigation]

In-pattern duration (outer points, 210 n mi; inner points, 90 n mi): 4 h

In-pattern duration with circumnavigation: 5 h 15 min

Note: for outer endpoint adjustments, every 0.5° bump inward/outward, subtracts/adds ~45 min from/to the pattern

Note: inner endpoint adjustments, going from 90 n mi to 60 n mi subtracts ~15 min from the pattern





**APPENDIX B**  
*Decision and Notification Process*

---

The decision and notification process is illustrated in Figs. B-1, B-2, and B-3. The typical timing of pre-flight activities is provided in Fig. B-4. The decision and notification process occurs in four steps:

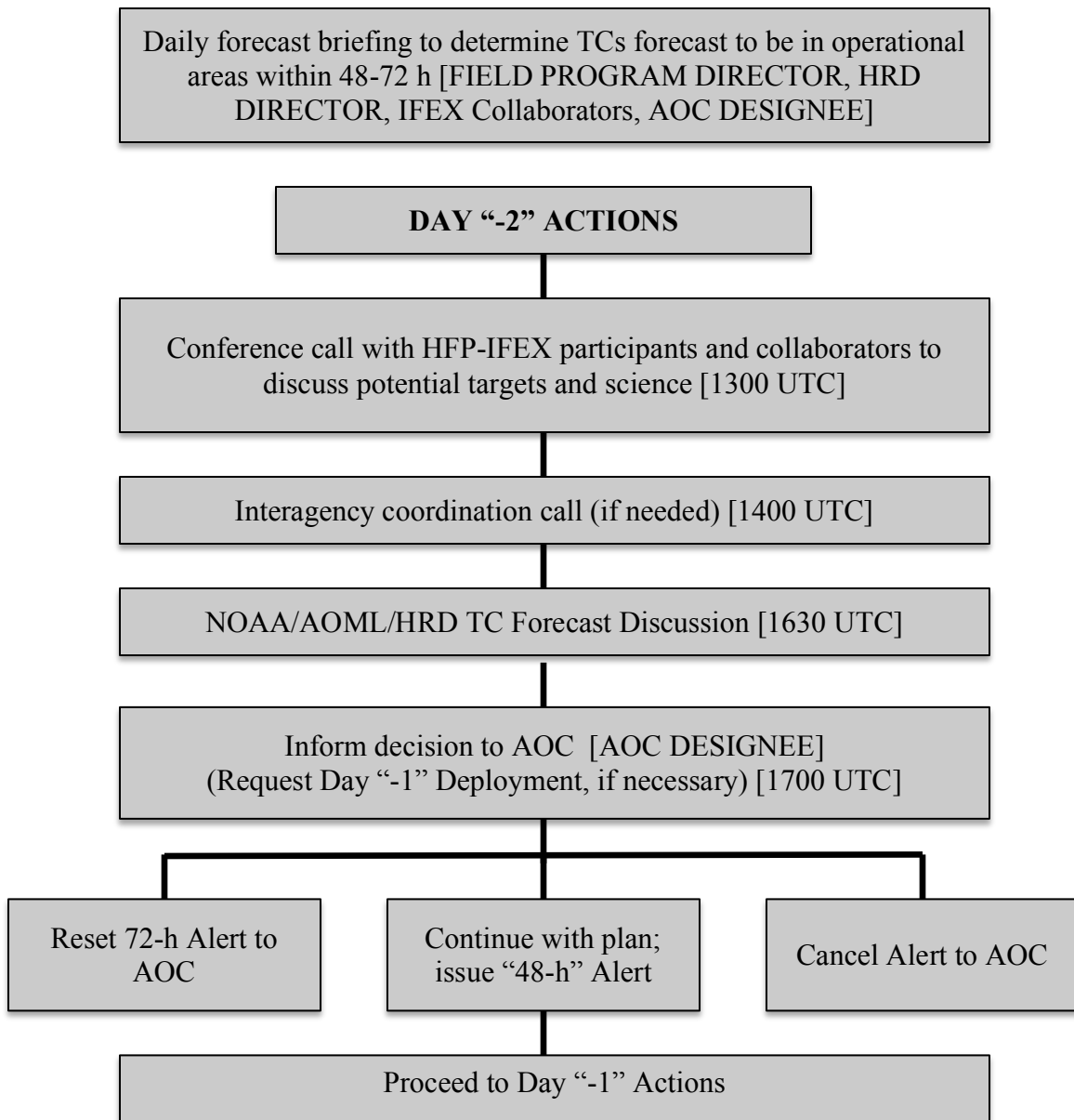
- 1) A research mission is determined to be probable within 72 h by [FIELD PROGRAM DIRECTOR]. Consultation with PIs, [HRD DIRECTOR] and [AOC DESIGNEE] determines: flight platform availability, crew and equipment status, and the type of mission(s) likely to be requested.
- 2) [FIELD PROGRAM DIRECTOR], [HRD DIRECTOR] or their designee, and PIs of relevant experiments meet to discuss possible missions and operational modes. [HRD DIRECTOR] or their designee provides approval to proceed on the mission objectives and strategy, and deployment logistics (i.e., travel, crewing).
- 3) The PIs, HRD SCIENCE CREW, and other personnel (visitors, IFEX Collaborators) are notified of mission objectives, deployment logistics by [FIELD PROGRAM DIRECTOR]. HRD SCIENCE CREW and other personnel are to inform [HRD ADMINISTRATIVE] of travel plans.
- 4) Secondary personnel (i.e., visitors) are notified by their primary affiliate.

**NOTE: Day “-3” requirements are not included below, but could be required for deployments to locations outside of the U.S., at the discretion of [AOC DESIGNEE]**

APPENDIX B  
*Decision and Notification Process*

\*\*Note: Time of briefings, conference calls, decisions, and deployments are dictated by timing limitations imposed by the AOC crew

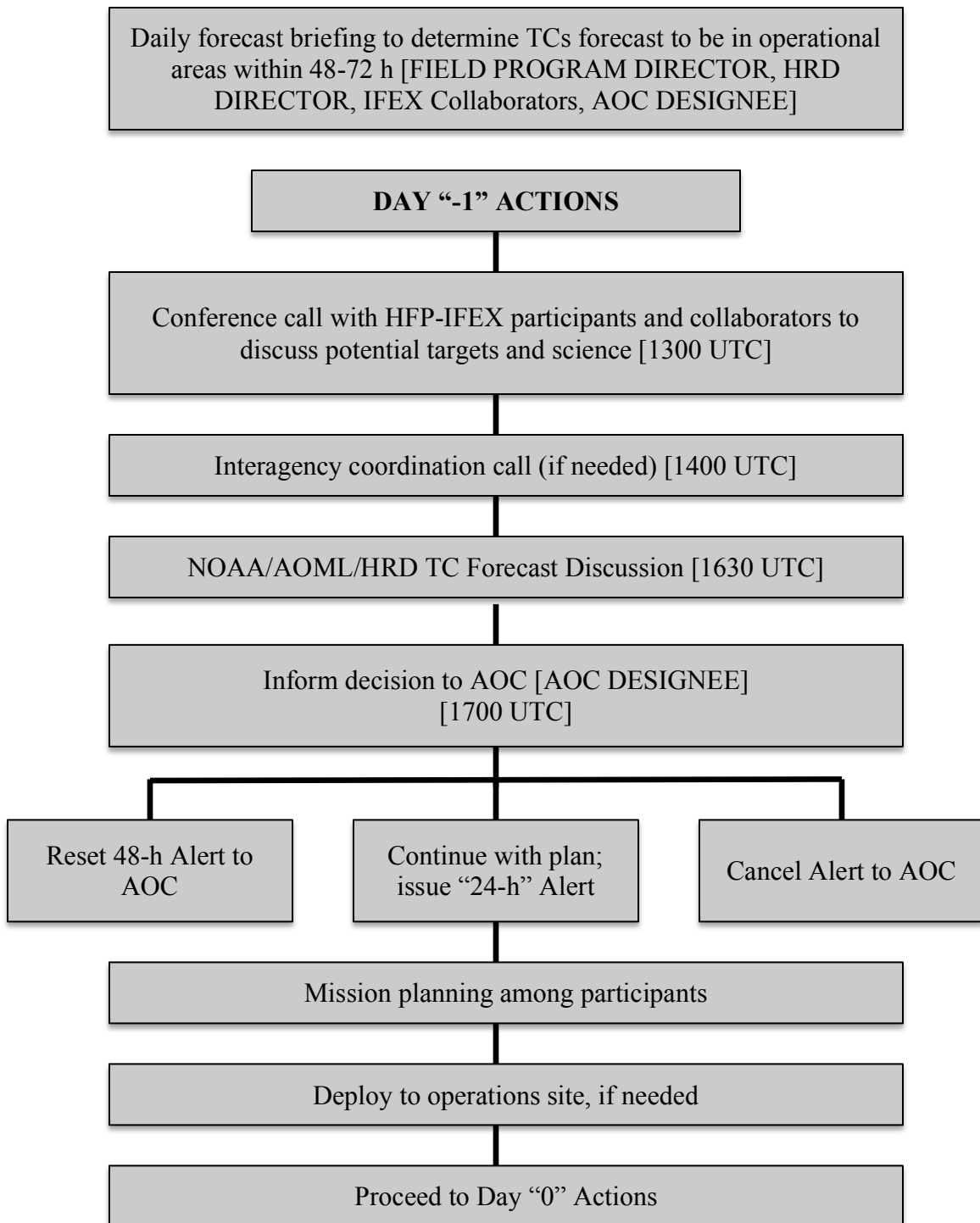
**Figure B-1.** Decision and notification process for Day “-2”



**APPENDIX B**  
*Decision and Notification Process*

\*\*Note: Time of briefings, conference calls, decisions, and deployments are dictated by timing limitations imposed by the AOC crew

**Figure B-2.** Decision and notification process for Day “-1”

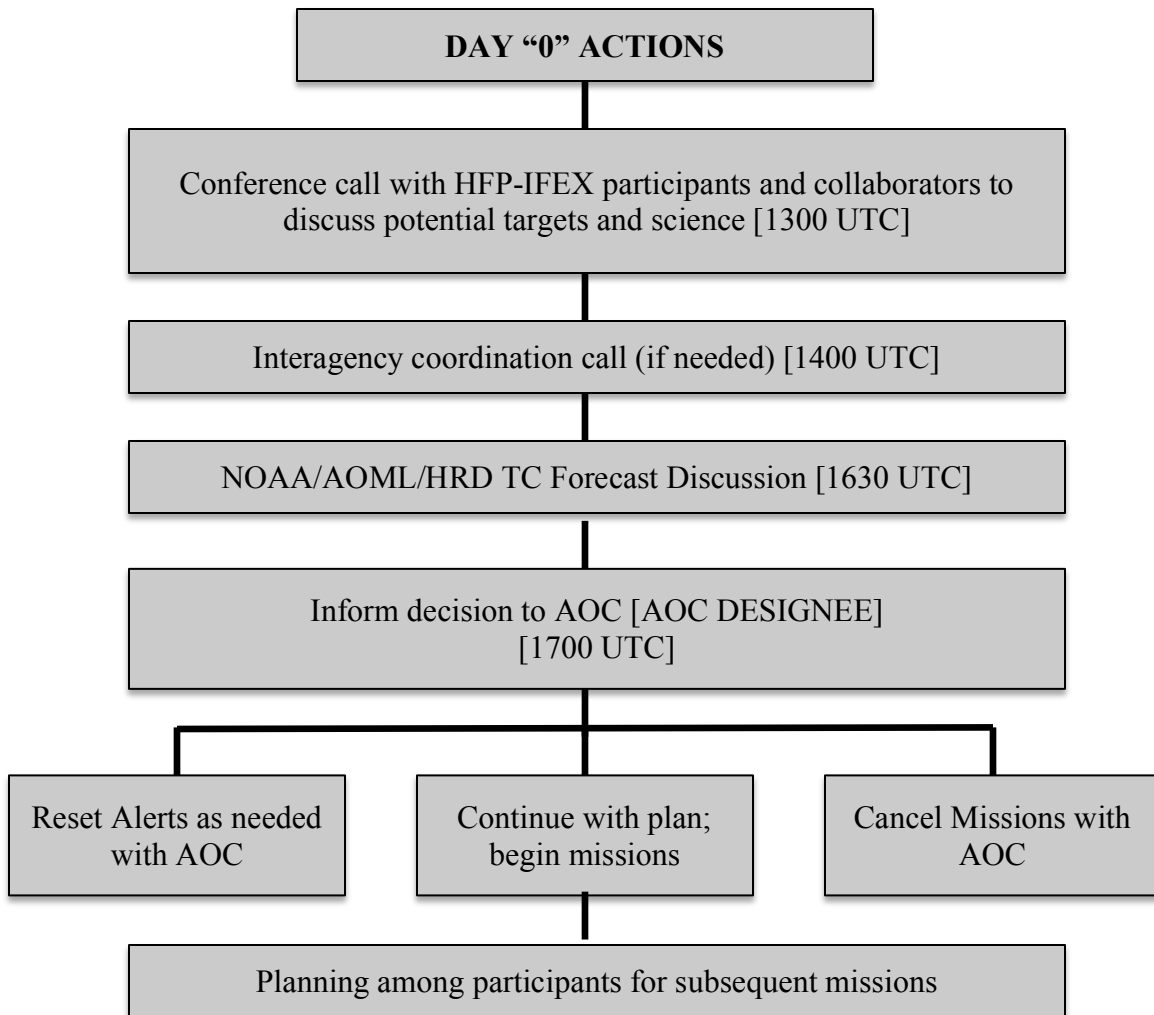


**APPENDIX B**  
*Decision and Notification Process*

---

\*\*Note: Time of briefings, conference calls, decisions, and deployments are dictated by timing limitations imposed by the AOC crew

**Figure B-3.** Decision and notification process for Day “0”

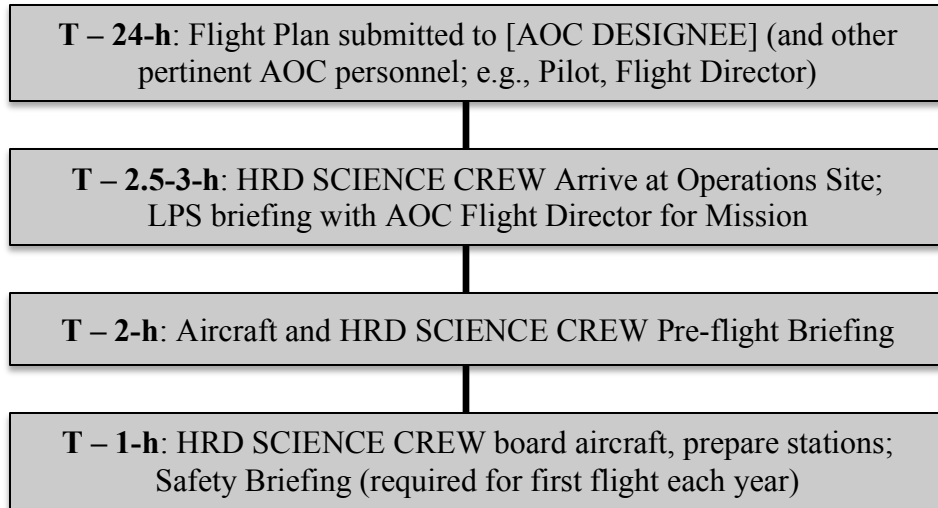


APPENDIX B  
*Decision and Notification Process*

---

\*\*Note: Time of briefings are dictated by timing limitations imposed by the AOC crew

**Figure B-4.** *Typical timing of pre-flight activities*



APPENDIX C  
*Principal Duties of HRD Scientific Personnel*

---

## 1. Safety

Flight operations are routinely conducted in turbulent conditions. Shock-mounted electronic and experimental racks surround most seat positions. Therefore, *for safety onboard the aircraft all personnel should wear a flight suit and closed toed shoes*. For comfort, personnel should bring a jacket or sweater, as the cabin gets cold during flight.

Smoking is prohibited within 50 ft of the aircraft while they are on the ground. No smoking is permitted on the aircraft at any time.

Section 4-401, of the NOAA Safety Rules Manual state that: “Don’t let your attention wander, either through constant conversation, use of cell phone or sightseeing while operating vehicles. Drivers must use caution and common sense under all conditions. Operators and passengers are not permitted to smoke or eat in the government vehicles. Cell phone use is permitted while car is parked.”

## 2. Conditions of Flight

Mission participants should be aware of the designated "conditions-of-flight." There are five designated basic conditions of readiness encountered during flight. The pilot will set a specific condition and announce it to all personnel over the aircraft's PA (public address) and ICS (interphone communications systems). All personnel are expected to act in accordance with the instructions for the specific condition announced by the pilot. These conditions and appropriate actions are shown below.

CONDITION 1: TURBULENCE/PENETRATION. All personnel will stow loose equipment and fasten safety belts.

CONDITION 2: HIGH ALTITUDE TRANSIT/FERRY. There are no cabin stations manning requirements.

CONDITION 3: NORMAL MISSION OPERATIONS. All scientific and flight crew stations are to be manned with equipment checked and operating as dictated by mission requirements. Personnel are free to leave their ditching stations.

CONDITION 4: AIRCRAFT INSPECTION. After take-off, crewmembers will perform wings, engines, electronic bays, lower compartments, and aircraft systems check. All other personnel will remain seated with safety belts fastened and headsets on.

CONDITION 5: TAKE-OFF/LANDING. All personnel will stow or secure loose equipment, don headsets, and fasten safety belts/shoulder harnesses.

APPENDIX C

*Principal Duties of HRD Scientific Personnel*

---

**3. General Information for All Scientific Mission Participants**

Mission participants are advised to carry the proper personal identification; i.e., travel orders, "shot" records (when appropriate), and passports. Passports will be checked by AOC personnel prior to deployment to countries requiring it. All participants must provide their own meals for in-flight consumption.

**4. HRD SCIENCE CREW Responsibilities**

FIELD PROGRAM DIRECTOR

- 1) Responsible to [HRD DIRECTOR] for the preparation and implementation of the HFPP
- 2) Only official communication link to AOC. Communicates flight requirements, patterns, and changes in mission to AOC crew (including [AOC DESIGNEE])
- 3) Only formal communication link between AOML and CARCAH during operations. Coordinates scheduling of each day's operations with AOC only after all (POD) reconnaissance requirements are completed between CARCAH and AOC
- 4) Works with PIs to select missions to be flown
- 5) Provides for pre-mission briefing of flight crews, HRD SCIENCE CREW, and others (as required)
- 6) Assigns duties and ensures safety of the HRD SCIENCE CREW
- 7) Coordinates press statements with NOAA/Public Affairs
- 8) Organizes necessary deployment debriefs and reports activities to [HRD DIRECTOR]

FIELD PROGRAM DEPUTY DIRECTOR

- 1) Assumes the duties of [FIELD PROGRAM DIRECTOR] in their absence
- 2) Assists [FIELD PROGRAM DIRECTOR] on any and all activities related to the HFP

PI(s)

- 1) Has overall responsibility for the experiment
- 2) Coordinates the project and sub-project requirements
- 3) Determines the primary modes of operation for appropriate instrumentation
- 4) Assists [FIELD PROGRAM DIRECTOR] in the selection and planning of missions for the experiment
- 5) Provides a written summary of the experiment accomplishments to [FIELD PROGRAM DIRECTOR] at the debrief

## 2018 NOAA/AOML/HRD Hurricane Field Program - IFEX

### APPENDIX C *Principal Duties of HRD Scientific Personnel*

---

#### LEAD PROJECT SCIENTIST [LPS]

- 1) Complete training and be familiar with any checklists
- 2) Has overall scientific responsibility for his/her aircraft mission
- 3) Communicates with the AOC Flight Director and makes in-flight decisions concerning alterations of: (a) flight patterns; (b) instrumentation operation; and (c) assignment of duties of HRD SCIENCE CREW
- 4) Acts as project supervisor on the aircraft and is the focal point for all interactions of project personnel with operational or visiting personnel
- 5) Conducts pre-flight and post-flight briefings for the flight crew. Completes formal checklists of safety, instrument operations, and data download (noting malfunctions, problems, etc.)
- 6) Provides a written report of each mission to [FIELD PROGRAM DIRECTOR], detailing issues encountered, interesting phenomena observed, (reasons for) changes in flight patterns and instrument status, and any other relevant details from each mission
- 7) Present mission summaries at experiment debrief

#### RADAR SCIENTIST

- 1) Complete training and be familiar with any checklists/guides
- 2) Prepares radar workstation for mission, including starting any software and radar displays
- 3) During the ferry to the storm, the radar scientist should check the performance of the radar (e.g., showing reflectivity, velocity in fore, aft scans in Tail radar)
- 4) Determines optimum meteorological target displays. Continuously monitors displays for performance of the radars and optimum mode of operations. Thoroughly documents modes and characteristics of the operations.
- 5) Communicates with ground radar scientists on the radar operations, resolves issues related to analysis software, and maintains logs
- 6) Downloads data onto media at the end of instrument operation
- 7) Provides a summary of the radar operation to the on-board LPS at the post-flight debriefing

#### DROPSONDE SCIENTIST

- 1) Complete training and be familiar with any checklists/guides
- 2) Prepares workstation, sets up software and directories to process and transmit dropsonde data
- 3) Processes dropsonde observations for accuracy
- 4) Generates and transmits TEMP drop messages
- 5) Downloads data onto media at the end of instrument operation
- 6) Provides a written pre-flight and post-flight status report and dropsonde summary to the on-board LPS at the post-flight debriefing



APPENDIX C

*Principal Duties of HRD Scientific Personnel*

---

CLOUD PHYSICS SCIENTIST

- 1) Has overall responsibility for the cloud physics project on the aircraft
- 2) Briefs the on-board LPS on equipment status before takeoff
- 3) Determines the operational mode of the cloud physics sensors (i.e., where, when, and at what rate to sample)
- 4) Operates and monitors the cloud physics sensors and data systems
- 5) Downloads data on media at the end of instrument operation
- 6) Provides a written pre-flight and post-flight status report and flight summary of each mission day's operations to the on-board LPS at the post-flight debriefing

BOUNDARY LAYER SCIENTIST

- 1) Ensures that the required number of AXCPs, AXBTs, and AXCTDs are on the aircraft for each mission
- 2) Operates the AXCP, AXBT, and AXCTD equipment (as required) on the aircraft
- 3) Briefs the on-board LPS on equipment status before takeoff
- 4) Determines where and when to release the AXCPs, AXBTs, and AXCTDs (as appropriate) subject to clearance by flight crew
- 5) Performs pre-flight, in-flight, and post-flight checks and calibrations
- 6) Provides a written pre-flight and post-flight status report and a flight summary of each mission day's operations to the on-board LPS at the post-flight debriefing

APPENDIX D  
Operational Maps

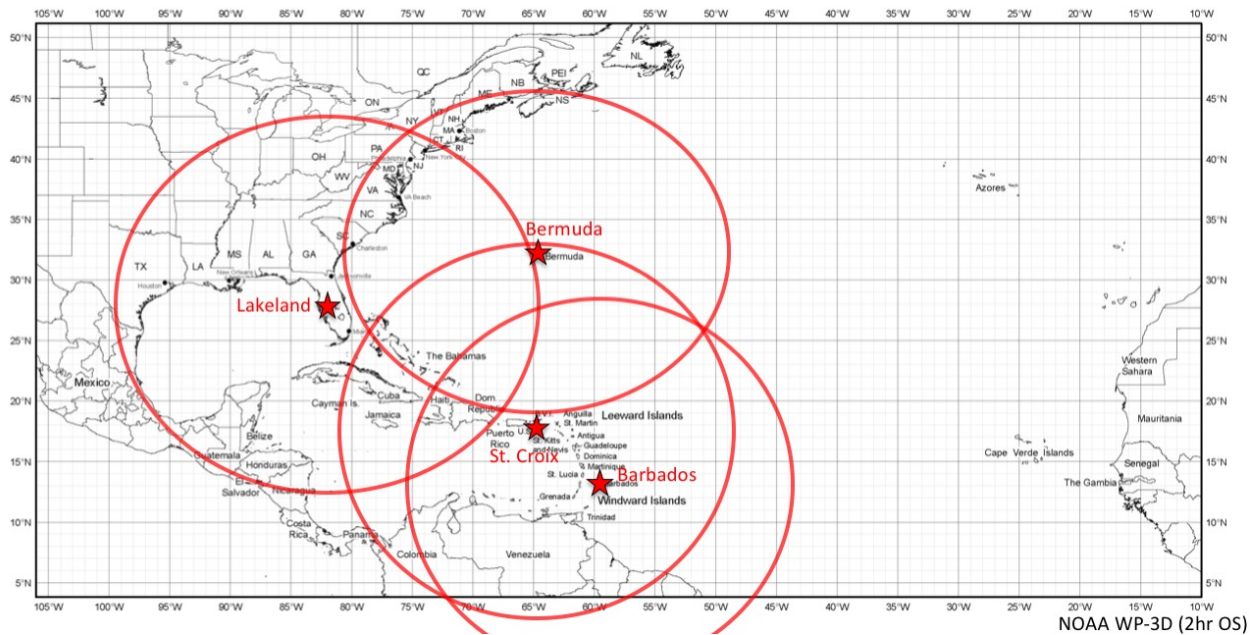


Figure D-1. Primary Atlantic operating bases and ranges (assuming ~2-h on-station time) for the P-3

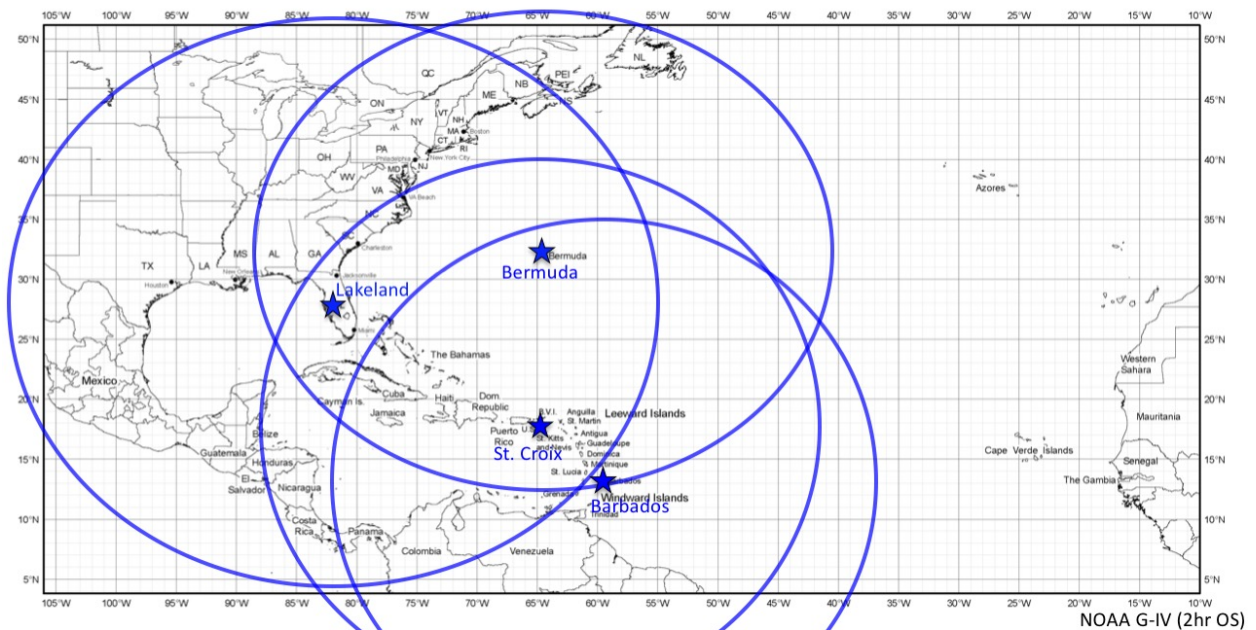


Figure D-2. Primary Atlantic operating bases and ranges (assuming ~2-h on-station time) for the G-IV

2018 NOAA/AOML/HRD Hurricane Field Program - IFEX

APPENDIX E  
Aircraft Instrumentation List

Table E-1. WP-3 (N42RF) instrumentation

Instrument	Parameter	PI	Group
<b>Navigational</b>			
INE1/2	lat, lon		AOC
GPS1/2	lat, lon		AOC
Honeywell HG9550 altimeter	Radar altitude		AOC
<b>Standard Meteorological</b>			
Buck1101c, Edgetech Vigilant, Maycom TDL	$T_g$		AOC
Rosemount temp	$T, T'$		AOC
Static pressure	$p$		AOC
Dynamic pressure	$p'$		AOC
Horizontal wind	$V_h$		AOC
Vertical wind	$w$		AOC
<b>Infrared Radiation</b>			
Side CO <sub>2</sub> radiometer	T		AOC
AOC down radiometer	SST		AOC
<b>Weather Radar</b>			
LF radar (MMR?)	R	Gamache	AOC
TA Doppler radar	V, R	Gamache	AOC
<b>Passive Microwave</b>			
AOC SFMR/pod	$V_{10}, Z$	Goldstein	AOC
2nd SFMR (until 8/15-31)	$V_{10}, Z$		
<b>Airborne Ocean Profiler</b>			
AOC (Mark 10/21) receivers for AXBTs, AXCTDs, AXCPs	T, S, u, v	Smith (N. Shay)	AOC (UM)
<b>Dropsonde Systems</b>			
GPS AVAPS Dropsonde-8CH	V, T, RH, p vs z	Smith	AOC
<b>Video Systems</b>			
Down video	F(%), WD	Cione	AOC
Right Side, and nose	LCL		AOC
<b>On board processing</b>			
PC/LINUX workstation	Radar - Radar processing, Web, xchat, Python 2.7, Numpy, Matplotlib	Hill	AOC
PC/LINUX workstation	LPS - xchat, Web, AAMPS	Hill	AOC
PC/LINUX workstation	Dropsonde - ASPEN, Web, xchat	Hill	AOC
Real-time data communications systems	FL, radar data	Chang, Carswell	NESDIS, RSS
<b>Active Microwave</b>			
IWRAP (CSCAT, KSCAT) (from 8/15-31)	$V_{10}, Z, V$ vs $z$	Chang	NESDIS
ProSensing WSRA (until 8/15-31)	HS, WPS, WDS	Fairall	ESRL, NHC
<b>Cloud Microphysics/Sea Spray</b>			
DMT CCP probe	Cloud particle spectra	R. Black	AOC
DMT PIP probe	Precipitation particle spectra	R. Black	AOC
DMT CAS probe	Aerosol/cloud droplet spectra	R. Black	AOC
DMT DAS processor		R. Black	AOC
SEA probe	liquid water	R. Black	AOC, HRD
<b>Weather Radar</b>			
Doppler Wind Lidar (until 8/15-31)	V, R	Atlas	HRD
Compact rotational Raman lidar (CRL) (from 8/15-31)	T, water vapor	J. Zhang, Z. Wang	HRD, Wyoming
<b>Turbulence Systems</b>			
Friehe radome gust probe system	U', V', W', T'	J. Zhang, Drennan	HRD, UM
<b>UAS</b>			
Coyote (P-3 deployed) (2 available?)	V, T, RH, p vs z and IR SST	Cione, Fairall	HRD, ESRL

2018 NOAA/AOML/HRD Hurricane Field Program - IFEX

APPENDIX E  
Aircraft Instrumentation List

Table E-2. G-IV (N49RF) instrumentation

Instrument	Parameter	PI	Group
<b>Navigational</b>			
INE1/2	lat, lon		AOC
GPS1/2	lat, lon		AOC
Honeywell HG9550 altimeter	Radar altitude		AOC
<b>Standard Meteorological</b>			
Buck1101c, Edgetech Vigilant, Maycom TDL	$T_d$		AOC
Rosemount temp	T, T'		AOC
Static pressure	p		AOC
Dynamic pressure	p'		AOC
Horizontal wind	$V_h$		AOC
Vertical wind	w		AOC
<b>Weather Radar</b>			
TA Doppler radar	V, R	Gamache	AOC
<b>Passive Microwave</b>			
SFMR	$V_{10}$ , Z	Goldstein	AOC
<b>Dropsonde Systems</b>			
GPS AVAPS Dropsonde-8CH	V, T, RH, p vs z	Smith	AOC
<b>On board processing</b>			
Real-time data communications systems	FL, radar data	Chang, Carswell	AOC
PC/LINUX Computer	radar data, sondes	Goldstein	AOC

APPENDIX F  
DOD/NWS RAWIN/RAOB and NWS Coastal Land-Based Radar Locations

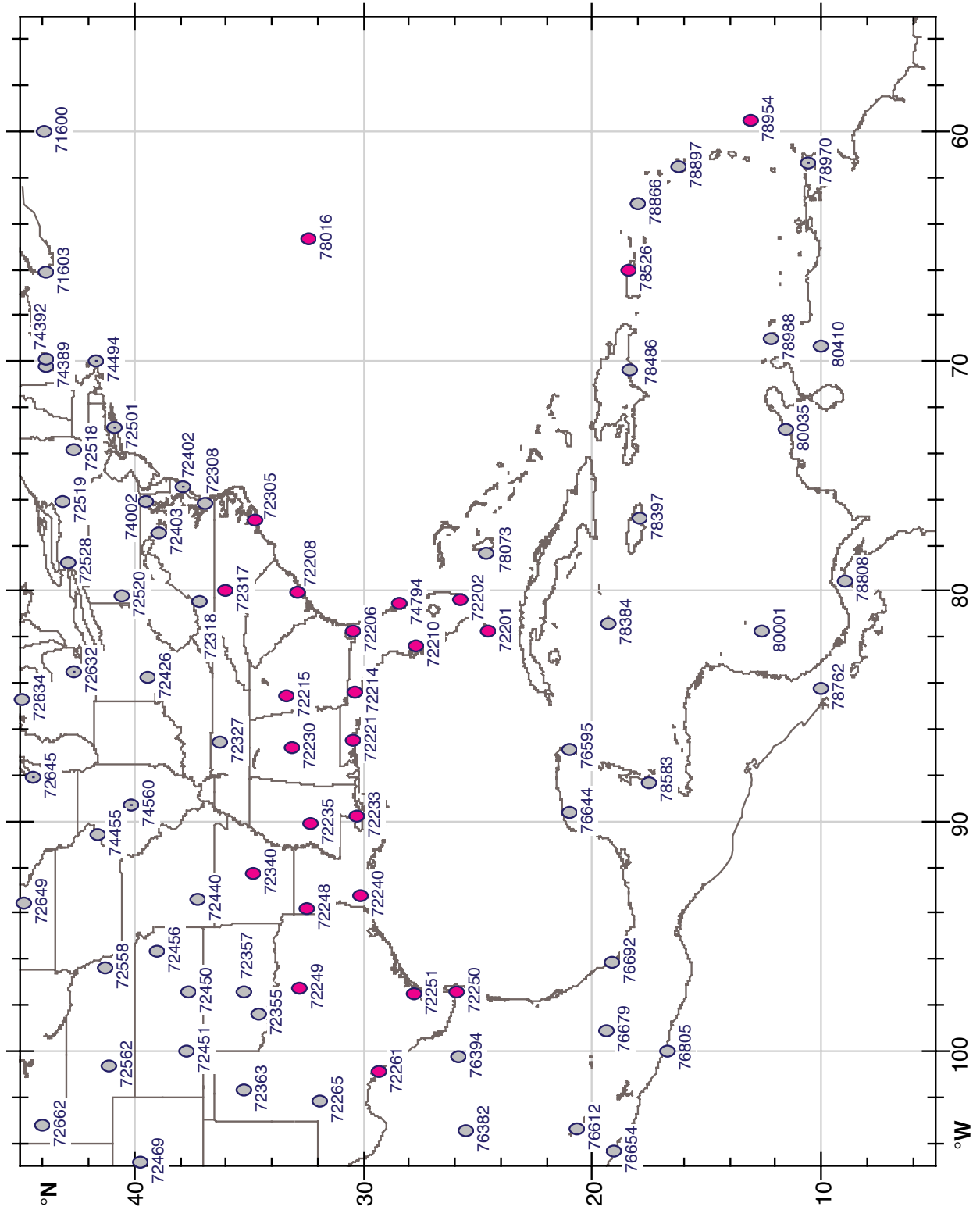


Figure F-1. Map of RAOB locations

APPENDIX F

DOD/NWS RAWIN/RAOB and NWS Coastal Land-Based Radar Locations

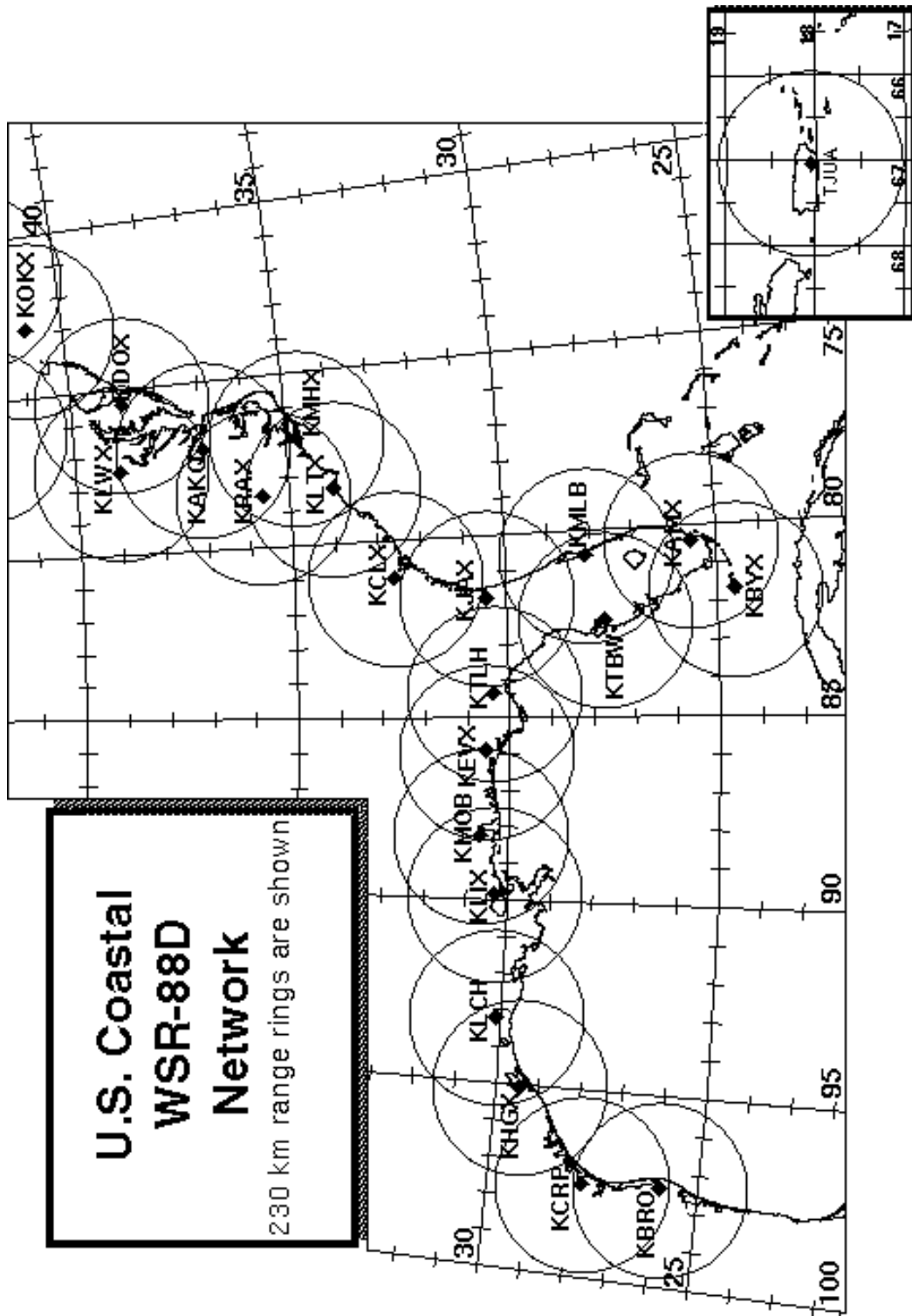


Figure F-2. Map of U.S. land-based radar locations

2018 NOAA/AOML/HRD Hurricane Field Program - IFEX

APPENDIX G  
Systems of Measure and Unit Conversion Factors

Table G-1. Systems of measure: Units, symbols, and definitions

Quantity	SI Unit	Early Metric	Maritime	English
length	meter (m)	centimeter (cm)	foot (ft)	foot (ft)
distance	meter (m)	kilometer (km)	nautical mile (n mi)	mile (mi)
depth	meter (m)	meter (m)	fathom (fa)	foot (ft)
mass	kilogram (kg)	gram (g)		
time	second (s)	second (s)	second (s)	second (s)
speed	meter per second (m s <sup>-1</sup> )	centimeter per second (cm s <sup>-1</sup> )	knot (kt) (nm h <sup>-1</sup> )	miles per hour (mph)
		kilometers per hour (km h <sup>-1</sup> )		
temperature-sensible	degree Celsius (°C)	degree Celsius (°C)	---	degree Fahrenheit (°F)
-potential	Kelvin (K)	Kelvin (K)	---	Kelvin (K)
force	Newton (N) (kg m s <sup>-2</sup> )	dyne (dy) (g cm s <sup>-2</sup> )	poundal (pl)	poundal (pl)
pressure	Pascal (Pa) (N m <sup>-2</sup> )	millibar (mb) (10 <sup>3</sup> dy cm <sup>-2</sup> )	inches (in) mercury (Hg)	inches (in) mercury (Hg)

Table G-2. Unit conversion factors

Parameter	Unit	Conversions
length	1 in	2.540 cm
	1 ft	30.480 cm
	1 m	3.281 ft
distance	1 n mi (nautical mile)	1.151 mi 1.852 km 6080 ft
	1 mi (statute mile)	1.609 km 5280 ft
	1° latitude	59.996 nm 69.055 mi 111.136 km
depth	1 fa	6 ft 1.829 m
mass	1 kg	2.2 lb
force	1 N	10 <sup>5</sup> dy
pressure	1 mb	102 Pa 0.0295 in Hg
	1 lb ft <sup>-2</sup>	4.88 kg m <sup>-2</sup>
speed	1 m s <sup>-1</sup>	1.94 kt 3.59 kph
	1° lat. 6 h <sup>-1</sup>	10 kt

## 2018 NOAA/AOML/HRD Hurricane Field Program - IFEX

### APPENDIX H *List of Acronyms*

---

ABL	atmospheric boundary layer
ADOS	Thermistor chain Autonomous Drifting Ocean Station
AMSR2	Advanced Microwave Scanning Radiometer 2
AOC	Aircraft Operations Center
AOML	Atlantic Oceanographic and Meteorological Laboratory
AXBT	airborne expendable bathythermograph
AXCP	airborne expendable current profilers
AXCTD	airborne expendable conductivity–temperature–depth probe
AEW	African easterly wave
AVAPS	Airborne Vertical Atmospheric Profiling System
AWRAP	Advanced Wind and Rain Airborne Profiler
CARCAH	Chief, Aerial Reconnaissance Coordinator, All Hurricanes
CB	convective burst
CBLAST	Coupled Boundary Layer Air-Sea Transfer
C-MAN	Coastal-Marine Automated Network
CCP	Cloud Combination Probe
CRL	Airborne compact rotational Raman LIDAR
CYGNSS	NASA Cyclone Global Navigation Satellite System
DA	data assimilation
DMT	Droplet Measurement Technologies, Inc.
DWL	Doppler Wind LIDAR
ECMWF	European Centre for Medium-Range Weather Forecasts
EMC	Environmental Modeling Center
EOL	Earth Observing Laboratory (NCAR)
ERC	eyewall replacement cycle
ET	extratropical transition
FL	flight level
GFS	Global Forecast System
G-IV	Gulfstream IV-SP aircraft
GMI	Global Precipitation Measuring Mission Microwave Instrument
GPS	global positioning system
GRIP	NASA Genesis and Rapid Intensification Processes experiment
GTS	global telecommunications system
HEDAS	Hurricane Ensemble Data Assimilation System
HFP	Hurricane Field Program
HFPP	Hurricane Field Program Plan
HRD	Hurricane Research Division
HWRP	Hurricane Weather Research and Forecasting (model)
ICS	interphone communications systems
IFEX	Intensity Forecast Experiment
IP	initial point
IWRAP	Imaging Wind and Rain Airborne Profiler
LIDAR	Light Detection and Ranging
LF	lower fuselage (radar)



**APPENDIX H**  
*List of Acronyms*

---

MCS	mesoscale convective system
MDR	main development region
MMR	Multi-mode Radar
NASA	National Aeronautics and Space Administration
NCAR	National Center for Atmospheric Research
NCEP	National Centers for Environmental Prediction
NCO	NCEP Central Operations
NESDIS	National Environmental Satellite, Data and Information Service
NHC	National Hurricane Center
NHOP	National Hurricane Operations Plan
NOAA	National Oceanographic and Atmospheric Administration
NPS	Naval Postgraduate School
NWS	National Weather Service
OMAO	Office of Marine and Aviation Operations
OSSE	observation system simulation experiment
OSE	observing system experiments
P-3	WP-3D aircraft
PA	public address
PIP	Precipitation Imaging Probe
POD	Plan of the Day
PREDICT	Pre-depression Investigation of Cloud-systems in the Tropics
RMW	radius of maximum wind
SAL	Saharan air layer
SEF	secondary eyewall formation
SFMR	Stepped Frequency Microwave Radiometer
SSMIS	Special Sensor Microwave Imager/Sounder
SST	sea surface temperature
TC	tropical cyclone
TCDC	tropical cyclone diurnal cycle
TD	tropical depression
TDR	tail Doppler radar
TPW	total precipitable water
TS	tropical storm
UAS	unmanned aerial system
WSRA	Wide Swath Radar Altimeter
WRF-ARW	Weather Research and Forecasting model – Advanced Research WRF

### **Acknowledgments**

The preparation of HRD's **Hurricane Field Program Plan** was a team effort. The authors would like to express their appreciation to: the HRD scientists that contributed information on specific experiments